VOLUME 47, NUMBER 3, SEPTEMBER 2024

# HADRONIC JOURNAL

Founded in 1978 by Prof. R. M. Santilli at Harvard University. Some of the past Editors include Professors S. L. Adler, A. 0. Barut, L. C. Biedenharn, N. N. Bogoliubov, M. Froissart, J.Lohmus, S. Okubo, Nobel Laureate Ilya Prigogine, M. L. Tomber, J. P.Vigier, J. Wess, Nobel Laureate Chen Ning Yang.

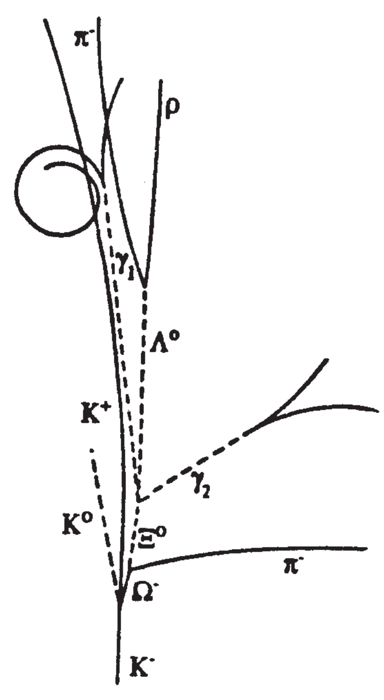




HADRONIC JOURNAL Volume 47, Number 3, September 2024

H P HADRONIC PRESS, INC.

# HADRONIC JOURNAL

Established in 1978 by Prof. R. M. Santilli at Harvard University Hadronic Journal and Algebras, Groups and Geometries have been regularly published since 1978 without publication charges and are among the few remaining independent refereed journals.

This Journal publishes advances research papers and Ph. D. theses in any field of mathematics without publication charges.

For subscription, format and any other information please visit the website http://www.hadronicpress.com

HADRONIC PRESS INC.
35246 U. S. 19 North Suite 215
Palm Harbor, FL 34684, U.S.A.
http://www.hadronicpress.com
Email: info@hadronicpress.com
Phone: +1-727-946-0427

# HADRONIC JOURNAL

ISSN: 0162-5519

Established in 1978 by Prof. R. M. Santilli at Harvard University Hadronic Journal and Algebras, Groups and Geometries have been regularly published since 1978 without publication charges and are among the few remaining independent refereed journals.

This Journal publishes advances research papers and Ph. D. theses in any field of mathematics without publication charges.

For subscription, format and any other information please visit the website http://www.hadronicpress.com

HADRONIC PRESS INC.
35246 U. S. 19 North Suite 215
Palm Harbor, FL 34684, U.S.A.
http://www.hadronicpress.com
Email: info@hadronicpress.com
Phone: +1-727-946-0427

HADRONIC JOURNAL Volume 47, Number 3, September 2024

H P HADRONIC PRESS, INC.

# HADRONIC JOURNAL

## VOLUME 47, NUMBER 3, SEPTEMBER 2024

**C. Wolf**
Department of Physics
North Adams State College
North Adams, MA 01247 USA

**V. M. Chabanov[1], B. N. Zakhariev[1]**
(All pictures of this report were prepared in collaboration with S. Brandt*, H. D. Dahmen* and T. Stroh*)
* Fachbereich Physik, Universitat Siegen, 57068 Siegen, Germany
[1] Laboratory of Theoretical Physics
Joint Institute for Nuclear Research
Dubna, 141980, Russia

**HADRONIC JOURNAL 47**, 263 - 273 (2024)
DOI 10.29083/HJ.47.03.2024/SC263



**COMPUTATIONAL ANALYSIS OF 1 kW PEMFC STACK: IV CHARACTERIZATION AND OPTIMIZATION**

**[1]Rajkrishna Sapkota, [2]Deepa Parajuli, [3]Shraddha Puri, [4]Ram Krishna Yadav, [5]Mukesh Shrestha, [6]Saddam Husain Dhobi**

[1]Central Department of Physics, Tribhuvan University, Kirtipur, Kathmandu, Nepal
[2]Department of Physics, Patan Multiple Campus, Tribhuvan University, Lalitpur Nepal
[3]Department of Physics, Amrit Science Campus, Tribhuvan University, Kathmandu, Nepal
[4]Electronic and Communication Engineering, National College of Engineering, Tribhuvan University, Nepal
[5]Electronic and Communication, Kathford International College of Engineering and Management, Tribhuvan University, Nepal
[6]Physical Science Unit, Nepal Academy of Science and Technology Khumaltar, Lalitpur, Nepal
saddam@ran.edu.np

Received May 25, 2024

## Abstract

This computational study focuses on the IV characterization (current-voltage-power) of a 1 kW-24 Vdc proton exchange membrane fuel cell (PEMFC) stack. Leveraging an online MATLAB package, we simulated the performance of a 42-cell stack, incorporating air and hydrogen flow rates. The simulation parameters included a stack efficiency of 46%, an air flow rate of 2400 lpm, and an operating temperature of 55 °C. Our objective was to comprehensively investigate the IV characteristics of the PEMFC over a 1-hour duration. The results demonstrate a linear relationship between current and voltage, with a maximum power output of 2 W and a voltage range of 0 to 45.5 V. The study contributes valuable insights into PEMFC dynamics, offering a computational approach for characterizing and optimizing performance. This work lays the foundation for further exploration of PEMFC behavior under varying conditions, paving the way for advancements in fuel cell technology.

**Keywords:** PEMFC, IV Characterization, Computational Simulation, Stack Efficiency

## 1 Introduction

Fuel cells have emerged as a promising technology for clean and efficient energy conversion, offering a viable alternative to traditional combustion-based power generation. Among various types of fuel cells, PEMFCs have garnered significant attention due to their high energy efficiency, low environmental impact, and versatile applications. As researchers and engineers strive to enhance the performance and viability of PEMFCs, computational analysis has become an indispensable tool in understanding the intricate dynamics of these systems. This article delves into the computational analysis of a 1 kW PEMFC stack, focusing on the crucial aspect of current-voltage (IV) characterization and subsequent optimization. The IV curve is a fundamental performance metric for PEMFCs, providing insights into the electrochemical processes within the cell and influencing the overall efficiency of the power generation system. By employing advanced simulation techniques and optimization algorithms, researchers aim to unravel the complexities associated with PEMFCs and tailor their operational parameters for optimal performance.

The research on the computational analysis of a 1 kW PEMFC stack with a focus on IV characterization and optimization is imperative for several compelling reasons. These reasons underscore the necessity of such investigations to advance the field of fuel cell technology and contribute to the broader goals of sustainable energy production: PEMFCs are known for their high efficiency in converting chemical energy into electrical energy. However, achieving and maintaining optimal efficiency levels is a complex task. This research aims to uncover opportunities for efficiency enhancement through detailed computational analysis, ultimately contributing to more effective and sustainable energy conversion processes. A comprehensive understanding of the IV characteristics is fundamental to deciphering the performance of PEMFCs. Computational analysis allows researchers to delve into the intricate electrochemical processes occurring within the fuel cell stack, providing insights into factors influencing performance. This knowledge is crucial for identifying bottlenecks, optimizing operating conditions, and improving overall system efficiency.

As PEMFC technology evolves, there is a need for continuous improvement in design to meet the increasing demands for energy efficiency and reliability. Computational analysis facilitates the exploration of various design

parameters, enabling researchers to optimize the geometry, materials, and operational conditions of the fuel cell stack. This optimization process is vital for achieving higher power density and longer operational lifetimes. The commercial viability of PEMFC technology is closely tied to the overall cost of production and operation. Computational analysis allows researchers to explore cost-effective design modifications and operational strategies without the need for extensive physical prototypes. Identifying cost-efficient solutions contributes to the economic feasibility of PEMFC technology, making it more competitive in the energy market. PEMFCs are recognized for their potential to provide clean energy with minimal environmental impact. Understanding the performance characteristics and optimizing PEMFC stacks can further enhance their environmental benefits by ensuring efficient energy conversion and reducing resource consumption. This aligns with the global imperative to transition towards cleaner and more sustainable energy sources.

## 2 Literature Review

The current era marks a pivotal moment for hydrogen, serving as a new energy vector that holds the potential to enhance global energy independence and facilitate decarbonization across various economic sectors. Electrolysis of water, involving the breakdown of $H_2O$ into oxygen and hydrogen gas through an electric current, is a key method to produce hydrogen sustainably. Utilizing a water electrolyzer and a fuel cell enables a seamless transition between electricity and hydrogen without on-site pollutant emissions. Amid prioritized objectives like reliability and lifespan, predicting the future applications of fuel cells remains challenging. Numerous studies have addressed this, focusing on fuel cell technology. This paper presents a model of a PEMFC using Matlab/Simulink, offering insights into the impact of different parameters on PEMFC efficiency and electricity production [1].

Fuel cells are a promising renewable energy source with the potential to offer secure, sustainable, and cost-effective energy solutions, contributing to economic, social, and environmental progress. PEMFCs utilizing polymers as electrolytes, have gained prominence due to their efficiency and versatility in various applications. The advantages of FCs include efficiency, cleanliness, economic, social, and environmental benefits, security, cost-effectiveness, and sustainable power generation. Despite their benefits, challenges such as high costs and maintenance requirements persist.

PEMFCs, among various types of fuel cells like phosphoric acid, molten carbonate, and solid oxide, stand out for their low operating temperature, fast start-up times, relatively lower component costs, high efficiency, and minimal environmental impact. Accurate modeling of PEMFCs is crucial for analysis and optimization, contributing to the development of more efficient, reliable, and environmentally friendly versions of the technology. Optimization algorithms play a critical role in determining PEMFC parameters, such as design, materials, operating temperature, and production rate, enhancing efficiency and cost-effectiveness [2].

Recent studies highlight the significance of perovskite proton conductivity, recommending Y-doped $BaZrO_3$ perovskite for electrochemical hydrogen FCs to improve efficiency [3]. Progress in barium zirconate proton conductors has also been reviewed, detailing current investigations to enhance hydrogen devices [4]. Optimizing PEMFC design variables involves traditional and metaheuristic optimization techniques. While traditional methods seek a single optimal solution, metaheuristic techniques, based on probabilistic methods, quickly find near-optimal solutions. Traditional techniques face challenges like slow convergence and difficulty handling complex nonlinear problems. Consequently, research papers increasingly focus on metaheuristic optimization algorithms for PEMFC parameter estimation due to their efficiency in addressing these challenges [2].

In 2011, the European Commission published the "Flight Path 2050" and set ambitious environmental goals for aviation. According to these goals, a 75% reduction in $CO_2$, a 90% reduction in $NO_X$, and a 60% reduction in noise emissions are targeted until 2050, specifically referring to typical aircraft manufactured in the year 2000. Given the increasing air travel demands, achieving these goals solely through evolutionary improvements of existing aviation technology appears challenging. It is widely acknowledged that hydrogen fuel cell systems can offer substantial improvements in civil aircraft design, including reduced noise, lower emissions, and enhanced fuel economy. This makes fuel cell-powered aircraft more aligned with the environmental objectives outlined in the "Flight Path 2050". To strengthen competencies in the aviation sector, weight reduction and reliability improvement of these fuel cell system designs are deemed crucial. The cooling subsystem within an aviation fuel cell system is identified as a critical component, accounting for up to 50% of the total system weight [4]. Efficient heat rejection is emphasized as vital for aviation fuel cell systems,

particularly as fuel cells in aviation move towards higher power outputs in the megawatt range for commercial airliners [5]. Existing studies have explored various cooling approaches, including using the aircraft surface for heat transfer, Outer Mold Line cooling, and innovative hydrogen cooling concepts. System reliability is paramount in aviation, often achieved through redundancy. Current standards require a minimum redundancy of 2.25 for fuel cell-powered airliners, but this increases the total system weight and limits payload capacity. To address this, a shift towards system simplicity is proposed, reducing the number of components and thereby improving reliability, reducing weight, and increasing the power-to-weight ratio [6].

## 3 Methods and materials

**Computational Framework:** This study leveraged a computational approach using an online MATLAB package to simulate the IV characteristics of a 1 kW-24Vdc PEMFC stack. MATLAB provides a versatile and powerful platform for numerical simulations, facilitating the modeling and analysis of complex systems like fuel cells.

**PEMFC Stack Design:** The simulation focused on a PEMFC stack with a power output of 1 kW and an operating voltage of 24Vdc. The stack consisted of 42 individual cells arranged in series, each operating under similar conditions. The nominal stack efficiency was set at 46%, reflecting the conversion efficiency of electrical power from hydrogen and air input.

**Operating Conditions:** The simulation considered operational parameters relevant to practical PEMFC systems. The air and hydrogen flow rates were integral components, with an air flow rate set at 2400 liters per minute (lpm). The simulation was conducted at an operating temperature of 55°C, representing a common operational range for PEMFCs.

**Simulation Duration:** The simulation spanned a duration of 1 hour, providing a comprehensive analysis of the IV characteristics over an extended period. This duration allowed for the observation of transient behavior, stability, and performance variations within the fuel cell stack.

**Computational Execution:** The online MATLAB basic package utilized for the simulation incorporated relevant algorithms and models for PEMFCs. The computation involved solving the governing equations of the fuel cell, considering factors such as electrochemical reactions, mass transport, and

thermal effects. The simulation was executed iteratively to capture the dynamic response of the PEMFC stack under varying load conditions.

**Data Collection and Analysis:** Data on current, voltage, and power characteristics were collected throughout the 1-hour simulation. Various performance metrics, such as power density, voltage efficiency, and current density, were computed to evaluate the overall performance of the PEMFC stack under the specified conditions. This computational study employed an online MATLAB package to simulate the IV characteristics of a 1 kW-24Vdc PEMFC stack. The design and operational parameters were carefully chosen to reflect real-world conditions, and the simulation methodology allowed for a detailed investigation of the fuel cell's performance over a 1-hour duration.

## 4 Simulation block Diagram

The simulation of a fuel cell system with a particular emphasis on the output generation based on specified constants (1), and input variables represent in leftside of stock cell. The simulation employs a model is treating as either a 1-D array or a matrix, depending on the configuration, shown in figure 1. The maximum value of the output is determined by the minimum or maximum of the input, with operators applied across the input vector in the case of multiple inputs. The simulation incorporates a general expression block, utilizing u as the input variable name for both air and fuel. This study provides a comprehensive understanding of the dynamics and behavior of the fuel cell system through a flexible and adaptable simulation framework, offering insights into the impact of specified constants and input variations on the system's performance.

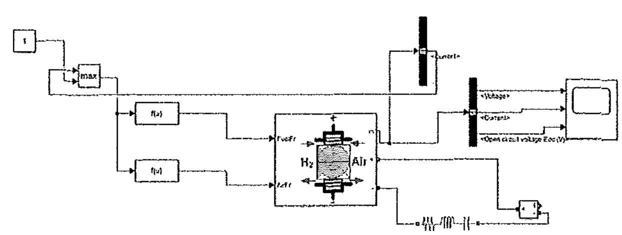


**Figure 1:** Block diagram and flow chart for simulation of fuel cell

## 5 Results and Discussion

The simulation focused on the transient response of a proton exchange membrane fuel cell (PEMFC) under constant fuel supply conditions, providing valuable insights into the dynamic behavior of the system. Figure 2 depicts the nature of current and voltage with time for a consistent supply of fuel and oxygen or air.

### 5.1 Voltage Fluctuation

The voltage fluctuation in the proton exchange membrane fuel cell (PEMFC) system exhibits distinct temporal patterns. Initially, between 0 to 750 seconds, the voltage fluctuation is comparatively lower, suggesting a relatively stable system during this period. However, from 750 seconds to 2750 seconds, there is a noticeable increase in voltage fluctuation, indicating a phase of heightened system dynamics. Beyond 2750 seconds, the voltage fluctuation decreases, emphasizing the system's ability to return to a more stable state. The voltage range of 44.5V to 45.5V throughout the experiment underscores the dynamic nature of the PEMFC system, potentially influenced by factors such as fuel supply variations and system response time.

### 5.2 Current Fluctuation

The current in the PEMFC system exhibits significant fluctuations over time, and these variations provide valuable insights into the system's dynamic behavior. Between 250 seconds and 600 seconds, the current fluctuation is observed to be lower, suggesting a period of relative stability. However, after 600 seconds, the current fluctuation increases and peaks at 1500 seconds, indicating a phase of heightened system dynamics. The sustained high fluctuation continues until 2750 seconds, after which the current fluctuation decreases, suggesting a return to a more stable state. The observed current range from $10^{-2}$ to $5x10^{-2}$ A signifies the dynamic response of the PEMFC system to changes in fuel supply and operational conditions.

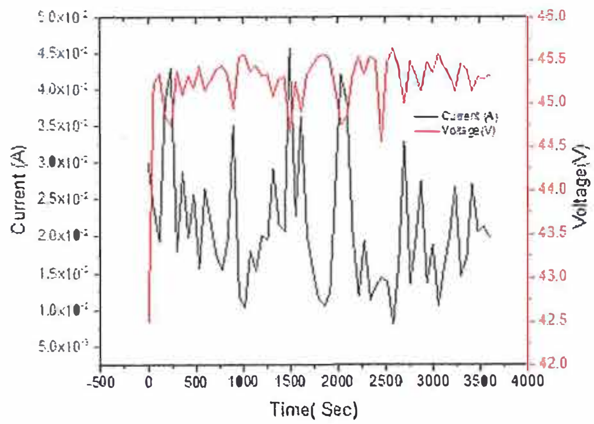


**Figure 2:** Fuel supply time vs Current and Voltage

Comparisons with previous studies, notably [7] Smith et al., reveal similarities in the fluctuation patterns of current and voltage. Despite differences in the voltage range and fluctuations, the shared characteristics indicate consistent behavior in PEMFC systems under certain conditions. This comparison highlights the reproducibility of certain dynamic phenomena in PEMFCs and provides additional context for interpreting the current study's results. It underscores the importance of understanding these fluctuations for designing and optimizing PEMFCs for practical applications. The dynamic performance and loading characteristics of the PEMFC system are crucial for evaluating its practical applicability. The study observes that successful loading occurs with a step current density of 1.5 $Acm^{-2}$ after activation, emphasizing the importance of controlled activation processes. Issues such as membrane dehydration are identified as significant factors affecting dynamic performance. The study's findings align with the broader goal of achieving favorable responses to high step currents, facilitating rapid loading to high-power output. These insights contribute valuable guidance for designing and controlling the dynamic loading of PEMFCs [8], enhancing their reliability and efficiency in diverse applications.

### 5.3 Voltage and Power Characteristics

Figure 3 illustrates the voltage and power characteristics of the PEMFC stack at different current densities. The observed nature of voltage demonstrates a linear decrease with increasing current density, indicating a typical behavior within the tested operational range. Conversely, the power exhibits a linear

increase with current density. The recorded maximum power reaches 2 W, while the voltage reaches a maximum of 45.5 V. Notably, the intersection point of power and voltage occurs at 0.03 A, indicating a critical operational point where both parameters align.

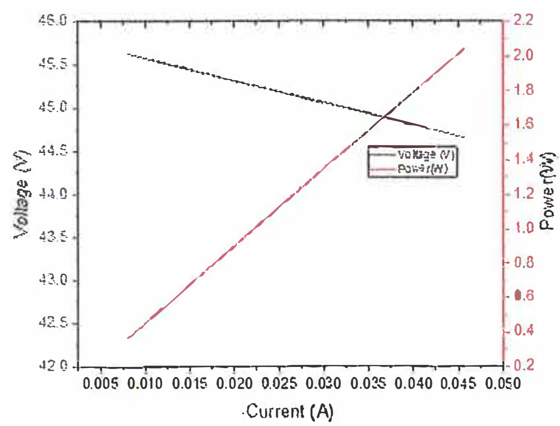


**Figure 3:** Current vs Voltage and Power

The voltage and power characteristics observed in this study align with the findings reported [9] Kuan et al., suggesting a consistent behavior across different experimental setups. This similarity provides corroborative evidence and reinforces the reproducibility of certain phenomena in PEMFCs. The linear relationship between voltage and current density, along with the intersection point, is a characteristic shared with the prior study, contributing to the broader understanding of PEMFC performance under varying conditions. To further evaluate the PEMFC stack, additional experiments were conducted using the Rigor fuel cell test system (RG24020) at 75 °C and 80% relative humidity. The polarization curve displayed a typical pattern, achieving an output power of 15.8 kW. The current experienced a decline from 270 A to 190 A at a stack voltage of 58.5 V, leading to a sharp drop in output power from 15.8 kW to 11.11 kW. These results closely resemble those reported by Xiong et al. [10], indicating a consistent trend in the impact of backpressure on PEMFC performance.

## 6 Conclusion

In conclusion, the investigation into the voltage and power characteristics of a homemade PEMFC stack reveals a linear decrease in voltage with increasing current density, while power exhibits a linear increase. The maximum recorded power and voltage reach 2 W and 45.5 V, respectively, with an interesting intersection point at 0.03 A. The congruence of these findings with the study by Kuan et al. [9] highlights the reproducibility of PEMFC behavior across different experimental setups. Additionally, the examination of backpressure effects on stack performance aligns with previous research, emphasizing the impact of pressure conditions on current, voltage, and power outputs. These insights contribute to a comprehensive understanding of PEMFC dynamics, guiding further research and practical applications. The observed trends underscore the importance of optimizing operational parameters for enhanced PEMFC performance in various environmental conditions.

## Reference

[1] S. El Aimani, Modeling and Simulation of a Hydrogen-based Proton Exchange Membrane Fuel Cell for Power Generation. Paper presented at the IEEE Global Power, Energy and Communication Conference (IEEE GPECOM 2023), Ramada by Wyndham Cappadocia, Cappadocia, Nevsehir, Turkey.

[2] H. Rezk, A. G. Olabi, S. Ferahtia, and E. T. Sayed, Energy, 255(2022).

[3] M. K. Hossain, T. Yamamoto, and K. Hashizume, Journal of Alloys and Compounds, 903 (2022).

[4] M. K. Hossain, S. M. K. Hasan, M. I. Hossain, R. C. Das, H. Bencherif, M. H. K. Rubel, M. F. Rahman, T. Emrose, and K. Hashizume, Nanomaterials, 12 (2022).

[5] H. Kellermann, A. L. Habermann, and M. Hornung, Aerospace, 7 (2020).

[6] A. Baroutaji, T. Wilberforce, M. Ramadan, and A. G. Olabi, Renewable and Sustainable Energy Reviews, 106(2019).

[7] P. J. Smith, W. R. Bennett, I. J. Jakupca, R. P. Gilligan, and L. G. Edwards, "Proton exchange membrane fuel cell transient load response," NASA/TM-20210018094, (2021).

[8] Z. Huang, J. Shen, S. H. Chan, and Z. Tu, Energy Conversion and Management, 226(2020).

[9] Y. D. Kuan, J. L. Lyu, T. R. Ke, M. F. Sung, and J.-S. Do, International Journal of Hydrogen Energy, 44(2019).

[10] Z. Xiong, H. Zhou, X. Wu, S. H. Chan, Z. Xie, and D. Dang, Molecules, 27 (2022).

**HADRONIC JOURNAL 47**, 275 - 293 (2024)
DOI 10.29083/HJ.47.03.2024/SC275


# THE ASTONISHING CONFLICT OF TIME DILATION WITHIN RELATIVITY

**Rodrigo de Abreu**
Departamento de Física, Instituto Superior Técnico
Universidade de Lisboa, 1049-001 Lisboa, Portugal
rabreu@tecnico.uslisboa.pt

Received April 13, 2024
Revised April 23, 2024

## Abstract

We show that if we assume the existence of a frame in vacuum where the one-way speed of light is $c$ ($c$ is the measured value of the two-way speed of light in vacuum) than for another frame moving with velocity $v_1$ in relation to that frame we can have time dilation, time contraction or no difference of proper times change at all. Therefore, the standard formulation is a result of a misinterpretation of the mathematical expression between the relation of the proper time of the moving frame in relation to the difference of times of Lorentzian clocks, the so-called time dilation. This is an astonishing conflict that standard formulation cannot solve. This result is easily obtained if we assume time dilation in relation to Einstein Frame (EF) the frame where the speed of light is isotropic.

**Keywords:** simultaneity, synchronization, Einstein frame, intrinsic desynchronization, Lorentz transformation, IST transformation, time dilation and contraction, Lorentz-FitzGerald contraction and dilation, resolution twin paradox

## 1. Introduction

Recently one more interesting article questioned the accuracy of the postulate of the constancy of the speed of light and the meaning of time dilation has been published [1]. In a first work [2] we address the failure of standard formulation in relation to the existence of Einstein Frame (EF) the unique frame where the one-way speed of light is isotropic [1, 2]. Now with the same token we address time dilation. This is a problem of semiotic where the problem of symbols and meaning is crucial as we formulate with the intrinsic desynchronization that necessitate the new symbol $t_L'$ for the Lorentzian time (https://en.wikipedia.org/wiki/Semiotics).

## 2. Time dilation and Lorentz Transformation

In a previous article "Special Relativity as a Simple Geometry Problem" [3] we obtain geometrically time dilation in relation to a frame where the speed of light is isotropic independently of the movement of the source. Therefore, we obtain the IST Transformation connected to Time Dilation and Lorentz-FitzGerald contraction [1-3]

$$x' = \frac{x - v_1 t}{\sqrt{\left(1 - \frac{v_1^2}{c^2}\right)}} \qquad (1)$$

$$t' = t\sqrt{\left(1 - \frac{v_1^2}{c^2}\right)} \qquad (2)$$

Indeed, consider frames $S$ and $S'$. $S$ is the $EF$ and $S'$ is a frame moving in a standard configuration in relation to $S$ with velocity $v_1$. This standard configuration is $S'$ moving through $x$ of $S$. O′ the origin of $S'$ coincide with O the origin of $S$ and O′ moves through the $x$ axis of $S$ with $v_1$. When O′ coincide with O the origin O′′ of another frame $S''$ coincide also with O′ and is moving from O′ through $x'=l_1$ with velocity $v_2$ in relation to $EF$. Therefore, we have time dilation with $v_2$

$$t'' = t\sqrt{\left(1 - \frac{v_2{}^2}{c^2}\right)} \qquad (3)$$

and Lorentz-FitzGerald contraction

$$x'' = \frac{x - v_2 t}{\sqrt{\left(1 - \frac{v_2{}^2}{c^2}\right)}} \qquad (4)$$

This is enough to obtain Lorentz Transformation through a change of coordinates based on the expression of intrinsic desynchronization introduced by us [4-9],

$$t_L' = t' - \frac{v_1}{c^2}x' \qquad (5)$$

Introducing (5) in (1) and (2) (and the similar procedure for (3) and (4)) we obtain [2, 3-116]

$$x'' = \frac{x' - v_E' t_L'}{\sqrt{\left(1 - \frac{v_E'^2}{c^2}\right)}} \qquad (6)$$

$$t_L'' = \frac{t_L' - \frac{v_E'}{c^2}x'}{\sqrt{\left(1 - \frac{v_E'^2}{c^2}\right)}} \qquad (7)$$

with

$$v_E' = \frac{dx'}{dt_L'} = \frac{v_2 - v_1}{1 - \frac{v_1 v_2}{c^2}} \qquad (8)$$

Therefore, if we consider the clock O′′ moving with Einstein speed $v_E'$ through $x'$ we obtain

$$x' = l_1 = v_E'\, t_L' \qquad (9)$$

Therefore, substituting (9) in (7)

$$t_L^{''} = \frac{t_L^{'}(1 - \frac{v_E^{'2}}{c^2})}{\sqrt{\left(1 - \frac{v'_E{}^2}{c^2}\right)}} = t_L^{'} \sqrt{\left(1 - \frac{v'_E{}^2}{c^2}\right)} \quad (10)$$

From (5) and (9)

$$t_L^{'} = t' - \frac{v_1}{c^2} v_E^{'} t_L^{'} \quad (11)$$

From (11)

$$t' = t_L^{'}\left(1 + \frac{v_1}{c^2} v_E^{'}\right) \quad (12)$$

Introducing (12) in (10) with $t' = \tau'$, and with $t_L^{''} = \tau''$ we obtain

$$\tau'' = \frac{\tau'}{\left(1 + \frac{v_1}{c^2} v_E^{'}\right)} \sqrt{\left(1 - \frac{v'_E{}^2}{c^2}\right)} \quad (13)$$

Therefore, the relation of $\tau''$ and $\tau'$ is not the relation that standard formulation confound as time dilation (relation (10)) since consider "Einstein synchronization" a synchronization [4-11].

Therefore, we can reapproach the twin paradox [23-25, 106-118]. Consider standard configuration previously referred:

Consider frames *S* and $S'$. *S* is the *EF* and $S'$ is a frame moving in a standard configuration in relation to *S* with velocity $v_1$. This standard configuration is $S'$ moving through *x* of *S*. O′ the origin of $S'$ coincide with O the origin of *S* and O′ moves through the *x* axis of *S* with $v_1$. When O′ coincide with O the origin O′′ of another frame $S''$ coincide also with O′ and is moving from O′ through $x'=l_1$ with velocity $v_2$ in relation to *EF*.

From (10) with $t_L^{''} = \tau_+^{''}$ and $t_L^{'} = \frac{l_1}{|v'_{E+}|}$ we obtain for the trip +

$$\tau_{+}'' = \frac{l_1}{|v'_{E+}|}\sqrt{\left(1 - \frac{{v'_{E+}}^2}{c^2}\right)} \qquad (14)$$

with $v'_{E+} = \frac{v_2 - v_1}{1 - v_1 v_2}$ when $v_2 > v_1$.

Similarly, for the returning trip $-$,

$$\tau_{-}'' = \frac{l_1}{|v'_{E-}|}\sqrt{\left(1 - \frac{{v'_{E-}}^2}{c^2}\right)} \qquad (15)$$

with $v'_{E-} = \frac{v_2 - v_1}{1 - v_1 v_2}$ when $v_2 < v_1$.

We have also that the proper time of $S'$ associated to trip + between the origin and $x'=l_1$ is (the proper time of any synchronized clock located in S′)

$$\tau_{+}' = \frac{l_1}{|v'_{+}|} \qquad (16)$$

with

$$v' = \frac{dx'}{dt'} = \frac{dx'}{dt_L'}\frac{dt_L'}{dt'} = v'_E \frac{dt_L'}{dt'} \qquad (17)$$

Since

$$t_L' = t' - \frac{v_1}{c^2}x' \qquad (18)$$

we obtain

$$\frac{dt_L'}{dt'} = 1 - \frac{v_1}{c^2}\frac{dx'}{dt'} = 1 - \frac{v_1}{c^2}v' \qquad (19)$$

Therefore, we obtain from (17) and (19)

$$v' = \frac{v'_E}{1 + \frac{v_1 v'_E}{c^2}} \qquad (20)$$

Therefore

$$\tau'_{+} = \frac{l_1}{|v'_{+}|} = \frac{l_1}{|v'_{E+}|}\left(1 + \frac{v_1\, v'_{E+}}{c^2}\right) \quad (21)$$

$$\tau'_{+} = \frac{l_1}{|v'_{+}|} = \frac{l_1}{|v'_{E+}|} + \frac{l_1 v_1}{c^2} \quad (22)$$

Similarly

$$\tau'_{-} = \frac{l_1}{|v'_{-}|} = \frac{l_1}{|v'_{E-}|}\left(1 - \frac{v_1\, |v'_{E-}|}{c^2}\right) \quad (23)$$

$$\tau'_{-} = \frac{l_1}{|v'_{-}|} = \frac{l_1}{|v'_{E-}|} - \frac{l_1 v_1}{c^2} \quad (24)$$

Finaly, we obtain the ageing of the “Earth twin” during the total trip,

$$\tau' = \tau'_{+} + \tau'_{-} = \frac{l_1}{|v'_{E+}|} + \frac{l_1}{|v'_{E-}|} \quad (25)$$

From (14) and (15) and (25) we conclude that the twin that return is the younger but without affirming the symmetry of the ageing that standard approach enunciate

$$\tau'' = \tau''_{+} + \tau''_{-} = \frac{l_1}{|v'_{E+}|}\sqrt{\left(1 - \frac{{v'_{E+}}^2}{c^2}\right)} + \frac{l_1}{|v'_{E-}|}\sqrt{\left(1 - \frac{{v'_{E-}}^2}{c^2}\right)} \quad (26)$$

From (25) and (26) we conclude that

$$\tau'' < \tau' \quad (27)$$

An astonishing conflict within relativity since Relativity affirm the equivalence of the frames and what we have is the preferred frame, *EF*. Therefore, we can understand the consistency of the asymmetry of (27) through (14) and (21)

$$\tau''_{+} = \frac{l_1}{|v'_{E+}|}\sqrt{\left(1 - \frac{{v'_{E+}}^2}{c^2}\right)} < \tau'_{+} \quad (28)$$

since, (22) is

$$\tau'_{+} = \frac{l_1}{|v'_{+}|} = \frac{l_1}{|v'_{E+}|} + \frac{l_1 v_1}{c^2} \quad (29)$$

Therefore

$$\tau''_{-} = \frac{l_1}{|v'_{E-}|}\sqrt{\left(1 - \frac{{v'_{E-}}^2}{c^2}\right)} < \tau'_{-} \quad (30)$$

since from (24)

$$\tau'_{-} = \frac{l_1}{|v'_{-}|} = \frac{l_1}{|v'_{E-}|} - \frac{l_1 v_1}{c^2} \quad (31)$$

Indeed when $v_2 < v_1, \tau'' < \tau'$ from (2) and (3).

Indeed from (2) and (3)

$$t'' = t' \frac{\sqrt{\left(1 - \frac{{v_1}^2}{c^2}\right)}}{\sqrt{\left(1 - \frac{{v_2}^2}{c^2}\right)}} \quad (34)$$

or

$$\tau'' = \tau' \frac{\sqrt{\left(1 - \frac{v_1{}^2}{c^2}\right)}}{\sqrt{\left(1 - \frac{v_2{}^2}{c^2}\right)}} \quad (35)$$

and therefore $\tau'' < \tau'$.

"De Abreu proposed to abandon the Relativity Principle in favor of 'restricted Relativity Principle' that allows the absolute space with a preferred reference system, referred to as 'the Einstein's lost frame'. This idea was future developed in [De Abreu 2002, 2004; De Abreu & Guerra 2005; Guerra & de Abreu 2006]. The velocity relative to the preferred reference system is said to be the absolute velocity, and a velocity relative to non-preferred system is said to be the Einstein velocity [De Abreu 2004]. The starting point of De Abreu (and jointly with Guerra) is the observation that the Einstein synchronization of clocks can be made in one and only one reference system. Analysis of the clock synchronization (related to one-way versus two-ways light velocity) leads Authors to consider the abandoning of the Relativity Principle (that all reference systems are equivalent)." [10, 11]

## Conclusion

We consider a clock moving in relation to a preferred frame, EF. This clock has time dilated in relation to the clocks of EF. Therefore, this clock can have time contracted in relation to other clock moving with other speed in relation to EF. And the rhythms are the same if the speed is the same. This resolves the time dilation conundrum and the Twin Paradox. This is an astonishingly conflict of Relativity that has been solved in the context of Relativity.

## References

1. Mateljević M (2024) Lorentz Transformation and time dilatation. Ann Math Phys 7(1): 016-022. DOI: 10.17352/amp.000104

2. de Abreu, R. The Astonishing Conflict of the Constancy of the One-Way Speed of Light within Relativity https://vixra.org/abs/2402.0086

3. de Abreu, R. and Guerra, V. Eur. J. Phys. 30, 2 (2009) Special relativity as a simple geometry problem - IOPscience

http://web.ist.utl.pt/d3264/papers/AG2009.pdf

4. de Abreu, R. The physical meaning of synchronization and simultaneity in Special Relativity
https://arxiv.org/abs/physics/0212020
http://ui.adsabs.harvard.edu/abs/2002physics..12020D/abstract

5. de Abreu, R. Reinterpretation of Lorentz Transformation and Resolution of Relativity Paradoxes
http://arxiv.org/abs/physics/0203025 ; EPS-12 Trends in Physics, Abstracts p. 270, Budapest (2002). http://vixra.org/abs/1505.0065

6. de Abreu, R. Deduction of Lorentz Transformation from the existence of absolute rest. Deduction of the speed of light in any frame of reference https://arxiv.org/abs/physics/0210023

7. Guerra, V. and de Abreu Foundations of Physics, On the Consistency between the Assumption of a Special System of Reference and Special Relativity Vol. 36, No. 12, December (2006) On the Consistency between the Assumption of a Special System of Reference and Special Relativity | SpringerLink

8. de Abreu, R. and Guerra, V. Eur. J. Phys. 29, 1 (2007) The principle of relativity and the indeterminacy of special relativity - IOPscience
https://iopscience.iop.org/article/10.1088/0143-0807/29/1/004
The principle of relativity and the indeterminacy of special relativity (ulisboa.pt)

9. Burde, G. I. Special Relativity with a Preferred Frame and the Relativity Principle
Journal of Modern Physics vol. 9, N° 8 (2018)
https://doi.org/10.4236/jmp.2018.98100

10. Zbigniew Oziewicz, How do you add relative velocities?
http://www.naturalphilosophy.org/pdf/group25.pdf

11. Zbigniew Oziewicz, Ternary relative velocity; astonishing conflict of the Lorentz group with relativity https://arxiv.org/abs/1104.0682

12. Kittel, C. Am. J. Phys. 42, 726 (1974) https://doi.org/10.1119/1.1987825

13. de Abreu, R. Gazeta de Física, vol. 21, Fasc. 3 (1998) https://www.spf.pt/magazines/GFIS/398/1153

14. Homem, G. Physics in a synchronized space-time. Master's thesis, Instituto Superior Técnico, Universidade Técnica de Lisboa, 2003

15. de Abreu, R. The Relativity Principle and the Indetermination of Special Relativity Ciência & Tecnologia dos Materiais, vol. 14, nº 1, p. 74 (2004), https://vixra.org/abs/2301.0139

16. de Abreu, R and Guerra, V. [physics/0512196] Is the assumption of a special system of reference consistent with Special Relativity? (arxiv.org)

17. de Abreu, R. and Guerra, V. Relativity – Einstein's Lost Frame (Extra]muros[, Lisboa, 2005), 1st ed. http://web.tecnico.ulisboa.pt/vguerra/papers/relshort.pdf

18. Guerra, V. and de Abreu, R. Special Relativity in Absolute Space: from a contradiction in terms to an obviousness https://arxiv.org/abs/physics/0603258

19. Guerra, V. and de Abreu, R. Foundations of Physics, On the Consistency between the Assumption of a Special System of Reference and Special Relativity Vol. 36, No. 12, December (2006) On the Consistency between the Assumption of a Special System of Reference and Special Relativity | SpringerLink

20. Guerra, V. and de Abreu, R. Eur. J. Phys. 26, 6 (2005) The conceptualization of time and the constancy of the speed of light – IOPscience

21. de Abreu, R. and Guerra, V. Eur. J. Phys. 29, 1 (2007) The principle of relativity and the indeterminacy of special relativity - IOPscience https://iopscience.iop.org/article/10.1088/0143-0807/29/1/004 The principle of relativity and the indeterminacy of special relativity (ulisboa.pt)

22. de Abreu, R. and Guerra, V. Eur. J. Phys. 30, 2 (2009) Special relativity as a simple geometry problem - IOPscience http://web.ist.utl.pt/d3264/papers/AG2009.pdf

23. de Abreu, R. and Guerra, V. EJTP Vol. 12 Issue 34, p183 (2015) http://www.ejtp.com/articles/ejtpv12i34p183.pdf Electronic Journal of Theoretical Physics (ejtp.com)

24. de Abreu, R. Guerra, V. Speakable and Unspeakable in Special Relativity:The Ageing of the Twins in the Paradox http://vixra.org/abs/1804.0320

25. de Abreu, R. Guerra, V. The Resolution of the Twin Paradox in a One-Way Trip http://vixra.org/abs/1805.0126

26. de Abreu, R. On the Experimental Determination of the One-Way Speed of Light (PDF) Rodrigo de Abreu Departamento de Física, Instituto ...vixra.org/pdf/1808.0646v2.pdf · Departamento de Física, Instituto Superior Técnico Universidade Técnica de Lisboa, 1049-001 - PDFSLIDE.NET https://vixra.org/abs/1808.0646

27. Einstein, A. Ann. Phys. 17, 132 (1905): "On the Electrodynamics of Moving Bodies", "Einstein's Miraculous Year, Five Papers That Changed the Face of Physics" Edited and Introduced by John Stachel, Princeton University Press (1998)

28. Consoli, M. Pluchino, A. Atti della Accademia Peloritana dei Pericolanti Vol. 96, No. S1, A2 (2018)

29. Kittel, C. Am. J. Phys. 42, 726 (1974) Larmor and the Prehistory of the Lorentz Transformations https://doi.org/10.1119/1.1987825

30. Andersen, F. PhD Thesis, NMBU (2017) · https://nmbu.brage.unit.no/nmbu-xmlui/handle/11250/2500054

31. Myrstad, J. A. Borderology: Cross-disciplinary Insights from the Border Zone, p. 93, Springer (2019) DOI: 10.1007/978-3-319-99392-8_8 http://dx.doi.org/10.1007/978-3-319-99392-8_8

32. Consoli, M. Pluchino, Michelson-Morley Experiments: An Enigma For Physics And The History Of Science, World Scientific (2019)
https://www.worldscientific.com/worldscibooks/10.1142/11209

33. Consoli, M. Pluchino, A. The CMB, Preferred Reference System, and Dragging
of Light in the Earth Frame, Universe (2021)
https://doi.org/10.3390/universe7080311

34. Haug, E The Return of Absolute Simultaneity? A New Way of Synchronizing Clocks Across Reference Frames
http://vixra.org/abs/1605.0057

35. Haug, E A Motion Paradox from Einstein's Relativity of Simultaneity
http://vixra.org/abs/1711.0408

36. de Abreu, R. Comment on "A Motion Paradox from Einstein´s Relativity of Simultaneity" http://vixra.org/abs/1810.0452

37. Geloni, G. Kocharyan, V. Saldin, E. https://arxiv.org/abs/1601.07738

38. Geloni, G. Kocharyan, V. Saldin, E. https://arxiv.org/abs/1610.04139

39. Geloni, G. Kocharyan, V. Saldin, E. https://arxiv.org/abs/1704.01843

40. de Abreu, R. Guerra http://vixra.org/abs/1906.0312
Comment on "Misconceptions Regarding Conventional Coupling of Fields and Particles in XFEL Codes"

41. Mansouri, R. and Sexl, R. Gen. Relat. Gravit. 8, 497 (1977)

42. Zbigniew Oziewicz, Ternary relative velocity; astonishing conflict of the Lorentz group with relativity, Vladimir Gladyshev, Editor, Physical Interpretations of Relativity Theory, Moscow 2007, pages 292-303, ISBN 978-5-7038-3178-6 https://arxiv.org/abs/1104.0682

43. Gianfranco Spavieri *et al* 2018 *J. Phys. Commun.* **2** 085009

44. Spavieri, G. PAIJ vol.1, Issue 1 (2017)

45. Consoli, M. Pluchino, A. Eur. Phys. J. Plus 133:295 (2018)

46. Burde, G. I. Special Relativity with a Preferred Frame and the Relativity Principle
Journal of Modern Physics vol. 9, N° 8 (2018)
https://doi.org/10.4236/jmp.2018.98100

47. Ricou, M. On the speed of light Physics Essays, Vol. 30, 461-468 (2017)

48. de Abreu, R. Guerra, V. Comment on "On the speed of light" by Manuel Ricou http://vixra.org/abs/1906.0310

49. Wutke, A.
https://www.researchgate.net/publication/326672264_Absolute_Simultaneity_and_Rest_Consistent_with_Special_Relativity_Science_or_Philosophy

50. Chandru Iyer 2018 *J. Phys. Commun.* **2** 118001

51. Potvin, G. Ether Interpretation of General Relativity, RESEARCHERS.ONE (2018)
https://www.researchers.one/article/2018-12-7

52. Grøn, Ø. Eur. J. Phys. 27, 885 (2006)
https://iopscience.iop.org/article/10.1088/0143-0807/27/4/019

53. Iyer, C. https://arxiv.org/abs/0811.0785

54. Iyer, C. Eur. J. Phys. 29, 4 (2008)
https://iopscience.iop.org/article/10.1088/0143-0807/29/4/L01/meta

55. Iyer, C. Prabhu, G. Am. J. Phys. 78 (2) (2010)

56. Iyer, C. Prabhu, G. https://arxiv.org/abs/0710.1594

57. Moller, C. Proc. of The Royal Soc. A vol. 270, Issue 1342 (1960)
https://doi.org/10.1098/rspa.1962.0220

- Schwartz, H. M. Am. J. Phys. 39, 1269 (1971)
  https://doi.org/10.1119/1.1976621
  A New Method of Clock Synchronization without Light Signals

58. Sears, F. W. Am. J. Phys. 37, 668 (1969)
    https://doi.org/10.1119/1.1975747
    Simultaneity without synchronized clocks

59. Ramakrishnan, A. Journal of Math. Anal. and App. 249, 243 (2000)

60. Bricmont, J. https://arxiv.org/pdf/1703.00294.pdf
    History of Quantum Mechanics or the Comedy of Errors

61. Giovanelli, M.
    https://www.researchgate.net/publication/338680431_Lorentz_Contraction_vs_Einstein_Contraction_Reichenbach_and_the_Philosophical_Reception_of_Miller'sEther-Drift_Experiments

62. Mamone-Capria, M. Journal for Foundations and Applications of Physics, vol.5, N° 2, 163 (2018) [1704.02587] On the Incompatibility of Special Relativity and Quantum Mechanics (arxiv.org)

63. Spavieri, G. Gillies, G. T. Haug, E. G., Sanchez, A. (2019): Light propagation and local speed in the linear Sagnac effect, Journal of Modern Optics, http://doi: 10.1080/09500340.2019.1695005

64. Unnikrishnan, C. The Theories of Relativity and Bergson's Philosophy of Duration and Simultaneity During and After Einstein's 1922 Visit to Paris. *Preprints* **2020**,2020010273 http://doi: 10.20944/preprints202001.0273.v1

65. Spavieri, G. Guerra, V. de Abreu, R. Gillies, G. T Eur. Phys. J. D. 47, 457 (2008)

66. Spavieri, G. Gillies, G. Haug, E. G., Sanchez, A. Applied Physics Research Vol. 11, No. 4 (2019)

67. Spavieri, G. and Haug, E. G. Why the Sagnac effect favors absolute over relative simultaneity Physics Essays, Vol. 32, 331-337 (2019)

68. Spavieri, G. Gillies, G. T. Haug, E. G. Journal of Modern Optics, vol. 68, Issue 4 (2021)

69. Salmon, W., 1977. "The Philosophical Significance of the One-Way Speed of Light," *Noûs*, 11: 253–292

70. https://plato.stanford.edu/entries/spacetime-convensimul/

71. Perez, I. https://arxiv.org/abs/1102.4837 On the experimental determination of the one-way speed of light

72. Guerra, V. de Abreu, R. Comment on: "From classical ether-drift experiments: the narrow window for a preferred frame" [Phys. Lett. A 333 (2004) 355] Phys. Lett. A 361, Issue 6 (2007)

73. Lewis, G. F. Barnes, L. A. The One-Way Speed of Light and the Milne Universe Publication of the Astronomical Society of Australia, vol. 38, (2021) https://arxiv.org/abs/2012.12037

74. R.J. Buenker, GPS-Compatible Lorentz Transformation that Satisfies the Relativity Principle, Journal of Astrophysics and Aerospace Technology, 3: 115. DOI: 10.4172/2329-6542.1000115.

75. Netchitailo, V. S. https://vixra.org/abs/2012.0222

76. Pagano, A., Pagano, E.V. EPJ H 44, 321-330 (2019) https://doi.org/10.1140/epjh/e2019-90058-4

77. Greaves, E. D., Michel Rodrigues, A., Ruiz-Camacho, J. Am. J. Phys. 77, 894 (2009)

78. de Abreu, Guerra, V. Comment on "A one-way speed of light experiment" (2009) https://www.researchgate.net/publication/45886873

79. Leaf, B. Philosophy of Science, vol. 22, Number 1 (1955) https://doi.org/10.1086/287387

80. Spavieri, G. Quintero, J. Unnikrishnan, C. Gillies, G. Phys. Lett. A 376(s 6-7):795-797 (2012) DOI: 10.1016/j.physleta.2012.01.010

81. Scott Blair, G. Relativity and Indeterminacy. *Nature* **170,** 582 (1952). https://doi.org/10.1038/170582a0

82. Hines, C. Relativity and Indeterminacy. *Nature* **170,** 582 (1952). https://doi.org/10.1038/170582a0

83. Mayantz, L. The enigma of probability in physics https://inis.iaea.org/search/search.aspx?orig_q=RN:18074404

84. Mayantz, L Beyond the quantum paradox, Taylor & Francis (1994)

85. Medvedev, S. Yu. Progress in Physics, vol. 10, 151 (2014) http://www.ptep-online.com/2014/PP-38-04.PDF

86. Del Santo, F. Gisin, N. http://philsci-archive.pitt.edu/id/eprint/18601 (2021)

87. Fleming, A. Matveev, V. Matvejev , O. https://www.researchgate.net/publication/264851293_Self-field_Theory_and_General_Physical_Uncertainty_Relations

88. Hill, J. Cox, B. Proc. Royal Soc. A (2012) https://doi.org/10.1098/rspa.2012.0340

89. Leubner, C. Aufinger, K. Krumm, P. Eur. J. Phys. 13, 170 (1992)

90. Drągowski, M., Włodarczyk, M. The Doppler Effect and the Anisotropy of the Speed of Light. *Found Phys* **50,** 429–440 (2020). https://doi.org/10.1007/s10701-020-00337-5

91. Ronald Anderson, S.J., Stedman, G.E. Distance, and the conventionality of simultaneity in special relativity. *Found Phys Lett* **5,** 199–220 (1992). https://doi.org/10.1007/BF00692800

92. de Abreu, R. Simultaneity and Synchronization by Rods as a Simple Geometry Problem https://vixra.org/abs/2103.0196

93. Dias Ferreira, L. Criticism to the Twin's Paradox, Colégio Valsassina, Lisbon, Portugal Universal Journal of Physics and Application Vol. 15(1), pp. 1 - 7 DOI: 10.13189/ujpa.2021.150101 Reprint (PDF) (412Kb)

94. de Abreu, R. Comment on "Criticism to the Twin's Paradox" by Luís Dias Ferreira https://vixra.org/abs/2107.0077

95. Borah, B. K. Schwarzschild-like solution for the gravitational field of an isolated particle on the basis of 7- dimensional metric, International Journal of Scientific and Research, vol. 3, Issue 10, October 2013

96. Borah, B. K. An Approach to New Concept of Time on the Basis of Four Fundamental Forces of Nature, International Journal of Scientific and Research Publications, vol. 3, Issue 6, June 2013

97. Borah, B. K. Unification of Four Fundamental Forces of Nature Developing 7- Dimensional Metric on The Basis of New Concept of Time https://www.worldwidejournals.com/international-journal-of-scientific-research- (IJSR)/article/unification-of-four-fundamental-forces-of-nature-developing-7andndash-dimensional-metric-on-the-basis-of-new-concept-of-time/NjU0OQ==/?is=1&b1=33&k=9

98. Homem, G. https://arxiv.org/abs/physics/0212050

99. de Abreu, R. The Energy-Entropy Principle https://arxiv.org/abs/physics/0207022

100. de Abreu, R. Guerra, V. The concepts of work and heat and the first and second laws of thermodynamics https://arxiv.org/abs/1203.2294

101. de Abreu, R. Guerra, V. Introducing thermodynamics through energy and entropy Am. J. Phys. 2012 https://aapt.scitation.org/doi/10.1119/1.3698160

102. Caratheodory, C. https://greatestgreeks.wordpress.com/2016/12/12/constantine-caratheodory/

103.Caratheodory, C. https://www.researchgate.net/publication/312057731_On_Caratheodory's_approach_to_relativity_and_its_relation_to_hyperbolic_geometry

104.de Abreu, R. The Concept of Mass as a Quantity Derived from Motion. https://vixra.org/abs/1505.0094

105.Mohazzabi, P. and Luo, Q. (2021) Has the Twin Paradox Really Been Resolved?. *Journal of Applied Mathematics and Physics*, **9**, 2187-2192. doi: 10.4236/jamp.2021.99138.

106.de Abreu, R. Comment on "Has the Twin Paradox Really Been Resolved?", viXra.org e-Print archive, viXra:2209.0045

107.de Abreu, R. Simultaneity and Synchronization, the Preferred Frame and the Principle of Relativity, viXra.org e-Print archive, viXra:2204.0060

108.Reference:https://www.physicsforums.com/threads/potential-energy-formula-_in-special-relativty.991687/

109.Reichenberger, Andrea (2018) The Clock Paradox: Luise Lange's Discussion REITCP-3 (philarchive.org)

110.Iyer, C. (2022) Importance of Synchronization in the observation of event coordinate DOI:10.36227/techrxiv.21657026

111.de Abreu, R. (2023) Proper Times, Time Dilation, Lorentz-FitzGerald Contraction and Distance, Time Ageing, Time Dilation-like and the Twin Paradox Conundrum Proper Times, Time Dilation, Lorentz-FitzGerald Contraction and Distance, Time Ageing, Time Dilation-like and the Twin Paradox Conundrum, viXra.org e-Print archive, viXra:2301.0029

112.de Abreu, R. (2023) An interesting case of Twins Paradox – Twins Approaching Each Other https://vixra.org/abs/2308.0109

113.de Abreu, R. (2023) The Time Dilation Conundrum and the Ageing of the Twins https://rxiv.org/abs/2301.0086

114.de Abreu, R. (2023) Simultaneity and Synchronization and Einstein´s Relative Simultaneity https://vixra.org/abs/2303.0053

115.Choi, Yang-Ho (2022) Multiple velocity composition in the standard synchronization https://ui.adsabs.harvard.edu/abs/2022OPhy...20...17C/abstract

116.Lambare, Justo On The Sagnac Effect and the Consistency of Relativity Theory https://doi.org/10.32388/UL1ZWZ

117.de Abreu, R. (2023) The Resolution of the Twin Paradox with Three Frames of Reference - A Mathematical and Physical Report https://vixra.org/abs/2307.0052

118.R.M. Santilli, Lie-isotopic Lifting of Special Relativity for extended Deformable Particles, , \textit{ Lettere Nuovo Cimento} {\bf 37}, 545-555 (1983),\\ www.santilli-foundation.org/docs/Santilli-50.pdf

119.R. M. Santilli, "Compatibility of Arbitrary Speeds with Special Relativity Axioms for Interior Dynamical Problems," American Journal of Modern Physics, {\bf 5}, 143 (2016),\\ http://www.santilli-foundation.org/docs/ArbitrarySpeeds.pdf

120.H. Ahmar, G. Amato, J. V. Kadeisvili, J. Manuel, G. West, and O. Zogorodnia, "Additional experimental confirmations of Santilli's IsoRedShift and the consequential lack of expansion of the universe, "Journal of Computational Methods in Sciences and Engineering,{\bf 13}, 321 (2013),\\ http://www.santilli-foundation.org/docs/IRS-confirmations-212.pdf

**HADRONIC JOURNAL 47**, 295 - 311 (2024)
DOI 10.29083/HJ.47.03.2024/SC295



# THEORETICAL FOUNDATIONS OF THE PARTICLE SPECTRUM

**Simon Davis**
Research Foundation of Southern California
8861 Villa La Jolla Drive #13595
La Jolla, CA 92307
sbdavis@resfdnsca.org

Received April 26, 2024
Revised August 19, 2024

## Abstract

A relation between the radii and masses of the quarks and leptons is established for each fermion generation. Kinematical calculations provide a proof of the essential stability of the proton at rest within the standard model together with conditions for the reaction $p \dashrightarrow uuu + e^- + \bar{\nu}_e$ with a $uuu$ composite state as a byproduct. The Koide relation reduces the scaling to a single number, and a theoretical explanation is given in terms of graded symmetries. The values of the masses of the each of the quarks are derived through nonperturbative infinite-genus effects.

**PACS: 14.65.Bt, 14.65.Dw, 14.65.Fy, 14.65.Ha, 21.30.Fe, 25.40.Qa**

**Keywords:** *quarks, nonperturbative effects, masses*

## 1. Introduction

There have been four major results in the production of the masses in the particle spectrum. The integer multiple rule is phenomenological law stating that many of the resonances have masses that are integer multiples of the pion [10] It can be phrased in terms of pion bubbles in the self-enery diagrams. The linear Regge trajectories in the graph of the angular momentum versus the squared mass [12] eventually led to the discovery of string theory, It may be conjectured that the linearity in both relations may be related, with the energy of the pions being converted into increases in the angular momentum and squared mass. The systematic formalism developed for the theory of the strong interactions introduced an SU(3) symmetry group with the hadron spectroscopy based on the quark model [6]. Finally, an empirical relation between the masses of the leptons in different generations [7] had been found, and it reflected an underlying discrete component of the automorphism group of the spinor space of the standard model, $S_3$ [5].

Therefore, the remaining problems in connection with the particle spectrum are the ratios of the quark and lepton masses, the origin of the scaling factor between the generations of leptons, the interpretation of the neutrino and its ratio of its mass to that of the lepton, and the derivation of the quark masses. Each of these topics will be considered in this investigation, and the solutions are described within a nonperturbative model.

The theoretical problem of the $\eta'$ mass can be solved only partially either through a quadrature formula consisting of the singlet and octet masses of the pseudoscalar multiplet, a pseudovector model of bound states of quarks and anti-quarks or the introduction of a Goldstone boson. None of these techniques yields the exact value of the $\eta'$ mass equal to 957.78 $MeV/c^2$. The first two configurations have a mass of approximately 831.08 $MeV/c^2$. The remainder cannot be predicted from the multiplet structure or perturbation theory, and therefore, it may be attributed to nonperturbative effects. Given the equality of the $\eta'$ wavefunction with $\frac{1}{\sqrt{6}}(u\bar{u} + d\bar{d} - 2s\bar{s})$. When the nonperturbative effects are identified with the ends of infinite-genus surfaces, its contribution is sufficient to generate the difference between the $\eta'$ mass and the initial estimate. It will be established further that the boundary components of the geometrical model of the $u$ and $d$ quarks is sufficient to produce the masses in the particle spectrum. Since the $s$ quark will be contructed from the chiral $u$ quark, the electron and these boundary components, the $s$ quark then does not have an effect on the nonperturbative component of the $\eta'$ mass. Then, it may be established that the $u$ and $u$ quarks have an infinite-genus components with masses of 61.85 $MeV/c^2$ and 64.85 $MeV/c^2$. The inverse proportionality of the self-energy of a charged particle with no composite structure and its radius yields a formula for the radii of the quarks. The derived value for the

radii of the chiral up and down quarks is demonstrated in §2 to compatible with. a conventional nearly point-particle model and the distance between quarks in the nucleon required for mass difference between the proton and the $\Delta^{++}$ baryon.

The mass scalings of the leptons in the three fermion generations depends their string representation together with the Koide relation. A theoretical explanation of the scaling coefficients is described in §3 based on massive representations of a superalgebra, and a generalization of this supersymmetry to a $\mathbb{Z}_4$ grading. Whereas the radii of the masses of the charged muon and $\tau$ lepton may be derived from $m_e$, from the self energy and the inverse proportionality with respect to the mass, the description of the neutrinos neutrinos in terms of linear extent of the string requires a proportionality between the mass of the neutrino and the radius. Then it follows that the size of the neutrino is considerably less, which is consistent with its almost pointlike structure.

The second and third generation quarks are much heavier and characterized by new quantum numbers such as strangeness. The entire hadronic spectrum may be represented by multiplets in the three dimensions of isospin, hypercharge and strangeness. Therefore, it is not unexpected that there exists a model of these quarks and baryons constructed from the first generation quarks, anti-quarks and the nonperturbative boundary components. The group theoretical transformations and the masses will place conditions on the complex of the $u$, $\bar{u}$, $d$ and $\bar{d}$ quarks. It is proven in §4 that the masses of $s$, $c$, $b$ and $t$ quarks is equal to a set of sums of the masses of the chiral $u$ and $d$ quarks and the infinite-genus ends. The number of first generation quarks and anti-quarks increases with the mass, and the radii of the heavier quarks becomes larger. The hadronic spectrum is established then through the same formula in terms of the quarks.

This phenomenological model requires a proof of the mass of the chiral quarks and the occurrence of the ends of surfaces of infinite genus in the string description of strongly interacting particles. One method for deriving the chiral mass would consists of developing the perturbative expansion of low energy effective theories of the hadronic interactions. The nonpertubative effect may be identified with the infinite-genus term in a generalization of the series expansion in string theory of a correlators of products of field strengths and the duals. The mass would have to be related to the potential energy of boundaries of these surfaces.

## 2. Radii of the Quarks in the First Fermion Generation and Proton Stability

Quarks have charge, isospin and colour, and therefore, the dynamics is governed by the electromagnetic, weak and strong nuclear forces at atomic scales. The contribution of the charge to the mass is known to be

$$(1) \qquad m_{elec} = \frac{e^2}{6\pi\epsilon_0 r c^2}$$
$$E_{elec}^{self-energy} = m_{elec}c^2 = \frac{3}{4}m_{tot}c^2$$

when there are only gravitational and electromagnetic interactions. This formula yields an inverse proportionality between the ratios of the masses and the ratios of the radii of particles acting only as a result of these two forces. Suppose, in the first instance, that this condition is valid for the electron and the up quark. An analysis of the mass of the $\eta'$ meson demonstrates that the perturbative mass, even with a vector component and a summation over quark annihilation diagrams, equals 831.08 $MeV/c^2$. Since the experimental value is 957.78 $MeV/c^2$, the remainder may be attributed to nonperturbative effects including an infinite-genus component that equals 126.6 $MeV/c^2$. This difference can be split into the the sum of a $u$ quark contribution of 61.85 $MeV/c^2$ and a $d$ quark contribution of 64.85 $MeV/c^2$, which can be deduced from the $\frac{1}{\sqrt{2}}(u\bar{u} + d\bar{d})$ sector of the boundary component, with mass $\frac{1}{2}(m_{u\bar{u}\infty} + m_{d\bar{d}\infty}) = \frac{1}{2}(2m_{u\infty} + 2m_{d\infty}) = m_{u\infty} + m_{d\infty}$, Both quarks would have the same mass from chiral perturbation theory, $m_{uc} = m_{dc} = 243.15 MeV/c^2$. Since the formula for the electromagnetic part of the mass requires a compact spherical model of the particle, it is this mass that will be substituted Then

$$(2) \qquad \frac{m_e}{m_{uc}} = \frac{e^2}{\left(\frac{2}{3}e\right)^2}\frac{r_{uc}^{(0)}}{r_e}$$

where $m_{uc}$ is the mass of the quark derived from breaking of chiral invariance, such that the nonperturative contribution equals nearly half of the difference between the perturbative mass of the $\eta'$ meson and its experimental value [4], $r_{uc}^{(0)}$ is the leading-order estimate of the quark radius. Given that the radius of the electron is $3 \times 10^{-16}m$,

$$(3) \qquad r_{qc}^{(0)} = \frac{4}{9}\frac{0.511\ MeV/c^2}{243.15\ MeV/c^2} \times 3 \times 10^{-16}m = 2.8021458298 \times 10^{-19}m,$$

which is closer to the experimental value than $2.1979 \times 10^{-19}m$ predicted for a quark mass of 310' $MeV/c^2$. There is a correction to this estimate from the

linear term in the strong interaction potential $V(r) = 1GeV/fm \times r$. Over the diameter of the quark, the accumulated potential energy is

$$(4) \qquad 1\ GeV/fm \times 2(2.8021458298 \times 10^{-19} m) = 0.56042916596\ MeV$$

With the inclusion of this energy, the mass must equal that given by the chiral gap. The value required in the Lorentz formula must be shifted to $242.58957087404\ MeV/c^2$. Substituting this value into the formula for $r_{uc}$ gives

$$(5) \qquad r_{uc} = 2.808563687 \times 10^{-19} m.$$

The effect of the weak interaction is negligible and this value for the radius can be compared with experiment. The radius of the electron is indicative of a prototype of the proton consisting of an electron and two positrons, which have barely enough space inside a nucleon. Then, the modern version of the proton formed by replacing these constituents by two up quarks and one down quark, which may be achieved by transferring a charge of $\frac{1}{3}e$ from each positron to the electron and placing it in an SU(3) gauge field to transform these particles to quarks with fractional charges. By contrast, the neutron cannot be formed by three charges of magnitude $e$. Instead, a fourth electron would be necessary to make the composite neutral and must combine with one of the up quarks in inverse beta decay $\bar{\nu}_e + e^- + p \rightarrow n$ and $\bar{\nu}_e + e^- + u \rightarrow d$ and, after the radiation of the neutron, the standard composition of the neutron in terms of an up quark and two down quarks is present. Beta decay $n \rightarrow p + e^- + \bar{\nu}_e$ causes the neutron to have lifetime of approximately 18 minutes.

The proton is known to be essentially stable at rest with a lifetime longer than $10^{32}$ years [11]. Grand unified theories have been developed with a superselection rule to prevent reactions with the mediation of leptoquarks or scalar fields, with the potential $p \rightarrow e^+\pi^0$ and other decays [3] allowed instead. The decay of the down quark in the proton, generating $uud \rightarrow uuu + e^- + \bar{\nu}_e$, nevertheless, may be considered. Suppose that the distance between the each pair of quarks is $d_{qq}$. Since

$$(6) \qquad E_{elec}(uud) = \frac{4}{9}\frac{e^2}{4\pi\epsilon_0 d_{qq}} - \frac{2}{9}\frac{e^2}{4\pi\epsilon_0 d_{qq}} - \frac{2}{9}\frac{e^2}{4\pi\epsilon_0 d_{qq}} = 0,$$

the location of equidistant quarks in the proton does not effect the binding energy. However, now let the $d$ quark decay to a $u$ quark, electron and an anti-eletrcon neutrino at the fixed location in the baryon. A reaction $d \rightarrow u + W^- \rightarrow u + e^- + \bar{\nu}_e$, together with $p \rightarrow (uuu) + e^- + \bar{\nu}_e$ may be considered with $m_{(uuu)\approx m_p}$ initially. By energy and momentum conservation

$$(7) \qquad \begin{aligned} E_d &= E_u + E_{W^-} \\ \vec{p}_d &= \vec{p}_u + \vec{p}_{W^-} \end{aligned}$$

A $d$ quark can decay into an $u$ quark and a $W^-$ boson with a non-zero scattering angle. The momentum transfer may be sufficient to deflect the entire $uuu$ state simultaneously in the same direction. Otherwise, this composite state would disintegrate with the third $u$ quark moving away from the other two quarks. In the latter circumstatnce, the alignment of the momentum vectors would require either the $W^-$ boson to move in the same or the opposite direction as the $u$ quark. The conservation laws then become either

(8)
$$\gamma_d m_d c^2 = \gamma_u m_u c^2 + \gamma_{W^-} m_{W^-} c^2$$
$$\gamma_d m_d v_d = \gamma_u m_u v_u + \gamma_{W^-} m_{W^-} v_{W^-} = 0$$

and

(9)
$$\frac{\gamma_{W^-}(v_d - v_{W^-})}{\gamma_u(v_u - v_d)} = \frac{m_u}{m_{W^-}}$$

when the $W^-$ boson moves in the same direction as the $u$ quark or

(10)
$$\gamma_d m_d c^2 = \gamma_u m_u c^2 + \gamma_{W^-} m_{W^-} c^2$$
$$\gamma_d m_d v_d = \gamma_u m_u v_u - \gamma_{W^-} m_{W^-} v_{W^-}$$

and

(11)
$$\frac{\gamma_{W^-}(v_d + v_{W^-})}{\gamma_u(v_u - v_d)} \frac{m_u}{m_{W^-}}$$

if the $W^-$ boson moves in the opposite direction to the $u$ quarks. Under both conditions, there exists a range of velocities $v_d$, $v_u \gg v_{W^-}$ and $v_d < v_u < \left[\left(1 - \frac{m_u^2}{m_d^2}\right)c^2 + \frac{m_u^2}{m_d^2}v_d^2\right]^{\frac{1}{2}}$ which include solutions to the above relations.

Therefore, even under the constraint of the alignment of momentum vectors in the reaction $p \rightarrow (uuu) + W^- \rightarrow (uuu) + e^- + \bar{\nu}^e$, the kinematics allow the transformation to the new composite state. The influx of a positive electostatic potential energy generates an increase in the mass of the $(uuu)$ state.

(12)
$$\frac{2.0395145184 \times 10^{-9} eVm}{d_{dd}}.$$

Given that $m_{\Delta^{++}} = 1272\ MeV/c^2$, equality of the shift in the electrostatic potential energy with the difference in the rest mass energies

(13)
$$m_{\Delta^{++}}c^2 - m_p c^2 = 333.5 MeV$$

requires

(14)
$$E_{elec}(uuu) = \frac{4}{9}\frac{e^2}{4\pi\epsilon_0 d_{qq}} \times 3 = \frac{4}{3}\frac{e^2}{4\pi\epsilon d_{qq}} = \frac{2.0395145184 \times 10^{-9} eVm}{d_{dd}}.$$

and

(15)
$$d_{qq} = 6.115485 \times 10^{-18} m.$$

If the only force at this distance is electostatic in origin, ther would be nothing preventing the $u$ quarks moving radially outwards and the composite state disintegrating. Consequently, the onset of the strong interactions is necessary to restore the constitution of the eventual $(uuu)$ state, which then as a mass increased by 333.5‘$MeV/c^2$. Equilibrium would be reached at a distance greater than or equal to $6.115485 \times 10^{-18} m$.

The kinematical conditions also may be given when the byproduct has a greater rest mass. The $\Delta^{++}$ baryon is both heavier than the proton and has angular momentum $\frac{3}{2}$. Given the decay $d \to u + W^- \to u + e^- + \bar{\nu}_e$, the reaction $p \to \Delta^{++} + W^-$ may be considered at non-zero momentum since charge, isospin and angular momentum are conserved. Again, the momentum vector of $\Delta^{++}$ wil be selected to be aligned along the direction of the motion of the proton, and similarly, $\vec{p}_{W^-} \parallel \vec{p}$. By the conservation of energy and momentum,

(16)
$$E_p = E_{\Delta^{++}} + E_{W^-}$$
$$\vec{p}_p = \vec{p}_{\Delta^{++}} + \vec{p}_{W^-}.$$

Suppose that $\vec{p}_{\Delta^{++}}$ and $\vec{p}_{W^-}$ are pointing in the same direction. Then

(17)
$$|\vec{p}_p| = |\vec{p}_{\Delta^{++}}| + |\vec{p}_{W^-}|$$

From the two equations

(18)
$$\gamma_p m_p c^2 = \gamma_{\Delta^{++}} m_{\Delta^{++}} c^2 + \gamma_{W^-} m_{W^-} c^2$$
$$\gamma_p m_p v_p = \gamma_{\Delta^{++}} m_{\Delta^{++}} v_{\Delta^{++}} + \gamma_{W^-} m_{W^-} v_{W^-},$$

(19)
$$\gamma_{\Delta^{++}} m_{\Delta^{++}} (v_p - v_{\Delta^{++}}) + \gamma_{W^-} m_{W^-} (v_p - v_{W^-}) = 0.$$

Since $m_p < m_{\Delta^{++}}$, $m_{W^-}$, $v_p > v_{\Delta^{++}}$, $v_{W^-}$. The above relation produces a contradiction because $v_p - v_{\Delta^{++}} > 0$ and $v_p v_{W^-} > 0$.

Now suppose that $\vec{p}_{\Delta^{++}}$ and $\vec{p}_{W^-}$ point in opposite directions. It follows that

(20)
$$|\vec{p}_p| = |\vec{p}_{\Delta^{++}}| - |\vec{p}_{W^-}|.$$

and

(21)
$$\gamma_p m_p v_p = \gamma_{\Delta^{++}} m_{\Delta^{++}} v_{\Delta^{++}} - \gamma_{W^-} m_{W^-} v_{W^-}.$$

Combining this equation with the energy conservation relation gives

(22)
$$\gamma_{\Delta^{++}} m_{\Delta^{++}} (v_p - v_{\Delta^{++}}) + \gamma_{W^-} m_{W^-} (v_p + v_{W^-}) = 0.$$

A contradiction results if $v_p - v_{\Delta^{++}} > 0$. Let $v_{\Delta^{++}} > v_p$. Then $\gamma_{\Delta^{++}} > \gamma_p$ and

(23)
$$\gamma_{\Delta^{++}} m_{\Delta^{++}} + \gamma_{W^-} m_{W^-} > \gamma_p m_p,$$

which contradicts the conservation of energy. Therefore, the reaction $p \to \Delta^{++} + W^-$ cannot occur when the momentum vectors are aligned. These contradictions can be circumvented by decreasing the components of the momentum along the direction of the $d$ quark motion and allowing the projection along of the $u$ quark and $W$ boson momenta along the perpendicular to cancel.

## 3. Scaling of the Masses of the Leptons

It is evident from beta decay that the down quark must contain an electron and the radius would be much larger than that of the up quark and approximately equal to $3 \times 10^{-16}m$. The difference in the masses of the up and down quarks may be attributed to nonperturbative effects [4]. The electron and the anti-neutrino then can be traced to characteristics of infinite-genus surfaces. Since the anti-neutrino is customarily regarded as a point particle, the identification with a point source of non-zero harmonic measure on the ideal boundary is consistent.

The relative size of the electron and neutrino may be described. Point sources on the ideal boundary represent ends of the Riemann surface, and with a boundary of the end being diffeomorphic to a circle, the electron and neutrino shall be viewed as circular strings. A spherical model of these particles would be generated from a rapid revolution of the string about its axis. With a uniform linear density, the greater extent yields the larger mass. By contrast with the Lorentz formula, the mass increases with the size of the circular arc.

The proportionality of the ratios of radii with the ratios of the masses yields

$$r_{\nu_e} = \frac{m_{\nu_e}}{m_e} r_e. \tag{24}$$

The electron neutrino mass is measured to be $0.007614\ eV$ and

$$\frac{m_e}{m_{\nu_e}} = 6.71132 \times 10^7. \tag{25}$$

It follows that

$$r_{\nu_e} = \frac{3 \times 10^{-16}m}{6.71132 \times 10^7} = 4.47 \times 10^{-24}m. \tag{26}$$

There is a scaling of the masses of the leptons from the first to second generations and second to third generations. Let $\sqrt{\frac{m_\mu}{m_e}} = a$ and $\sqrt{\frac{m_\tau}{m_e}} = b$. By the Koide relation [7],

$$1 + a^2 + b^2 = \frac{2}{3}(1 + a + b)^2. \tag{27}$$

A rearrangement of terms gives the quadratic equation

$$b^2 - 4(1+a)b + (1 - 4a + a^2) = 0. \tag{28}$$

Of the two solutions to this equation,

$$2(1+a) \pm \sqrt{3}(a+2), \tag{29}$$

the lesser root is excluded because $m_\tau > m_\mu$. The larger root is

$$b = (2+\sqrt{3})a + 2(1+\sqrt{3}). \tag{30}$$

The values $a \approx 14.5$, $b \approx 59.578$ generate the experimental charged lepton mass ratios.

A theoretical basis for the mass scales of the leptons in the fermion generations requires an explanation of the relation between the supercharges and the number 14.5. The example of a massive representation of N = 2 Poincare superalgebra

$$\begin{aligned} \{Q^a_\alpha, Q_{\dot{\alpha}b}\} &= 2\sigma^\mu{}_{\alpha\dot{\alpha}} P_\mu \delta^a{}_b \\ \{Q^a_\alpha, Q^b_\beta\} &= 2^{\frac{3}{2}} \epsilon_{\alpha\beta}\epsilon^{ab} Z \\ \{Q^\dagger_{\dot{\alpha}a}, Q^\dagger_{\dot{\beta}b}\} &= 2^{\frac{3}{2}} \epsilon_{\dot{\alpha}\dot{\beta}}\epsilon_{ab} Z \end{aligned} \tag{31}$$

furnishes the anticommutators

$$\begin{aligned} \{a_\alpha, a^\dagger_\beta\} &= \delta_{\alpha\beta}(M + \sqrt{2}Z) \\ \{b_\alpha, b^\dagger_\beta\} &= \delta_{\alpha\beta}(M - \sqrt{2}Z), \end{aligned} \tag{32}$$

where

$$\begin{aligned} a_\alpha &= \frac{1}{2}\left(Q^1_\alpha + \epsilon_{\alpha\beta}(Q^2_\beta)^\dagger\right) \\ b_\alpha &= \frac{1}{2}\left(Q^1_\alpha - \epsilon_{\alpha\beta}(Q^2_\beta)^\dagger\right). \end{aligned} \tag{33}$$

The central charge then can decrease the trace of the anticommutators of supercharges. For example, when the number of spinor indices is increased from 2 to 4 in an N = 4 superalgebra, tracing of a set of anticommutators can give a factor of $16(M - 3\sqrt{2}Z)$. Setting the parameter $Z$ of internal rotations commuting with the supersymmetry generators equal to $\frac{1}{48}M$, the factor becomes $(16 - \sqrt{2})M$.

The ratio $\sqrt{\frac{m_\mu}{m_e}}$ can be set equal to $16 - \sqrt{2}$ only if the supercharges rather than the masses are scaled by this factor. Therefore, a $\mathbb{Z}_4$ graded symmetry

that squares to a supersymmetry is necessary. One of the anticommutation relations of the $\mathbb{Z}_4$ graded algebra would have the form

$$\{Q_{\frac{1}{2}}{}^{a}{}_{\tilde{\alpha}\tilde{\gamma}}, Q_{\frac{1}{2}}^{b\,\dagger}{}_{\tilde{\gamma}\tilde{\beta}}\} = (\gamma^{\mu})_{\tilde{\alpha}\tilde{\gamma}}(Q_{\mu})_{\tilde{\gamma}\tilde{\beta}}\delta^{a}{}_{b}, \tag{34}$$

where two indices $(\alpha\tilde{\alpha})$ correspond to a single four-component index. Since $\tilde{\alpha}\tilde{\gamma}$ can cover only four indices, the elements of $(\gamma^{\mu})_{\tilde{\alpha}\tilde{\gamma}}$ belong to the diagonal. Then $(\gamma^{\mu})_{\tilde{\alpha}\tilde{\gamma}}(Q_{\mu})_{\tilde{\gamma}\tilde{\beta}}$ can be written as $(\gamma^{\mu})_{\alpha\alpha}(Q_{\mu})_{\beta}\delta^{\alpha\beta}$, where repeated indices are summed and $Q_0$ is set equal to the supercharge $Q$. The scales of the supercharges may be arranged to increase by $16-\sqrt{2}$ from the first to the second generation, while there would be an overall scaling of $(16-\sqrt{2})^2$ for the masses.

The ratio of the lifetimes of the muon and $\tau$ lepton is known to be a constant multiple of the ratio of the fifth powers of the masses. By contrast, the Lorentz formula requires the ratio of the radii to be proportional to the inverse of the ratio of the masses. It follows that

$$\begin{aligned} r_{\mu} &= \frac{m_e}{m_{\mu}} r_e = 1.4509 \times 10^{-18} m \\ r_{\tau} &= \frac{m_e}{m_{\tau}} r_e = 8.628 \times 10^{-20} m \end{aligned} \tag{35}$$

Corrections resulting from the weak interactions may be deduced from the width of the resonances $\Gamma = \frac{G_F^2 E_0^5}{60\pi^3}$. Setting $E_0$ equal to $m_{\mu}c^2 = 105.658\ MeV$ or $m_{\tau}c^2 = 1777\ MeV$, the shifts in the mass are found to be

$$\begin{aligned} \Delta m_{\mu} &= 10^{-14} MeV/c^2 \\ \Delta m_{\tau} &= 1.61 \times 10^{-8} MeV/c^2 \end{aligned} \tag{36}$$

and the effect on the masses and radii is negligible.

There have been various figures given for the masses of the neutrinos for each flavour and the mass eigenstates [8]. A comparison with the Koide relation is compatible with a normal hierarchy. The neutrino mass matrix [1] requires a mixing angle [2] larger than the Cabibbo angle. Generally, the masses derived from the mass matrix and the eigenstates yield an inverted hierarchy with values of $m_{\nu_{\mu}}$ and $m_{\nu_{\tau}}$ which are generally not sufficiently large [9]

## 4. Quarks in the Second and Third Fermion Generations

The mass of the strange quark exceeds that of two $\bar{u}$ anti-quarks in chiral perturbation theory by less than 1 $MeV/c^2$, when the value $m_{\bar{u}c} = 243.15\ MeV/c^2$ is used. Combining two $\bar{u}$ anti-quarks with a positron produces a composite

system of charge $-\frac{1}{3}e$ with mass

(37) $$2m_{\bar{u}c} + m_{e^+} = 486.811\ MeV^2.$$

Beginning with a $dd$ state, a charge of $\frac{1}{3}e$ would have to be added without introducing a $\bar{d}$ anti-quark. Instead, contact with a $\bar{d}$ anti-quark must result in the transfer of the charge $\frac{1}{3}e$ and a recoil of the anti-quark for this configuration to model a particle of charge $-\frac{1}{3}e$ and mass nearly equal to $m_s$.

Both composite systems, however, do not satisfy a mandatory condition on the representation theory of $\mathrm{SU}(3)_c$. Quarks transform under the **3** representation and anti-quarks belong to the $\overline{\mathbf{3}}$ representation of SU(3). Since the positron is an SU(3) singlet state, it is not tenable for $\bar{u}\bar{u}e^+$ to transform under this group identically to the strange quark $s$. Similarly, the $dd^{\left(\frac{1}{3}\right)}$ state transforms under the $\mathbf{3} \times \mathbf{3} = \mathbf{8} \oplus \mathbf{1}$ representation, which is also different.

An alternative configuration consistent with representation theory of $SU(3)$ would be the a $ue^-$ state together with four-infinite genus components with a mass

(38)
$$\begin{aligned} m_{uc} + m_{e^-} + 4m_{u\infty} &= 243.15\ MeV/c^2 + 0.511\ MeV/c^2 + 4(61.85\ MeV/c^2) \\ &= 491.061\ MeV/c^2. \end{aligned}$$

The sum of the radii of the chiral up quark and the boundary of the infinite-genus components equals

(39) $$r_{uc} + 4r_{u\infty} = r_{uc} + 4\frac{61.85}{0.511}r_{e^-} = 1.45244618676 \times 10^{-13}m$$

which is much too large for the strange quark to fit inside a baryon from the decuplet that includes the $\Omega^-$. Instead, the boundary of the infinite-genus surface must be wrapped around the fundamental constituent up quark. Its final radius is measured to be $5.95268 \times 10^{-19}m$. Setting

(40) $$2\pi \sum_{n=0}^{N} (2.808563687 \times 10^{-19}m + n\Delta x) = 2\pi(1.45244618676 \times 10^{-13}m),$$

it follows that

(41)
$$\begin{aligned} N &= 3.31562 \times 10^5 \\ \Delta x &= 9.4827406 \times 10^{-25}m. \end{aligned}$$

The electrostatic potential energy between the $u$ quark and the electron

(42) $$V_{ue^-}^{elec} = -\frac{2}{3}\frac{e^2}{4\pi\epsilon_0 d_{ue^-}} = -\frac{1.0705775916 \times 10^{-9}eVm}{d_{ue^-}}.$$

must be included in the computation. When this electroatic energy is discharged into the bound state during the process of fusion at a distance of

$d_{ue^-} = 3\times 10^{-16}m$, $V_{ue^-}^{elec} = 3.598591972\ MeV$ yielding $m_s = 491.061\ MeV/c^2 - 3.598591972\ MeV/c^2 = 487.462408028\ MeV/c^2$ which belongs to the range of experimental error.

The charmed quark may be described as a complex consisting of $dd$, $u$ and $\bar{d}\bar{d}$, with one $u$, two $d$ and two $\bar{d}$ infinite-genus components. Then the mass would be

$$(43)\qquad \begin{aligned} m_c &= m_{uc} + 2m_{dc} + 2m_{\bar{d}c} + m_{u\infty} + 2m_{d\infty} + 2m_{\bar{d}\infty} \\ &= 5(243.15\ MeV/c^2) + 4(64.85\ MeV/c^2) + 61.85\ MeV/c^2 \\ &= 1543\ MeV/c^2 \end{aligned}$$

which is consistent with the mass of the $J/\psi$ particle. The electrostatic potential energy of the complex describing the $c$ quarks is $V_{elec}^{c} = 2V_{elec}^{ud} + 2V_{elec}^{u\bar{d}} + V_{elec}^{dd} + V_{elec}^{\bar{d}\bar{d}} + 2V_{elec}^{d\bar{d}hor.} + V_{elec}^{d\bar{d}diag.}$. When the $u$ quark is placed centrally in a square with $d$ and $\bar{d}$ quarks at the corners, $V_{elec}^{ud} + V_{elec}^{u\bar{d}} = 0$ and $V_{elec}^{dd} + V_{elec}^{\bar{d}\bar{d}} + 2V_{d\bar{d}hor.} = 0$. The remainder is

$$(44)\qquad 2V_{elec}^{d\bar{d}diag.} = -\frac{2}{9}\frac{e^2}{4\pi\epsilon_0 d_{d\bar{d}diag.}} = -\frac{3.598591972\times 10^{-10}eVm}{d_{d\bar{d}diag.}}.$$

When the distance between the $d$ and $\bar{d}$ quarks across the diagonal of the square array is $8.3688185395\times 10^{-18}m$, the mass of the charmed quark is reduced to $1.5\ GeV/c^2$.

The quarks in the third fermion generation require many more components. The $\Upsilon$ resonance at an energy of $9.46\ GeV$ is a $1^-$ $b\bar{b}$ state if $m_b \approx 4.73\ GeV/c^2$. The following configuration

$$\begin{array}{ccccccccccc} u & & \bar{u} & u & & \bar{u} & u & & \bar{u} \\ & d & & & \bar{d} & & & d & \\ u & & \bar{u} & u & & \bar{u} & u & & \bar{u} \end{array}$$

has a mass equal to

$$(45)\qquad \begin{aligned} &6m_{uc} + 6m_{\bar{u}c} + 2m_{dc} + m_{\bar{d}c} + 6m_{u\infty} + 6m_{\bar{u}\infty} + 2m_{d\infty} + m_{\bar{d}\infty} \\ &\quad = 4584\ MeV/c^2 \end{aligned}$$

The difference from the experimental value of the $b$ quark mass can be explained through the addition of infinite-genus components neighbouring quarks and anti-quarks and a reduction as a result of the electrostatic potential energy. If the $d$ and $\bar{d}$ quarks are placed symmetrically between the $uu$ and $\bar{u}\bar{u}$ pairs, the electrostatic energies involving the $u$ and $\bar{u}$ quarks will cancel with the exception of neighbouring the diagonal interaction between $u$ and $\bar{u}$ quarks. When the planar array is replaced by a connected three-dimensional

configuration, there is a negative electrostatic potential energy between the $\bar{u}\bar{u}$ in the third complex and the $uu$ pair in the first complex. If the three complex are arranged in an equilateral triangular form, the distances between the central $d$ and $\bar{d}$ quarks will become equal.

Then the electrostatic potential energy of the entire supercomplex would be

$$(46) \qquad 12V_{u\bar{u}} + V_{dd} + V_{d\bar{d}} + 2V_{\bar{d}d} + V_{dd} + V_{d\bar{d}} = 12V_{u\bar{u}} + 2V_{\bar{d}d}$$

These electrostatic energies equal

$$(47) \qquad V_{elec}^{u\bar{u}diag.} = -\frac{4}{9}\frac{e^2}{4\pi\epsilon_0 d_{u\bar{u}diag.}} = \frac{7.197183944 \times 10^{-10} eVm}{d_{u\bar{u}diag.}}$$

$$V_{elec}^{d\bar{d}} = \frac{1}{9}\frac{e^2}{4\pi\epsilon_0 d_{d\bar{d}}} = -\frac{1.799295986 \times 10^{-10} eVm}{d_{d\bar{d}}}.$$

The length of the diagonal from the $u$ to $\bar{u}$ quark is $\sqrt{2}$ times that of the length of side of a single complex. The distance between the $d$ and $\bar{d}$ quarks would equal the length of this side.

When the distance between the surfaces of the $d$ and $\bar{d}$ quarks is $6.335412 \times 10^{-18}m$,

$$(48) \qquad V_{elec}^{u\bar{u}} = -80.3290105 \; MeV$$

$$V_{elec}^{d\bar{d}} = -28.4 \; MeV$$

The net electrostatic potential energy is

$$(49) \qquad 12V_{u\bar{u}} + 2V_{d\bar{d}} = -1020.748126 \; MeV.$$

The strong interaction potential would contribute significantly to the energy unless it drops rapidly to zero beyond a range between $10^{-18}m$ and $10^{-17}m$. Since $6m_{u\infty} + 6m_{\bar{u}\infty} + 2m_{d\infty} + m_{\bar{d}\infty} = 12(61.85 \; MeV/c^2) + 3(64.85 \; MeV/c^2) = 936.75 \; MeV/c^2$, the mass of the entire supercomplex of 15 elements is

$$(50) \qquad 4584 \; MeV/c^2 + 936.75 \; MeV/c^2 - 1020.748126 \; MeV/c^2$$
$$= 4500.001874 \; MeV/c^2.$$

It may be noted that the sum of the masses of the supercomplexes and the boundary components gives $4584 \; MeV/c^2 + 936.75 \; MeV/c^2$. Therefore, the $\Upsilon$ resonance would be created by a fusion of the $b$ and $\bar{b}$ quarks with the electrostatic potential energy of a single complex approximately equal to $-184.81\overline{66} \; MeV$, which can be achieved by increasing the distances between the $d$ and $\bar{d}$ quarks to $8.1781346 \times 10^{-18}m$.

The top quark is much heavier with a mass of 175 $GeV/c^2$. Let $n$ be number of complexes of the form

$$\begin{array}{ccccccc} d & & \bar{d} & & d & & \bar{d} \\ & u & & or & & \bar{u} & \\ d & & \bar{d} & & d & & \bar{d} \end{array}$$

Each complex has a chiral mass of $5(243.15\ MeV/c^2) = 1215.75\ MeV/c^2$. Given that there are infinite-genus components of surfaces emanating from each of the chiral quarks, the entire mass contributed by $n$ complexes

(51)
$$n(1215.75\ MeV/c^2)+4n(64.85\ MeV/c^2)+n(61.85\ MeV/c^2) = n(1537\ MeV/c^2).$$

Setting $n$ equal to 113, it would equal 173.681 $GeV/c^2$. Given that there are two other infinite-genus ends originating from the central 113 $u$ and $\bar{u}$ quarks, their connections generate another

(52)
$$226(61.85\ MeV/c^2) = 13.9781\ GeV/c^2.$$

Adding the two masses gives an estimate in excess of $m_t$ by 12.6591 $GeV/c^2$. The remainder of the supercomplex would close to form an electrically neutral structure.

There is a reduction in energy resulting from the electrostatic forces between the a three-dimensional polygonal configuration with alternating central $u$ and $\bar{u}$ quarks. With 57 $u$ quarks and 56 $\bar{u}$ quarks in the complex, the electrostatic potential energies amongst the central quarks and anti-quarks cancel except for $56 \times 2\ V_{elec}^{u\bar{u}}$. The diagonal interactions yield $113 \times 4\ V_{elec}^{d\bar{d}}$.

Setting $d_{u\bar{u}} = 1.09104255722 \times 10^{-17} m$ and $d_{d\bar{d}} = 1.54296713803 \times 10^{-17} m$,

(53)
$$\begin{aligned} V_{elec}^{u\bar{u}} &= -65.9661146814\ MeV \\ V_{elec}^{d\bar{d}} &= -11.6612722439\ MeV \end{aligned}$$

The mass is reduced by 12.6590998986 $GeV$ to $m_t \doteq 175\ GeV/c^2$.

## 5. **Conclusion**

The mass spectrum of hadrons has been successfully described through the quark model and the spin coupling formula. Further regularities in the integer multiple rule, Regge trajectories and the Koide relation have resulted in substantial understanding of the elementary particle interactions. The patterns in the fermion multiplets of the standard model have yet to be entirely elucidated. The quarks are found to have a mass generated by chiral perturbation theory and a nonperturbative portion that may be attributed to the

infinite-genus term in a string theoretic version of a series expansion of expectation values of products of field strengths. Many of the conventional methods may be adapted to the chiral mass of the up quark, which is 243.15 $MeV/c^2$. This value is sufficient to establish an inverse proportionality of the ratio of the masses of the up quark and the electron to the ratio of the radii by the Lorentz formula. A similar calculation yields the radii of the muon and $\tau$ lepton. Since the beta decay requires the reaction $d \rightarrow u + e^- + \bar{\nu}_e$, and the difference between the masses of the up and down quarks is a nonperturbative effect, the electron and the anti-neutrino are identified with characteristics of the end of an infinite-genus surface. By constrast with the Lorentz formula, the extent of the boundary circle representing the two particles is proportional to the mass, given a uniform linear density. Then the radius of the anti-neutrino is computed to be eight orders of magnitude less than that of the electron. The analogue of the beta decay for the proton, converting a uud to a uuu state, is found to be kinematically impossible when its momentum is zero or aligned with the momentum vectors of the byproducts in the intermeidate channel as a result of the larger rest mass of the $\Delta^{++}$ baryon. Therefore, it is verified that a proton at rest is stable within the standard model, and a similar conclusion is valid when it has momentum unless a composite $uuu$ state of lesser rest mass is created or the momentum transfer allows a non-zero scattering angle.

The Koide relation for the masses of the charged leptons has a theoretical explanation in terms of an anticommutation relation for the supercharges and an approximation for disparate masses. Definining two variables $a$ and $b$ equal to $\frac{\sqrt{m_\mu}}{\sqrt{m_e}}$ and $\frac{\sqrt{m_\tau}}{\sqrt{m_e}}$ respectively, a quadratic equation for $b$ in terms of $a$ may be derived, with the solution $=(2+\sqrt{3})a+2(1+[\sqrt{3})$. The derivation of the scaling of the first generation, $a$, requires the introduction of a coefficient in the trace of the anticommutators of the form $16 - \sqrt{2}$, which is possible with central charges in the algebra. A consideration of four-dimensional superalgebras reveals that this factor can be introduced for masses. However, consistency with the scaling $a$ requires that it is present for supercharges, which requires a $\mathbb{Z}_4$ graded supersymmetry. The specific form of each of the anticommutation relations, and the central charge, would be a necessary for this theoretical explanation to be valid.

Given the infinite-genus components representing the nonperturbative contributions to the $u$ and $d$ masses, various models may be constructed for the quarks in the second and third fermion generations. Group theory of the $SU(3)_c$ makes it mandatory that the configurations transform under the **3** representation. An equivalence between the strange quark and a combination of the up quark and the electron can be completed when four-infinite-genus components are added, the electron is scattered and the ideal boundary is wrapped around the chiral quark. Complexes of up and down quarks and the

anti-quarks with five elements yield a composite system that satisfies this condition, with the correct net charge. Then a sequence of identical copies of the complex and the antiparticle version would comprise a much larger structure which models the more massive quarks. The central quarks are attached to two infinite-genus components in the third generation, and there is a reduction resulting from the electrostatic potential energy. By this technique, the $c$, $b$ and $t$ quarks can be described by 1, 3 and 113 complexes. This sequence must be explained for a rigorous theory of the structures of the quarks.

## REFERENCES

[1] G. Altarelli, *Neutrino 2004: concluding talk,* Nucl. Phys. B. Proc. Suppl. **143** (2005) 470–478.

[2] C. Amsler et al. (Particle Data Group), *Review of Particle Physics, Sect. 13: Neutrino mass, mixing and flavor change,* Phys. Lett. **667B** (2008) 163–171.

[3] F. Arampura, G. Amelino-Camelia, F. Buccella, O. Pisanti, L. Rosa and T. Tusi, *Proton decay and neutrino masses in SO(10)*, Il Nuovo Cim. A **108** (1995) 375–400.

[4] S. Davis, *The Mass of the ninth resonance of the pseudoscalar multiplet,* Hadr. J. **38** (2015) 31–52.

[5] S. Davis, *The coset space of the unified field theory,* Appl. Sci. **20** (2018) 54–101.

[6] M. Gell-Mann, *The eightfold way: a theory of the strong interaction symmetry,* Caltech Report (1961).

[7] Y. Koide, *Fermion-boson two-body model of quarks and leptons and Cabibbo mixing,* Lett. Nuovo Cim. **34** (1982) 201–205.

[8] Y. Koide, H. Nishiura, K. Matsuda, T. Kikuchi, and T. Fukuyama, *Universal texture of quark and lepton mass matrices and a discrete symmetry* $\mathbb{Z}_3$, Phys. Rev. **D66** (2002) 093006:1–11.

[9] N. Li and B. Q. Ma, *Estimate of neutrino masses from Koide's relation,* Phys. Lett. **609B** (2005) 309–316.

[10] Y. Nambu, *An empirical mass spectrum of elementary particles,* Prog. Theor. Phys. **9** (1952) 595–596.

[11] H. Nishino et al. (Super-Kamiokande Collaboration), *Search for proton decay via* $p \rightarrow e^+\pi^0$ *and* $p \rightarrow \mu^+\pi^0$ *in a large water Cherenkov deterctor,* $Phys.Rev.Lett.$ **102**(2009)141801 : 1 – –5.

[12] T. Regge, *Introduction to complex orbital momenta,* Il Nuovo Cim. **14** (1959) 951–976.

**HADRONIC JOURNAL 47**, 313 - 328 (2024)
DOI 10.29083/HJ.47.03.2024/SC313



# SUPERSTRING AMPLITUDES AND ELEMENTARY PARTICLES

**Simon Davis**
Research Foundation of Southern California
8861 Villa La Jolla Drive #13595
La Jolla, CA 92307
sbdavis@resfdnsca.org

Received April 26, 2024
Revised August 15, 2024

## Abstract

It has been shown recently that superstring states are organized into supermultiplets for the massless fundamental modes and solitons representing excited states. Summation of superstring amplitudes yields an expression that has poles when the momenta of the external states have specific values. It is established that only the residues and not the mass can be shifted by higher genus terms in the superstring perturbation series. The masses of elementary particles will not be generated by radiative corrections in superstring theory. Quantization of the energy levels does occur for the excited modes and the solitons. The superstring must be replaced by a hadronic string to achieve a phenomenologically viable theory of the particle spectrum. A linear spacing for the masses can be derived from the pion bubble model. The vibrational modes of the string between the quark and anti-quark in the pion then generates square-root variations from the integer multiple rule for the excited states of hadrons.

**PACS: 11.25.Db, 11.25.Sq, 14.20.Gk, 14.40.Be**

**Keywords:** *superstring amplitudes, hadronic string, integer multiple rule*

## 1. Introduction

While solitons described by extreme black hole geometries might be used to representing elementary particles, excited states generally have a Planck mass, and it is useful to restrict consideration to the massless sector. The feasibility of such a truncation is raised by connections between Type IIA string theory and eleven-dimensional supergravity [23] [24].

An alternative approach of the derivation of the elementary particle spectrum would follow from characteristics of superstring amplitudes with massless external states. It may be recalled that the energy levels of string states are defined by a Fourier mode expansion and expectation values of of operators satisfying a Virasoro algebra. A quantization of energy is introduced. The superstring amplitudes will have poles at the on-shell masses of excited modes defined by the external vertex operators. It is analogous to the poles of the Koba-Nielsen amplitudes in bosonic string scattering. Corrections to the masses at sufficiently high order are prevented, however, by nonrenormalization theorems. Given the quantization of on-shell energies, it would follow that there is a theoretical basis for the integer-multiple rule for the elementary particle spectrum in a superstring model.

An evaluation of resonance poles in superstring correlation functions yields a series of corrections to the residues without affecting the masses. The absence of a mass renormalization would be expected from the finiteness of the superstring perturbation series at each order and summed over the genus for a range of the string coupling. Therefore, higher-genus terms cannot shift the massless states to the masses of elementary particles.

The predicted values of the masses based on the excited states of the superstring would not be considered to be phenomenologically viable. It is necessary to replace the superstring by a hadronic string. If the hadronic string model has supersymmetry, this symmetry would be present in the spectrum [10], which may be valid for two multiplets with a tetraquark resonance. By contrast, a nonsupersymmetric hadronic string model can generate the known spectrum, but the quantum theory has problems of consistency similar to that of the bosonic string.

The integer multiple rule, nevertheless, characterizes a branch of both the meson and baryon resonances. An explanation through pion bubble diagrams [11] is compatible with validity of the rule for the $\gamma$ branch. This method then may be combined with the hadronic string model to derive a realistic spectrum and a square root variation from the integer multiple rule for the excited states.

## 2. Scattering Amplitudes

The poles of string amplitudes have integer spacings. The scattering amplitude with $N$ vertex operators would be

$$(1) \qquad \sum_g \kappa_{str}^{2g-2} \int_{M_g} d\mu_{WP} \int_{\Sigma_g} \prod_{i=1}^{n} d^2 z_i \sqrt{g(z_i)} \langle V_1(z_1) \ldots V_N(z_N), \rangle.$$

where $V_i(z_i)$ is the $i^{th}$ vertex operator, $d\mu_{WP}$ is the Weil-Petersson measure on the moduli space $M_g$ of complex metrics on a Riemann surface of genus $g$ and $\kappa_{str}$ is the string coupling. The path integral of the time ordered product would be evaluated through the Wick contractions of the operators, which yields

(2)

$$\begin{aligned}
&\Big\langle 0 \Big| \left(1 + ip_1 \cdot X(z_1) - \frac{1}{2!}(p_1 \cdot X(z_1))^2 - \frac{i}{3!}(p_1 \cdot X(z_1))^2 + \ldots\right) \\
&\quad \left(1 + ip_2 \cdot X(z_2) - \frac{1}{2!}(p_2 \cdot X(z_2))^2 - \frac{i}{3!}(p_2 \cdot X(z_2))^3 + \ldots\right) \\
&\quad \left(1 + ip_N \cdot X(z_N) - \frac{1}{2!}(p_N \cdot X(z_N))^2 - \frac{i}{3!}(p_N \cdot X(z_n))^3 + \ldots\right) \Big| 0 \Big\rangle \\
&\quad = \langle 0|0\rangle + i \sum_i \langle 0|p_i \cdot X(z_i)|0\rangle - \sum_{i<j} \langle 0|p_i^\mu p_j^\nu X_\mu(z_i) X_\nu(z_j)|0\rangle \\
&\quad + \sum_{i<j<k<\ell} \langle 0|p_i^\mu p_j^\nu X_\mu(z_i) X_\nu(z_j)|0\rangle \langle 0|p_k^\rho p_\ell^\sigma X_\rho(z_k) X_\sigma(z_\ell)|0\rangle \\
&\quad + \frac{1}{(2!)^2} \cdot 2 \sum_{i<j} p_i^\mu p_j^\nu p_j^\rho p_j^\sigma \langle 0|X_\mu(z_i) X_\rho(z_j)|0\rangle \langle 0|X_\nu(z_i) X_\sigma(z_j)|0\rangle \\
&\quad + \sum_{i<j<k} p_i^\mu p_j^\nu p_j^\rho p_k^\sigma \langle 0|X_\mu(z_i) X_\nu(z_j)|0\rangle \langle 0|X_\rho(z_j) X_\sigma(z_k)|0\rangle \\
&\quad - \frac{1}{(3!)^2} 6 \sum_{i<j} p_i^\mu p_i^\nu p_i^\lambda p_j^\rho p_j^\sigma p_j^\tau \langle 0|X_\mu(z_i) X_\rho(z_j)|0\rangle \langle 0|X_\nu(z_i) X_\sigma(z_j)|0\rangle \langle 0|X_\lambda(z_i) X_\tau(z_j)|0\rangle \\
&\quad - \frac{1}{(2!)^3} 2^2 \sum_{i<j<k} p_i^\mu p_i^\nu p_j^\lambda p_j^\rho p_k^\sigma p_k^\tau \langle 0|X_\mu(z_i) X_\lambda(z_j)|0\rangle \langle 0|X_\nu(z_i) X_\sigma(z_k)|0\rangle \\
&\qquad \langle 0|X_\rho(z_j) X_\tau(z_k)|0\rangle
\end{aligned}$$

(3)

$$-\frac{1}{(2!)^2}2\sum_{i<j<k<\ell} p_i^\mu p_j^\nu p_j^\lambda p_k^\rho p_k^\sigma p_\ell^\tau \Big[\langle 0|X_\mu(z_i)X_\nu(z_j)|0\rangle\langle 0|0X_\lambda(z_j)X_\sigma(z_k)|0\rangle$$

$$\langle 0|X_\rho(z_k)X_\tau(z_\ell)|0\rangle$$

$$\ldots\ldots\ldots\ldots\ldots\ldots + \langle 0|X_\mu(z_i)X_\rho(z_k)|0\rangle\langle 0|X_\nu(z_j)X_\sigma(z_k)|0\rangle\langle 0|X_\lambda(z_j)X_\tau(z_\ell)|0\rangle$$

$$+ \langle 0|X_\mu(z_i)X_\tau(z_\ell)|0\rangle\langle 0|X_\nu(z_j)X_\rho(z_k)|0\rangle\langle 0|X_\lambda(z_j)X_\sigma(z_k)|0\rangle\Big]$$

$.. +$ *correlation functions with coincident fields*

$+$ *expectation values of normal ordered products of operators*

$+ \ldots .$

The general combination is

(4) $$(p_{i_1}\cdot p_{j_1})^{r_1}\ldots(p_{i_m}\cdot p_{j_m})^{r_m}(G(z_{i_1},z_{j_1}))^{r_1}\ldots(G(z_{i_m},z_{j_m}))^{r_m}$$
$$r_1+\ldots.+r_m=n.$$

Suppose that $i_1,\ j_1,\ i_2,\ j_2,\ \ldots,\ i_m,\ j_m$ are different. The combinatorial factor from the expansion of the correlation function is

(5) $$\frac{1}{(r_1!)^2}\ldots\frac{1}{(r_m!)^2}r_1!\ldots r_m! = \frac{1}{r_1!\ldots r_m!}.$$

From the expansion of the exponential $exp\left(-\sum_{i<j}p_i^\mu p_j^\nu\langle 0|X_\mu(z_i)X(z_j)|0\rangle\right)$ is

(6) $$\frac{1}{n!}\begin{pmatrix} & n & \\ r_1 & \ldots & r_m\end{pmatrix} = \frac{1}{r_1!\ldots r_m!}.$$

If some of the indices $i_1,\ j_1,\ i_2,\ j_2,\ \ldots.i_m\ j_m$ coincide, an alternate labelling $k_1,\ldots,k_\ell$ of the expression is

(7)
$$(p_{k_1}\cdot p_{k_2})^{r_1}(p_{k_2}\cdot p_{k_3})^{r_2}\ldots(p_{k_{i_0}}\cdot p_{k_{i_0+1}})^{r_{m_0}}\ldots(p_{k_{\ell-1}}\cdot p_{k_\ell})^{r_m}G(z_{k_1},z_{k_2})^{r_1}\ldots G(z_{k_{\ell-1}},z_{k_\ell})^{r_m}.$$

where $p_{k_1}$ appears $r_{k_1} = r_{k_1,s_{11}} + \ldots + r_{r_1,s_{1,t_1}} = r_{k_1}$ times, ..., $p_{k_\ell}$ appears $r_{k_\ell} = r_{k_\ell,s_{\ell,1}} + \ldots + r_{k_\ell,s_{\ell,t_\ell}} = r_{k_\ell}$ times. The combinatorial factor from the expansion of the correlation function is

(8)
$$\frac{1}{r_{k_1}!...r_{k_\ell}!}\begin{pmatrix} r_{k_1} \\ r_{k_1,s_{11}}...r_{k_1,s_1,t_1}\end{pmatrix}...\begin{pmatrix} r_{k_\ell} \\ r_{k_\ell,s_{\ell,1}}...r_{k_\ell,s_\ell,t_\ell}\end{pmatrix} r_1!...r_m!$$
$$= \frac{1}{r_{k_1,s_{11}}!...r_{k_1,s_1,t_1}!...r_{k_\ell,s_{\ell,1}}!...r_{k_\ell,s_\ell,t_\ell}!} r_1!...r_m!$$
$$= \frac{1}{r_1!...r_m!}.$$

The expansion of the exponential again gives $\frac{1}{r_1!...r_m!}$. Therefore, the coefficients are equal, and expression for the correlation function is given by

(9)
$$\prod_{i<j} exp\left(-p_i \cdot p_j G(z_i, z_j)\right)$$

with $G(z_i, z_j)\eta^{\mu\nu} = \langle 0|X^\mu(z_i), X^\nu(z_j)|0\rangle$. and not including the normalization of the Green function. The Green function for the free scalar field on the complex plan would satisfy

(10)
$$\partial\bar{\partial}G(z_i, z_j) = \delta(z_i - z_j)$$

The solution is

(11)
$$G(z_i, z_j) = \frac{1}{\pi} ln\ |z_i - z_j|$$

since

(12)
$$\partial\bar{\partial}\ \frac{1}{2}(ln\ z + ln\ \bar{z}) = \left[\bar{\partial}\left(\frac{1}{z}\right) + \partial\left(\frac{1}{\bar{z}}\right)\right]$$

and

(13)
$$-\frac{i}{2}\int dz d\bar{z}\left[\bar{\partial}\left(\frac{1}{z}\right) + \partial\left(\frac{1}{\bar{z}}\right)\right] = -\frac{i}{2}\frac{1}{2}\left[\int_C \frac{dz}{z} + \int_C \frac{d\bar{z}}{\bar{z}}\right].$$
$$= -\frac{i}{4}2 \cdot 2\pi i = \pi.$$

On a Riemann surface, two delta function sources are necessary for consistency with Stokes' theorem, and a summation over image charges under the action

of a uniformizing Schottky group gives

(14)

$$
\begin{aligned}
G_{QS}(P,R) = \frac{1}{\pi}\Bigg[\sum_{\alpha} ln\ &\frac{z_P - V_\alpha z_R}{z_Q - V_\alpha z_S}\frac{z_Q - V_\alpha z_S}{z_Q - V_\alpha z_R} \\
&- \frac{1}{2\pi}\sum_{m,n=1}^{g} Re\ \{v_m(z_P) - v_m(z_Q)\}(Im\ \tau)^{-1}_{mn} Re\{v_n(z_R) - v(z_S)\}\Bigg] \\
v_n(z) = \sum_{\alpha}{}^{(n)} ln\left(\frac{z - V_\alpha \xi_{1n}}{z - V_\alpha \xi_{2n}}\right) &\qquad v_n(z) - v_n(T_m z) + 2\pi i \tau_{mn},
\end{aligned}
$$

where $R$ and $S$ represent the sources, $\tau$ is the period matrix, and $\{v_n,\ n = 1,,,.g\}$ is the set of integrals of canonical basis of homolorphic differentials and the sum over elements $\{V_\alpha\}$ over the free group $\langle T_1^{\pm 1}, ..., T_g^{\pm 1}\rangle$, $\Sigma^{(n)}$ does not include those products of generators that have $T_n^{\pm 1}$ as the right-most factor. The final expression

$$
(15) \qquad \prod_{i<j} e^{-\frac{\pi}{2} p_i \cdot p_j G(z_i, z_j)}
$$

then would be required to obtain an integral of the form

(16)

$$
\begin{aligned}
f(z_1^0, z_3^0, z_3^0) \int_\Delta d^2 z_4 |z_4 - z_1^0|^{1-\frac{p_1 \cdot p_4}{2}} &\prod_{\alpha \neq I}{}' \left| \frac{z_4 - V_\alpha z_1^0}{z_4 - V_\alpha z_4} \frac{z_1^0 - V_\alpha z_4}{z_1^0 - V_\alpha z_1^0} \right|^{-\frac{p_1 \cdot p_4}{2}} \\
\times \prod_{m,n} exp &\left[\frac{p_1 \cdot p_4}{8\pi} Re\{v_m(z_4) - v_m(z_1^0))(Im\ \tau)^{-1} Re(v_n(z_r) - v_n(z_1^0))\}\right] \\
\times\ (similar\ &factors\ with\ z_1^0 \rightarrow z_2^0,\ z_3^0,\ p_1 \rightarrow p_2,\ p_3).
\end{aligned}
$$

The four-point finite-genus amplitude, for example, then may be expressed in the Schottky group coordinate parameterization of moduli space by

(17)

$$
\begin{aligned}
&\int_{F_g} d^2z\ |z-z_1^0|^{-\frac{p_1\cdot p_4}{2}}|z-z_2^0|^{-\frac{p_2\cdot p_4}{2}}|z-z_3^0|^{-\frac{p_3\cdot p_4}{2}}\,\Phi(z,\bar z) \\
&= \int_0^{2\pi}\int_{|z-z_1^0|\le\Lambda} d\theta\ d|z-z_1^0|\ |z-z_1^0|^{1-\frac{p_1\cdot p_4}{2}}\sum_{\ell=0}^{\infty}\sum_{m=0}^{\infty}\frac{(z-z_1^0)^\ell(\bar z-\bar z_1^0)^m}{\ell!m!} \\
&\qquad\qquad \partial^\ell\bar\partial^m\{|z-z_2^0|^{-\frac{p_2\cdot p_4}{2}}|z-z_3^0|^{-\frac{p_3\cdot p_4}{2}}\,\Phi(z,\bar z)\}_{z=z_1^0} \\
&\quad + \int_0^{2\pi}\int_{|z-z_2^0|\le\Lambda} d\theta\ d|z-z_2^0|\ |z-z_2^0|^{1-\frac{p_2\cdot p_4}{2}}\sum_{\ell=0}^{\infty}\sum_{m=0}^{\infty}\frac{(z-z_2^0)^\ell(\bar z-\bar z_2^0)^m}{\ell!m!} \\
&\qquad\qquad \partial^\ell\bar\partial^m\{|z-z_1^0|^{-\frac{p_1\cdot p_4}{2}}|z-z_3^0|^{-\frac{p_3\cdot p_4}{2}}\,\Phi(z,\bar z)\}_{z=z_2^0} \\
&\quad + \int_0^{2\pi}\int_{|z-z_3^0|\le\Lambda} d\theta\ d|z-z_3^0|\ |z-z_3^0|^{1-\frac{p_3\cdot p_4}{2}}\sum_{\ell=0}^{\infty}\sum_{m=0}^{\infty}\frac{(z-z_3^0)^\ell(\bar z-\bar z_3^0)^m}{\ell!m!} \\
&\qquad\qquad \partial^\ell\bar\partial^m\{|z-z_1^0|^{-\frac{p_1\cdot p_4}{2}}|z-z_2^0|^{-\frac{p_2\cdot p_4}{2}}\,\Phi(z,\bar z)\}_{z=z_3^0} \\
&\quad + finite \\
&= \sum_n \frac{\Lambda^{-\frac{p_1\cdot p_4}{2}+2n+2}}{-\frac{p_1\cdot p_4}{2}+2n+2}\frac{1}{(n!)^2}(\partial\bar\partial)^n\{|z-z_2^0|^{-\frac{p_2\cdot p_4}{2}}|z-z_3^0|^{-\frac{p_3\cdot p_4}{2}}\,\Phi(z,\bar z)\}_{z=z_1^0} \\
&\quad + \sum_n \frac{\Lambda^{-\frac{p_2\cdot p_4}{2}+2n+2}}{-\frac{p_2\cdot p_4}{2}+2n+2}\frac{1}{(n!)^2}(\partial\bar\partial)^n\{|z-z_1^0|^{-\frac{p_1\cdot p_4}{2}}|z-z_3^0|^{-\frac{p_3\cdot p_4}{2}}\,\Phi(z,\bar z)\}_{z=z_2^0} \\
&\quad + \sum_n \frac{\Lambda^{-\frac{p_3\cdot p_4}{2}+2n+2}}{-\frac{p_3\cdot p_4}{2}+2n+2}\frac{1}{(n!)^2}(\partial\bar\partial)^n\{|z-z_1^0|^{-\frac{p_1\cdot p_4}{2}}|z-z_2^0|^{-\frac{p_3\cdot p_4}{2}}\,\Phi(z,\bar z)\}_{z=z_3^0} \\
&\quad + finite
\end{aligned}
$$

where the domains of the integrals are divided into $\{z||z-z_i^0|\le\Lambda\}\cup F_g/\{z||z-z_i^0|\le\Lambda\}$, $i=1,2,3$ in the Schottky covering surface $C\cup\infty/\cup_{n=1}^g(D_{T_n}\cup D_{T_n^{-1}})$, where $\Phi(z,\bar z)$ is a regular function. The poles in the amplitude occur at $s,\ t,\ u=8(n-1)$, beginning with the tachyon and progressing to excited levels. When $n=0$, the poles occur at $s,\ t,\ u=-8$, which would describe an intermediate tachyon resonance. Another linear dependence, such as $4n-12$, which would arise if the exponents included $-p_i\cdot p_4$ without the factor of $\frac{1}{2}$, yields intermediate states with squared center-of-mass energies equal to -12 and, after iteration of the scattering calculation, a set of resonances with arbitrarily large negative energies. Consequently, the factor of $\frac{\pi}{2}$ would be present in the factor (15), and the tachyon vertex operator actually must have

the form $e^{i\sqrt{\frac{\pi}{2}}p\cdot X(z)}$. The spacings are determined by the tension of the string. Therefore, the energies can range from Planck to hadronic scales.

An $N$-point correlation function in superstring theory would be equal to

$$(18) \qquad \langle V_1 \,...\, V_N\rangle = \sum_{g=0} \kappa^{2g-2} \int_{sM_g} d\mu_{WP} \prod_{i=1}^{N} d^2 z_i \langle V_1(z_1) \,...\, V_N(z_N)\rangle$$

Expanding about a particle resonance

$$(19) \qquad \sum_{g=0} \kappa^{2g-2} \sum_{k=1}^{g-1} A_k \frac{1}{p^2 - m^2} A_{g-k}$$

It may be recalled that the upper bound for the amplitude at genus $g$ is given by the maximum over the interior and the compactification divisor. The integral over Schottky group parameters over the interior, which is the complement of the neighbourhood of the divisor, is less than $\frac{B^g}{g!}$, where the quotient by $g!$ results from the restriction to the fundamental domain of the supermodular group [6]. Summing over the interior and the components of the compactification divisor describing two components, the bound for the sum over the amplitudes would be

$$(20) \quad \kappa^{2g-2}\left[\frac{B^g}{g!} + \sum_{\substack{g_1+g_2=g \\ 1\le g_1, g_2 \le n-1}} \frac{B^{g_1}}{g_1!}\frac{B^{g_2}}{g_2!}\right] = \kappa^{2g-2} B^g \left[\frac{1}{g!} + \sum_{\substack{g_1+g_2=g \\ 1\le g_1,\, g_2 \le n-1}} \frac{1}{g_1!}\frac{1}{g_2!}\right].$$

Let

$$(21) \qquad S_{2,g} = \sum_{\substack{g_1+g_2=g \\ 1\le g_1, g_2\le g-1}} \frac{1}{g_1!}\frac{1}{g_2!}$$

Since

$$(22) \qquad e^{x_1+x_2} = \sum_{g=0}^{\infty} \frac{(x_1+x_2)^g}{g!} = \sum_{g=0}^{\infty} \sum_{g_1+g_2=g} \frac{x_1^{g_1}}{g_1!}\frac{x_2^{g_2}}{g_2!},$$

$$(23) \qquad e^2 = \sum_{g=0}^{\infty} \frac{2^g}{g!} = \sum_{g=0}^{\infty} \sum_{g_1+g_2=g} \frac{1}{g_1!}\frac{1}{g_2!} = \sum_{g=0}^{\infty} S_{2,g}$$

and

$$(24) \qquad S_{2,g} = \frac{2^g}{g!}.$$

Then

$$\sum_{\substack{g_1+g_2=g \\ 1\leq g_1,g_2\leq n-1}} \frac{1}{g_1!}\frac{1}{g_2!} = S_{2,g} - \frac{1}{g!} - \frac{1}{g!} = \frac{2^g-2}{g!} \qquad g \geq 1. \tag{25}$$

The magnitude of the amplitude is less than

$$\kappa^{2g-2}\ |B|^g \left[\frac{1}{g!} + \frac{2^g-2}{g!}\right] = \kappa^{2g-2}\ |B|^g\ \frac{2^g-1}{g!}. \tag{26}$$

Then the summation of the factorizations over the particle resonance is bounded by

$$\sum_{g=0}^{\infty} \kappa^{2g-2}\ |B|^g\ \frac{2^g-1}{g!}\ \frac{1}{p^2-m^2}. \tag{27}$$

The series converges for all values of the coupling, and the mass of the resonance remains invariant.

Infrared divergences resulting from propagation of tachyon states in bosonic string are cancelled by supersymmetry. Then there are massless states propagating along thin tubes created by pinching the separating cycle between the genus $k$ and genus $g = k$ components of a surface of genus $g$. After these resonances are excited states of the string. The problem with this model is that the excited states of a Planck size string have Planck masses, which is too large for the elementary particle spectrum. The viability of a model of the particle spectrum based on superstring amplitudes would depend on existence of corrections to the mass of the resonance. It is evident from the above series that there is no mass renormalization in superstring perturbation theory. Only the residues, representing couplings to different channels in the scattering process [3], are altered by radiative corrections in the superstring perturbation series.

The nonperturbative contribution to the amplitude arises from the infinite-genus boundary components. The amplitude given by the integral over the set of effectively closed surfaces with zero harmonic measure would have the same form as finite-genus amplitudes and not affect the masses of resonances. However, there exists a class of surfaces beyond this category of $O_G$ surfaces that represent the nonperturbative phenomena in the theory. A nonvanishing capacity of the ideal boundary yield a non-zero potential for the surface through the integration of the normal derivative of the harmonic measure [16]. The potential energy can be set equal to the energy of the infinite-genus boundary component. When there is no other dynamics, this energy would be proportional to a non-zero rest mass.

It is known also that the masses of leptons may be estimated through radiative corrections [20]. If the Planck strings are replaced by hadronic string with tensions that are multiplied by a factor $\left(\frac{\ell_P}{R_{hadr.}}\right)^2$, the masses of the excited states become more realistic. There is still a large difference between the masses of the hadrons and the leptons.

The formula for the mass of the electron in a quantum theory of radiating oscillators is precise, however, and it is indicative of the necessity of methods which are valid for the finite size. The equation for a radiating electron in an electromagnetic field is

$$m\ddot{x} - \frac{2e^2}{3c^3}\frac{d^3x}{dt^2} = eE \tag{28}$$

with $E = E_\omega cos(\omega t)$ has the solution

$$x(t) = -\frac{eE_\omega}{m\omega^2} cos\ \zeta_w cos(\omega t - \zeta_\omega) \tag{29}$$

where $tan\ \zeta_\omega = -\frac{\omega}{\omega_0}$. The Hamiltonian may be given by

$$H' = 4\pi c^2 \Omega^{-1} \sum_s \omega_s^{-2} \Big[ (\sum_i e_i \beta_i sin\ \vartheta_{si} cos \zeta'_{si} sin(\Gamma_{si} + \zeta'_{si}))^2 + (\sum_i e_i cos\ \zeta'_{si} cos(\Gamma_{si} + \zeta'_{si}))^2 \Big] \tag{30}$$

and $\vartheta_{si}$ is the angle between the wave with index $s$ and the velocity $\vec{\beta}_i$, while $\zeta'_{si} = arc\ tan\left(-\frac{\omega'_{si}}{\omega_0}\right)$, with $\omega_0 = \frac{3mc^3}{2e^2}$ and $\omega'_{si} = \omega_s(1 - \beta_i cos\ \vartheta_{si})(1 - \beta_i^2)^{-\frac{1}{2}}$, and $\Gamma_{si} = \frac{\omega_s r_i cos\ \vartheta_{si}}{c} +$ [17]. For a single particle at rest, $\beta_i = 0$ and $\zeta'_{si} = \zeta_s$. It follows that

$$E_i^0 = \frac{4\pi c^2}{\omega} e_i^2 \sum_s \omega_s^{-2} cos^2 \zeta_s cos^2(\Gamma_{si} + \zeta_s). \tag{31}$$

Replacing the sums by an integral,

$$E_i^0 = \frac{4\pi c^2}{\omega} e_i^2 \frac{\omega}{2\pi^2 c^3} \int d\omega \left(1 + \frac{\omega^2}{\omega_0^2}\right)^{-1} cos^2(\Gamma_{si} + \zeta_s) \tag{32}$$

and setting $\langle cos^2(\Gamma_{si} + \zeta_s)\rangle = \frac{1}{2}$,

$$\langle E_i^0 \rangle = \frac{e_i^2}{\pi c} \int_0^\infty \left(1 + \frac{\omega^2}{\omega_0^2}\right)^{-1} d\omega = \frac{e_i^2 \omega_0}{2c} = \frac{e_i^2}{2c}\frac{3}{2}\frac{m_i c^2}{e_i^2} = \frac{3}{4} m_i c^2. \tag{33}$$

For the interaction between two charges, it may be noted that $cos(\Gamma_{si} + \zeta_s) cos(\Gamma_{sj} + \zeta_s) = \frac{1}{2} cos(\Gamma_{si} + \Gamma_{sj} + 2\zeta_s) + \frac{1}{2} cos(\Gamma_{si} - \Gamma_{sj})$ and, when $cos_{\vartheta_s} = 0$,

$\frac{1}{2}cos(\Gamma_{si}\Gamma_{sj}) = \frac{1}{2}cos\left(\frac{\omega_s(r_i-r_j)cos\,\vartheta_s}{c}\right) = \frac{1}{2}cos\left(\frac{\omega_s r_{ij}}{c}\right)$. Let $r_{ij} = r$, $\frac{\omega r}{c} = ux_0$ and $x_0 = \frac{r}{r_0}$, where $r_0 = \frac{2e^2}{3mc^2}$. Then

(34)

$$E^0_{ij} = \frac{e^2}{c}\frac{2}{\pi}\int_0^\infty du\frac{c}{r}x_0 sin(ux_0)(1+u^2)^{-1} = \frac{e^2}{r_0}\frac{2}{\pi}\int_0^\infty dusin(ux_0)(1+u^2)^{-1}.$$

The evaluation of the sum of oscillator contributions is the equivalent of a one-loop calculation of the self-energy of the electron. There also would be higher-order contributions in the diagrammatic expansion of quantum field theory. If the action may be included in a supersymmetric model, a nonrenormalization theorem may be used to render corrections to be vanishing. When supersymmetry is not present, the magnitude of any higher-order terms would have to be bounded.

A classical theory with form factors would begin with the replacement of the current by $e\int_{-\infty}^{\infty} v_\mu F(R^2)$ in the source term $\int j^\mu(x)A_\mu(x)d^4x$, where $F(R^2) = \frac{1}{4\pi^2}\int e^{-iK\cdot R}g(K^2)d^4K$, $g(K^2) = \frac{K_0^4}{4\pi^2(K_0^4+K^4)}$, and terms in the electron equation include $\left(M^2 + e^2\frac{C_0}{2r_0}\right)\dot{v}_\mu - \frac{2}{3}e^2(\ddot{v}_\mu + \dot{v}^2 v_\mu) + \ldots$, where $\frac{C_0}{r_0} = \int_{-\infty}^{\infty} H(\sigma^2)d\sigma$ and $H(R^2) = -4\pi\int\frac{g^2(K^2)}{K^2}e^{-iK\cdot R}d^4K$ [4][18].The electromagnetic contribution to the energy is equal to $\frac{2}{3}\frac{e^2}{r_0}$ if

$$r_0\int_{-\infty}^{\infty} H(\sigma^2)\,d\sigma = \frac{4}{3}. \tag{35}$$

## 3. Integer Multiple Rule

The integer multiple rule has been observed amongst leptons and hadrons. It may be noted that the formula for the masses of dyons in N = 4 super-Yang-Mills theory [22] verify the integer multiple rule when either the electric or the magnetic charge is significantly larger [5]. The dyons represent nonperturbative states in string theory.

Nevertheless, shifts in the masses of hadronic states are expected to be derived from radiative corrections. By the formula for the bosonic string amplitude, it is evident that the poles occur at

$$\frac{p_i\cdot p_j}{2} = 2n+2 \tag{36}$$

or $s,\ t\ ,u = 8\,(n-1)$. Consequently, the squared center-of mass energy scales as the square root of $n$. The path integral formalism is developed to compute the scattering amplitudes of $N$ massless bosons with vertex operators

$V_0 = \varepsilon_\mu(\partial x^\mu - ip_\nu\psi^\mu\psi^\nu)e^{ip\cdot x}$ and $V_{-\frac{1}{2}} = u^\alpha(p)S_\alpha(z)S_g^{-\frac{1}{2}}(z)e^{ip\cdot x}$ and $2n$ massless fermions with vertex operators $V_{-\frac{1}{2}} = u^\alpha(p)S_\alpha(z)S_g^{-\frac{1}{2}}(z)e^{ip\cdot x}$ with ghost charge $-\frac{1}{2}$ and $V_{\frac{1}{2}} = u^\alpha(p)S_\alpha(z)S_g^{\frac{1}{2}}e^{ip\cdot x}$ with ghost charge $\frac{1}{2}$, where $S_\alpha$ and $S_g^{\pm\frac{1}{2}}$ are spin fields [1]. The fermionic scattering amplitudes

(37)

$$A_N = \int dz\omega(z)d\xi\omega_\xi \prod_{j=3}^{N} dz_j\omega(z_j) \sum_{n=0}^{\infty} \frac{(\omega\xi)^{-p_1\cdot p_2+\vec{q}_{\alpha_1}\cdot\vec{q}_{\alpha_2}-\frac{1}{4}+n+1}}{n!}$$
$$\nabla_{z_i}^n[\Theta_R(z_1,z_2)F(z_1,z_2,z_j)]|_{z_1=z_2=z}$$

$$F(z_1,z_2,z_j) = \prod_{j=3}^{N} \Theta(z_i,z_j)^{\vec{q}_{\alpha_1}\cdot\vec{q}_j+\vec{p}_1\cdot\vec{p}_j+\frac{g_j}{2}}\Theta(z_2,z_j)^{\vec{q}_{\alpha_2}\cdot\vec{q}_j-\vec{p}_2\cdot\vec{p}_j+\frac{g_j}{2}}$$
$$\prod_{a=1}^{5}\Theta_m\left(q_{\alpha_i,a}\int_P^{z_1}\omega + q_{\alpha_2,a}\int_P^{z_2} + \sum_{j,a}\int_P^{z_j}\omega\right)$$
$$\left[\Theta_m\left(-\frac{1}{2}\int_P^{z_1}\omega - \frac{1}{2}\int_P^{z_2}\omega + \sum_j g_j\int_P^{z_j}\right)\omega\right]^{-1}K_{ij}$$
$$Kij = \prod_{2\le i\le j}[\Theta(z_i,z_j)]^{\vec{q}_i\cdot\vec{q}_j}{}_{-i}\cdot\vec{p}_j\cdot g_i\cdot g_j$$

where $p_1$ and $p_2$ are momenta of gauge bosons, $\vec{q}_{\alpha_1}$ and $\vec{q}_{\alpha_2}$ are fermion charges of the spin field, $\omega = \omega^A\frac{\partial\Theta(u^A)}{\partial u^A}\Big|_{u^i=0}$, with $\{\omega^A,\ A=1,...,g\}$ is a canonical basis of holomorphic one-forms, $\xi$ is the tangent vector to the geodesic connecting $z_1$ and $z_2$ in a normal coordinate expansion on the Riemann surface and $g_i$ is the ghost charge, has poles at $p_1\cdot p_2 = \vec{q}_{\alpha_1}\cdot\vec{q}_{\alpha_2} - \frac{1}{4} + n + 1$ [1]. The squared center of mass energy is scaling linearly with the level number. Recalling that, in a center-of-mass frame, $s^2 = (p_1+p_2)^2$, it would equal

$$s = p_1^2 + p_2^2 + 2\vec{q}_{\alpha_1}\cdot\vec{q}_{\alpha_2} + 2\left(n+\frac{3}{4}\right). \tag{38}$$

Setting $s$ at the resonances equal to $M^2$, where $M$ is the mass of the intermediate state, when the vertex operators represent massless states with null momentum vectors,

$$M^2 = 2\vec{q}_{\alpha_1}\cdot\vec{q}_{\alpha_2} + 2\left(n+\frac{3}{4}\right). \tag{39}$$

The masses of the charged particles may be deduced from the dyon and Lorentz Formulae. It is feasible to demonstrate the integer multiple rule for more massive resonances. The use of the nonperturbative formula for the electron, however, would require introduce additional charges.

The intermediate vector boson in the fundamental interactions has integer spin to conserve angular momentum in the scattering of fermions with half-integer spin. By contrast, Regge amplitudes can have poles at the squared mass of baryons with half-integer spin. Baryons are massive compound states that have quantum numbers of the resonances on the Regge trajectories. The electron is an elementary particle that generally could be interpreted as an incoming or outgoing state and not as a resonance produced by the scattering.

Nevertheless, the formula (39) may be checked in this regard. The values of the inner products may be $\vec{q}_{\alpha 1} \cdot \vec{q}_{\alpha 2} = -\frac{3}{4}, \frac{1}{4}, \frac{5}{4}$. Then, when $n = 0$ and the spin field scalar product is $\frac{1}{4}$,

$$M_{n=0}^2 = 2 \cdot \frac{1}{4} + 2 \cdot \frac{3}{4} = 2 \tag{40}$$

The ratio of the fermion contribution to the entire expression is $\frac{3}{2} : 2 = \frac{3}{4}$, which is identical to that of the Lorentz formula for the electromagnetic contribution to the mass of the electron. Since the equality (40) describes the squared mass instead of the mass, an alternative mechanism for describing a spin-$\frac{1}{2}$ intermediate state would be necessary. The existence of the poles in the scattering amplitude reflects the quadratic form of the propagator for integer spin particles. When the intermediate state has half-integer spin, it must be modified to be linear in $\frac{1}{p-m}$. Since

$$\frac{1}{p^2 - m^2} = \frac{1}{p+m}\frac{1}{p-m}, \tag{41}$$

it follows that if singularity in the scattering amplitude occurs at $p = m$, the pole in the fermion propagator would arise if $(p-m)\psi = 0$, where $\psi$ is the spin-$\frac{1}{2}$ field, and the product would be $\frac{1}{2m}\frac{1}{p-m}$. The factor $(\omega\xi)^{-p_1 \cdot p_2 + \vec{q}_{\alpha 1} \cdot \vec{q}_{\alpha 2} - \frac{1}{4} + n + 1}$ in the integrand of the superstring amplitude arises from the representation of theta functions producing the expectation value of the product of pairs of fermion vertex operators, $V_{-\frac{1}{2}}$ and $V_{\frac{1}{2}}$, and the poles in the scattering amplitude may be found through an expansion in a Taylor series. The poles of the fermion propagator would be expected to arise from a factor with an exponent with a linear function of the momentum. The production of an intermediate spin-$\frac{1}{2}$ particle, however, requires one of the fermionic incoming particles to be replaced by a bosonic particle, with the effect of leaving an unpaired fermion in the expectation value. The contraction of factors in $V_0$ and $V_{\pm\frac{1}{2}}$ would include that of $e^{ip \cdot x}$ and $\partial x_\mu$, which yields after integration

over the Riemann surface, yields, a linear function of the momentum. It would also introduce only a single fermion charge of the spin field $q_\alpha$

Setting this linear function equal to the mass at the pole of the amplitude then would yield the equation, since $p^2$ gives $2\nu$, half of the rest of the exponent for $p$ would give

$$M^{spin-\frac{1}{2}} = \frac{1}{2}|\vec{q}_\alpha| + \left(n + \frac{3}{4}\right). \tag{42}$$

for a fermionic intermediate state. Since $|q_\alpha| = \frac{1}{2}$, when $n = 0$,

$$M_{n=0}^{spin-\frac{1}{2}} = \frac{1}{2} \cdot \frac{1}{2} + \frac{3}{4} = 1 \tag{43}$$

and the contribution of the matter fields would be $\frac{3}{4}$ of the mass of the spin-$\frac{1}{2}$ particle since the remainder would result from the spin field of the superstring.

The ratio of the masses of the $\gamma$ branch of the meson and baryon spectrum to the pion mass satisfies an integer multiple rule [2][12] [15][19]. Fractional powers may result from a variety of potentials in the modeling of hadronic spectra [14]. Since the energy levels are defined for the scattering of two string states in a fixed channel, it would be best to consider the integer spacing for the squares of masses amongst the corrections to the fundamental mass spectrum within each particle multiplet. The Gell-Mann-Okubo mass rule is known to be linear for fermions and quadratic for mesons [13] [21], which describe bound states of two quarks, and therefore, a resonance resulting from the interaction of two strings.

Given a collection of pion bubbles in a meson with a mass larger by a factor of $v$, the poles in the string amplitudes would yield corrections $\delta M$ for each pion that are proportional to $\frac{1}{v}\sqrt{n}$. Given $k$ excited energy levels of the open string between the quark and anti-quark in each pion, there would be $kv$ excited states of the meson.

## 4. Conclusion

The masses of the elementary particles are known to satisfy an integer multiple rule. It has been determined that this rule follows from the masses of nonperturbative string states which are dyons in N = 4 super-Yang-Mills theory. The perturbative string amplitudes have poles at values of $s$, $t$ and $u$ that increase linearly with the level number of the excited state of the intermediate resonance. It follows that this radiative process then yield quadratic corrections to a fundamental energy spectrum. The problem of the linear proportionality of masses with the level number may be resolved for half-integer spin particles by transferring the pole of the resonance to the factor $\frac{1}{\not p - m}$ and

integer-spin particles through pion bubbles since the ratio of the mesons in the $\gamma$ branch. The validity of the pion bubble model for the $\gamma$ branch follows from the decay $\pi^0 \rightarrow 2\gamma$ for each pion. The Gell-Mann-Okubo mass rule is conjectured to be the primary method for predicting masses differences in the hadron multiplets.

Phenomenologically realistic values of the masses would be derived from the hadronic string rather than the superstring. Without supersymmetry, the infrared divergences resulting from tachyon states must be removed. There exists a method for ensuring finiteness of the string theory having only modular invariance and breaking of supersymmetry [9] through a matching of states in different sectors. The tachyon then would not generate the problems for such a model that occur for the bosonic string.

Given the meson resonances in the $\gamma$ branch which have masses that are integer multiples of $m_{\pi^0}$ or $m_{\pi^-}$, excited states resulting from the quantized vibrational modes of the open string connecting the quark and the anti-quark that differ from the mass of the resonance $M$ by $\delta M$, where $\delta M \propto \frac{1}{v}\sqrt{n}$. There will be $kv$ energy levels when the open string has $k$ excited energy levels.

The variation from this rule for the $\nu$ branch is indicative of an extra contribution to the masses, which may be related to the infinite-genus boundary component that is found to be sufficient to explain a nonperturbative contribution to the $\eta'$ mass [7].

Lepton masses would not be predicted by the current string models. A recent study of the generation of lepton masses is based on the division algebra modules in the spinor space of the standard model [8]. The infinite-genus boundary component is not required. However, the interaction between quarks and leptons in the weak interactions is indicative of a connection between the ideal boundaries of infinite-genus surfaces and the $\nu$ branch of the meson and baryon resonances. The electromagnetic contribution to the mass of a charged particle is given by the Lorentz law which depends on its radius. The formula for the energies of a set of elementary particle states therefore would include the combination of the integer multiple rule and a Lorentz term that represents symmetry breaking.

## REFERENCES


[1] G. Aldazabal, M. Bonini and C. Nunez, Covariant Superstring *Fermionic amplitudes, vertex operators and picture changing*, Nucl. Phys. **B319** (1989) 342–366.

[2] D. Akers, *Further evidence for magnetic charge from hadronic spectra*, Int. J. Theor. Phys. **33** (1994) 1817–1829.

[3] D. M. Asner, C. Hanhart and E. Klempt, *Resonances, Sec. 48,* in Review of Particle Physics, Particle Data Group, Chin. Phys. C bf 40 (2016) 100001: 1–1808.

[4] M. Chrétien and R. E. Peierls, *A study of gauge-invariant non-local interactions*, Proc. Roy. Soc. **A223** (1954) 468–481.

[5] S. Davis, *Supersymmetric fixed points for elementary particle masses*, Balkan J. Phys. **21** (2013) 1–15.

[6] S. Davis, *A resolution of the integration region problem for the supermoduli space integral*, Int. J. Mod. Phys. **A29** (2014) 1450190:1–60.

[7] S. Davis, *Nonperturbative contributions to the massive propagator in a class of strong interactions*, Bull. Pure Appl. Sciences **37D** (2018) 137–145.

[8] S. Davis, The physical interpretation of the spinor conditions for the wave wquation, RFSC-19-07.

[9] K. R. Dienes, *Modular invariance, finiteness and misaligned supersymmetry: new constraints on the numbers of physical string states*, Nucl. Phys. **B429** (1994) 533–588.

[10] H. G. Dosch, *Supersymmetry across the hadronic spectrum*, Adv. High Energy Phys. (2017) 8627918:1–6.

[11] E. Elbaz, *A geometrical approach to elementary particles*, Il Nuovo Cim. **63A** (1981) 257–320.

[12] H. Fröhlich, *Speculations on the masses of particles*, Nucl. Phys. **7** (1958) 148–149.

[13] M. Gell-Mann, *The eightfold way: a theory of strong interaction symmetry* (1961), California Institute of Technology Synchrotron Laboratory Report CTSL-20.

[14] A. E. Inopin, *Hadronic Regge trajectories in the resonance energy region*, hep-ph/0110160.

[15] E. L. Koschmieder, *The masses of the mesons and baryons. Part I. The integer multiple rule*, Bull. Class. Acad. Sci. Roy. Belg. **X** (1999) 281–283.

[16] Z. Kuramochi, *Mass distribution on the ideal boundaries of abstract Riemann surfaces. I*, Osaka Math J. **8** (1956) 119–137; II, Osaka Math. J. **8** (1956) 145–186.

[17] A. Landé, *Finite self-energies in radiation theory*, Part I, Phys. Rev. **60** (1941) 121–127.

[18] H. McManus, *Classical electrodynamics without singularities*, Proc. Roy. Soc. **A195** (1948) 323–336.

[19] Y. Nambu, *An empirical mass spectrum of elementary particles*, Prog. Theor. Phys. **7** (1952) 595–596.

[20] C. R. Nappi and B. A. Ovrut, *Supersymmetric extension of the* $SU(3) \times SU(2) \times U(1)$ *Model*, Phys. Lett. **B113** (1982) 175–179.

[21] S. Okubo, *Note on unitary symmetry in strong Interactions*, Prog. Theor. Phys. **27** (1962) 949–966.

[22] A. Sen, *Electric-magnetic duality in string theory*, Nucl. Phys. **B404** (1993) 109–126.

[23] P. K. Townsend, *The =eleven-dimensional supermembrane revisited*, Phys. Lett. **B350** (1995) 184–187.

[24] E. Witten, *String theory dynamics in various dimensions*, Nucl. Phys. **B443** (1995) 85–126.

**HADRONIC JOURNAL 47**, 329 - 352 (2024)
DOI 10.29083/HJ.47.03.2024/SC329


# DISCRETE TIME QUANTUM THEORY AND MARKOV ENVIRONMENTAL INFLUENCES AS PROBES TO THE COMPOSITE STRUCTURE OF ELEMENTARY PARTICLES

**C. Wolf**
Department of Physics
North Adams State College
North Adams, MA 01247 USA

## Abstract

The belief that the substratum has a discrete grainy-like structure at some small scale follows from the natural scale set by of the Planck length and the assumption that the concept of quantum correlations preceded any primitive notion of space and time. Dealing with the present formalism of quantum theory, it is possible to incorporate the notion of a discrete time interval into the theory through a discrete time difference amended Schrodinger equation. One of the consequences of such a theory is that it leads to discrete time corrections to spin precession frequencies and spin-flip frequencies that depend on the internal structure of composite particles. Thus the theory provides us with a potential probe to the composite structure of quarks, leptons, gauge bosons and Higgs particles. It is also possible that due to the environment a quantum system might be subject to Markov environmental influences that perturb a quantum system with an assumed Hamiltonian. In this case also it turns out that these Markov effects are sensitive to the internal structure of composite particles and thus provide a probe to compositeness. The following discussion suggests various models that may probe for both discrete time difference effects and Markov environmental influences. It is hoped that future precision measurements of spin-precession frequencies, spin flip frequencies as well as spectral shifts in atomic systems may lend support to these models.

P.A.C.S. - 03.65 - Quantum Theory, Foundations

Reprinted from: Gill, Tepper L., Editor, "*New Frontiers in Physics, Vol. II*" Hadronic Press, ISBN 1-57485-014-8, p. 51-75 (1996)

## 1. Introduction

The present theory of elementary particles has brought with it a degree of unification embodied in the presence of a gauge symmetry ($SU(3)_C$ X $SU(2)_L$ X $U(1)_Y$) along with the beautiful idea of gauge invariance leading to a calculable, renormalizable theory.[1] However, because of the presence of arbitrary Yukawa couplings to calculate fermionic masses and mixing angles as well as arbitrary values of coupling constants, vacuum angles and CP violating phases, the need for the number of free parameters is excessive (about 18).[2] Also the asymmetry created by the chiral structure of the weak interactions and the contrived Higgs sector to break the electroweak symmetry has prodded most theorists to believe that there has to be a more fundamental theory. Alternates to the standard model are G.U.T. unification leading to large fermion multiplets and fermion mass relations,[3] technicolor theory suggesting composite structure to the Higgs sector,[4] Supergravity embodied in SU(5) supergravity or SU(5) X U(1) supergravity[5] reducing the number of free parameters to 5 and 3 respectively, and superstrings with only a minimum number of free parameters leading to unification of gravity and particle interactions at or near the Planck scale.[6] The other attempt at unification involves the notion of compositeness suggesting that in analogy with atoms, nuclei and hadrons that all particles (quarks, leptons, gauge bosons and Higgs particles) have a finer layer of structure.[7] We also believe that at some scale the arena of space and time becomes discrete and grainy-like in structure. When a discrete quantum theory is imposed on a composite system, it turns out that certain measureables reveal the composite structure that otherwise would lie hidden beneath a quantum formalism embedded in the continuum. This is the primary purpose of the study, not to discuss the rigor or "lack of it" portrayed by the particular discrete quantum theory that we use,[8, 9] but rather to emphasize that independent of the formalism certain revealing features of composite particles emerge from a discrete quantum theory.

## 2. Discrete Time Quantum Theory and Elementary Particle Substructure

The motivation to study the composite structure of quarks, leptons, gauge bosons and Higgs particles emerges from the enormous success of SU(3) (Flavor) to describe the Hadron spectrum and the well known fact that all previous systems (atoms, nuclei, hadrons) reveal a composite structure.[10, 11] After the initial success of the standard model numerous composite schemes were proposed usually with a hypercolor binding mechanism to keep the preons together.[12, 13, 14, 15, 16, 17] Also since quarks and leptons are light relative to the composite scale (A ≈ 100 Gev) there must be a "chiral flavor" symmetry or supersymmetry protecting the quarks and leptons from acquiring large masses.[18] Two of the most popular composite models are the Rishon Model of Harari[19] and the scalar-fermion model by Fritzsch and Mandelbaum.[20] The Rishon model builds quarks and leptons out of three preon composites with only two fundamental preons T, V, $\left(T\left(q = \frac{1}{3}\right),\ V(q = 0)\right)$. The Fermion-scalar model considers a fermion doublet $\begin{pmatrix} q = \frac{1}{2} \\ q = -\frac{1}{2} \end{pmatrix}$ and two scalar bosons, one of charge $\frac{1}{6}$, the other of charge $-\frac{1}{2}$. The doublet coupled to the scalar boson of $q = \frac{1}{6}$ generating quarks, the doublet coupled to the scalar of $q = -\frac{1}{2}$ generates the

leptons. Higher generations add additional hypergluons. For the Rishon model higher generations are built by adding $(3T+3\overline{T})$ to each successive generation. It is clear from these two models also that the number of preons is generation dependent. To imprecise probes it would be difficult to probe for the number of preons, however if the internal dynamics of the preons (constituents of quarks, leptons and gauge bosons) is a discrete time quantum theory it turns out that observables calculated for the composite system will in the zeroth approximation yield the usual Q.M. values with corrections expressed in terms of a discrete time interval and composite parameters. If the discrete time interval is a random variable being the left over fragment of pregeometric "quantum correlations" then to calculate the discrete time interval for the composite system we can apply the central limit theorem expressing the composite discrete time interval in terms of a fundamental discrete time interval and the number of preons. For a spin precessing lepton[21] we have calculated the precession frequency in an external magnetic field, we find

$$\omega = \frac{4}{\tau}\sin^{-1}\left(E\tau\right) \tag{2.1}$$

when $E = \dfrac{e\hbar B}{2m}$

($\tau$ = discrete time interval).

Here the probability of up and down spin is equal at t = 0.

Eq. (2.1) gives

$$\omega \propto \frac{eB}{m} + \frac{e^3 B^3}{96 m^3} \tau^2 \qquad (2.2)$$

(e = charge of lepton, m = mass of lepton, B = z component magnetic field). If there are n preons in the lepton we have from the central limit theorem

$$\tau = n\tau_0, \quad (\tau_0 = \textit{fundamental discrete time interval})$$

and

$$\omega \propto \frac{eB}{m} + \frac{e^3 B^3}{9Ln^3}\left(n^2 \tau_0^2\right) \qquad (2.3)$$

Eq. (2.3) would give an $n^2$ dependence of the precession frequency. Thus measuring $\omega$ for different leptons would ascertain the number of preons in each lepton. We have also applied this idea to the decay of

$$(K_L, K_S), (B_S, B_L) - - - (X_L, X_S)$$

using a discrete time asymmetric quantum theory,[22] the result for the short and long level states is

$$\psi_{L,S} = \begin{pmatrix} a_1 \\ a_2 \end{pmatrix}_{L,S} e^{-\frac{2}{\tau}\sin^{-1}\left(\frac{E_{L,S}\tau}{2\hbar}\right)it} e^{-\frac{2(r_0)_{L,S}}{\tau}\left(\tan\frac{r_0\tau}{2}\right)\epsilon t} \qquad (2.4)$$

here

$$r_0 = -\frac{2}{\tau}\sin^{-1}\left(\frac{E_{o_{L,S}}\tau}{2\hbar}\right)$$

$\tau$ = discrete time interval,
$\epsilon$ = time asymmetry parameter.

Both $\tau$, $\epsilon$ should depend on the number of preons in the system (for instance $\bar{S}d$, $S\bar{d}$ ) and thus very precise measurements of the lifetime should reveal

$$\tau = n\tau_0,\ \epsilon = n\epsilon_0 \ or\ \tau = \sqrt{n}\tau_0,\ \ \epsilon = \sqrt{n}\epsilon_0,$$

The relations $\tau = \sqrt{n}\tau_0$, $\epsilon = \sqrt{n}\epsilon_0$ follow if $\tau$ and $\epsilon$ represent the width of a random distribution corresponding to n random variables. The relations $\tau = n\tau_0$, $\epsilon = n\epsilon_0$ follow if $\epsilon$, $\tau$ are the average over a random distribution of n random variables.

In addition to the above probes to discreteness and composite structure we have applied discrete time spin polarization precession to a spin one gauge boson with internal (2 preon composite) structure. The result was a combination of two sinusoidal functions

for the $<S_x>$ with the frequencies depending on the internal coupling parameters.[23] Also for elementary particles with internal dyon-fermion properties[24] and elementary particles with heavy preons moving in extra dimensions[25] within the composite particle we have calculated spin flip frequencies in an external magnetic field and demonstrated that they are sensitive to both the discrete time interval $\tau$ and the internal composite structure mentioned above. The models discussed in Ref. (21, 22, 23, 24, 25) all represent possible probes to both the discreteness of time and composite structure, though particular simplified systems were used the general ideas have far ranging applications.

## 3. Markov Environmental Effects on a Quantum System

In the famous paper of Einstein, Padolsky and Rosen[26] it was emphasized that quantum theory is incomplete and elements of reality were missing from the theory. Quantum theory is based on "subjective probability" while classical theory is based on objective determinism. Whatever interpretation of Q.M. one subscribes to [27, 28, 29, 30] we must reckon with the fact that whenever probability appears in the interpretation of the theory there may be a composite probability theory beneath the observable world or perhaps Markov processes adjoined to the normal laws of probability. In this regard we have assumed that the Schrodinger theory on the preon or substructure level is adjoined to Markov processes that represent environmental effects possibly generated by fluctuations of the space-time continuum related to the original pre-geometric origin of space-time.[31, 32, 33] As we will express below, Markov processes represent the correction to a continum Q.M. that a discrete non-causal world generate at the present stage of cosmic evolution. Perhaps in the very early primitive stages of cosmological evolution they were the dominant quantum effects operative before time became realized as a continuous variable. It might also be that the time scale set by an individual Markov jump might be different than

that of the usual time and thus two independent time-like variables would appear in the theory. As an example consider a spin ½ system

in a z component magnetic field with energy $E_{\pm} = \pm \frac{e}{2m}\hbar B$ , (q = -e)

The solution to the Schrodinger equation is

$$\Psi = C_1 \alpha e^{-\frac{iE_+ t}{\hbar}} + C_2 \beta e^{-\frac{iE_- t}{\hbar}} \tag{3.1}$$

Here $|C_1|^2 + |C_2|^2 = 1$ . If an addition to the Schrodinger dynamics we have a Markov process operative as described by the transition matrix

$$\begin{array}{c c} & \begin{array}{cc} + & - \end{array} \\ \begin{array}{c} + \\ - \end{array} & \begin{pmatrix} 1-q & q \\ p & 1-p \end{pmatrix} \end{array} \tag{3.2}$$

then after n steps if the initial probability of up is ½ and down is ½ we have[34]

$$\begin{aligned} P(+)_n &= \frac{p}{p+q} + (1-p-q)^n \left( \frac{1}{2} - \frac{p}{p+q} \right) \\ P(-)_n &= \frac{q}{p+q} + (1-p-q)^n \left( \frac{1}{2} - \frac{q}{p+q} \right) \end{aligned} \tag{3.3}$$

Here
$P(+)_n$ = probability of spin + ½ after n steps,
$P(-)_n$ = probability of spin - ½ after n steps.

Now in Eq. (3.1) we replace $C_1 = \sqrt{P(+)_n}$, $C_2 = \sqrt{P(-)_n}$,

we have

$$\Psi = \sqrt{P(+)_n}\, e^{-\frac{iE_+ t}{\hbar}} \alpha + \sqrt{P(-)_n}\, e^{-\frac{iE_- t}{\hbar}} \beta \tag{3.4}$$

giving

$$<S_x> = \hbar\sqrt{P(+)_n P(-)_n} \cos \frac{eB}{m} t \tag{3.5}$$

Then if $p \neq q$, the amplitude of $<S_x>$ has a certain chaotic behavior associated with n. Also we expect p, q to depend on B for high magnetic fields. For low magnetic fields we have $p = q$ and

$$<S_x> = \frac{\hbar}{2} \cos\left(\frac{eB}{m}\right) t \tag{3.6}$$

which is the usual expression for $<S_x>$. Thus a chaotic behavior of $<S_x>$ and a final state amplitude of

$$\hbar \sqrt{P(+)_n P(-)_n} \rightarrow \hbar \sqrt{\frac{pq}{(p+q)^2}}$$

would signal Markov environmental effects. If we have a spin 1

gauge boson
(q = -1) made of two preonic fermions, we have ($M_\omega$ = mass of gauge boson)

$$\Psi = C_1 \alpha\alpha e^{-\frac{iE_+ t}{\hbar}} + C_2 e^{-\frac{iE_0}{\hbar}t}\left(\frac{\alpha\beta+\beta\alpha}{\sqrt{2}}\right) + C_3 e^{-\frac{iE_-}{\hbar}t}\beta\beta \quad (3.7)$$

Here

$$H = \frac{e_p}{m_p}\left(S_{z_1}+S_{z_2}\right)B\begin{pmatrix} q_1 = -e_p \\ q_2 = -e_p \end{pmatrix}$$

where $|e_p| = \frac{e}{2}$, $m_{p_1} = m_{p_2} = \frac{M_\omega}{2}$ for the preons.

Also

$$E_+ = \frac{e}{M_\omega}\hbar B$$

$$E_0 = 0 \quad (3.8)$$

$$E_- = -\frac{e}{M_\omega}\hbar B$$

If we choose

$$\Psi = \sqrt{P(+)_n P(+)_n}\, e^{-\frac{iE_+}{\hbar}t}\, \alpha\,\alpha$$

$$+\left(\sqrt{P(+)_n P(-)_n}\,\alpha\,\beta + \sqrt{P(-)_n P(+)_n}\,\beta\,\alpha\right) e^{-\frac{iE_0}{\hbar}t} \tag{3.9}$$

$$+\sqrt{P(-)_n P(-)_n}\, e^{-\frac{iE_-}{\hbar}t}\, \beta\,\beta$$

(where again $P_{1,2}(+)_0 = \frac{1}{2}$, $P_{1,2}(-)_0 = \frac{1}{2}$ and both preons have same p, q, then $P(\pm)_n$ is same for preon 1 and 2) we find

$$< S_{x_1} + S_{x_2} > = 2\hbar \cos \frac{eB}{M_\omega} t$$
$$\times \left(\sqrt{P^3(+)_n P(-)_n} + \sqrt{P(-)_n^3 P(+)_n}\right) \tag{3.10}$$

If the preons are not the same we still must have

$$\mathrm{H} = \frac{e_1}{m_1} S_{z_1} B + \frac{e_2}{m_2} S_{z_2} B \tag{3.11}$$

where $\frac{e_1}{m_1} = \frac{e_2}{m_2}$ $(q_1 = -e_1,\ q_2 = -e_2)$ but $e_1 \neq e_2$, $m_1 \neq m_2$.

$\left(\frac{e_1}{m_1} = \frac{e_2}{m_2}\ \textit{is to insure that the } S_z = 0 \textit{ state has } E = 0\right)$

In this case we still have $\frac{e_1}{m_1} = \frac{e_2}{m_2} = \frac{e}{M_\omega}$ and

$$E_+ = \frac{e}{M_\omega}\hbar B$$

$$E_0 = 0 \tag{3.12}$$

$$E_- = -\frac{e}{M_\omega}\hbar B$$

however, the Markov process for preon 1 might have a different p, q than for preon 2 because it is seen different by B (external field). Thus we write

$$\Psi = \sqrt{P_1(+)_n P(+)_n}\, e^{-\frac{iE_+}{\hbar}t}\,\alpha\,\alpha$$

$$+\left(\sqrt{P_1(+)_n P_2(-1)_n}\,\alpha\,\beta + \sqrt{P_1(-)_n P_2(+)_n}\,\beta\,\alpha\right) e^{-\frac{iE_0}{\hbar}t} \tag{3.13}$$

$$+\sqrt{P_1(-)_n P_2(-)_n}\, e^{-\frac{iE_-}{\hbar}t}\,\beta\,\beta$$

at t = 0

$$P_1(+)_0 = P_2(+)_0 = \frac{1}{2},\ P_1(-)_0 - P_2(-)_0 = \frac{1}{2} \qquad (3.14)$$

and

$$<S_x>_0 = \Psi^+\left(S_{x_1} + S_{x_2}\right)\Psi = \hbar$$

however at $n \neq 0$, $t \neq 0$ we have

$$<S_x>_{n,t} = \Psi^+\left(S_{x_1} + S_{x_2}\right)\Psi \qquad (3.15)$$

giving upon using Eq. (3.13)

$$<S_{x_1} + S_{x_2}> = \hbar\begin{pmatrix} \sqrt{P_1(+)_n^2 P_2(+)_n P_2(-)_n} \\ +\sqrt{P_1(+)_n P_1(-)_n P_2(+)_n^2} \\ +\sqrt{P_1(-)_n P_1(+)_n P_2(-)_n^2} \\ +\sqrt{P_1(-)_n^2 P_2(+)_n P_2(-)_n} \end{pmatrix} \cos\frac{eB}{M_\omega}t \qquad (3.16)$$

here $P_1(+)_n$, $P_1(-)_n$ are given by Eq. (3.3) with $p = p_1$, $q = q_1$, and $P_2(+)_n$, $P_2(-)_n$ are given by Eq. (3.3) with $p = p_2$, $q = q_2$.

In Eq. (3.16) if $p_1 = p_2 = q_1 = q_2$

$$< S_{x_1} + S_{x_2} > \; = \hbar \cos \frac{eB}{M_\omega} t \tag{3.17}$$

which is the usual expression for a spin 1 gauge boson. In general $P_1(+1)_n$, $P_1(-)_n$, $P_2(+)_n$, $P_2(-)_n$ will vary with n, and B (external field). For low fields we expect the expression (Eq. (3.17)) to hold. For high fields, however, $p_1$, $q_1$, $p_2$, $q_2$ will depend on B. The experimental problem is to compare Eq. (3.16) with experimental measurements of $< S_{x_1} + S_{x_2} >$ for discrete steps (n). If the expression (Eq. (3.16)) fits the data better than Eq. (3.10) it would suggest a preonic substructure with different preons. If the formula (Eq. (3.10)) fits the data, it would suggest a preonic substructure with identical preons.

The above discussion has outlined probes to both the discrete nature of time induced by pre-geometric fluctuations from Minkowski space-time and fundamental Markov environmental corrections to Q.M. through discrete time quantum jumps specified by n. If we also set $t = n\tau_0$ in Eq. (3.16) then we relate the Markov time ordering process to the usual time order specified by t. In two previous studies[35, 36] we have outlined a variety of discrete time phenomena and Markov environmental processes and in the following two tables we summarize the predictions for each model for the average spin polarization with $< S_x >_{t = n = 0} = \frac{\hbar}{2}$ for fermions and

$< S_x >_{t = n = 0} = \hbar$ for bosons.

Table I

| | **Type of Theory** | **$<S_x>$ for spin ½ fermions ($q = -e$) ($P(+)_n$, $P(-)_n$ from Eq. 3.3)** | |
|---|---|---|---|
| 1 | Normal quantum theory with no Markov influence | $<S_x> = \frac{\hbar}{2} \cos \frac{eB}{m} t$ | (Ref. 35) |
| 2 | Discrete time difference Q.M. with no Markov influence | $<S_x> = \frac{\hbar}{2} \cos\left( \frac{4}{\tau} \sin^{-1}\left( \frac{eB\tau}{4m} \right) t \right)$ | (Ref. 35) |
| 3 | Normal quantum theory with Markov environmental influence | $<S_x> = \hbar\sqrt{P(+)_n P(-)_n} \cos\left( \frac{eB}{m} \right) t$ | (Ref. 35) |
| 4 | Discrete time difference Q.M. with Markov environmental influence | $<S_x> = \hbar\sqrt{P(+)_n P(-)_n}$ $\cos\left( \frac{4}{\tau} \sin^{-1}\left( \frac{eB\tau}{4m} \right) t \right)$ | (Present Study) |

5 Pure discrete time theory with no Markov environmental influence

$$<S_x> = \frac{\frac{\hbar}{2}(1-\phi)\cos\frac{eBt}{m} + \phi\frac{\hbar}{2}(-1)^n}{(1-\phi)+(-1)^n\phi\cos\frac{eBt}{m}}$$

$$(\phi = \epsilon_1 + \epsilon_2)$$

Ref. 35)

( $t \to \frac{n\tau}{2}$, $\epsilon_1$, $\epsilon_2$ are asymmetry parameters necessary to specify initial time solution)

## Table II

| **Type of Theory** | **$<S_x>$ for spin 1 gauge boson (q = -e) ($P(+)_n$, $P(-)_n$ from Eq. 3.3)** | |
|---|---|---|
| 1 Normal Q.M. behavior with no Markov environmental effects on 2 preon composite gauge boson (identical preons) | $<S_x> = \hbar\cos\frac{eB}{M_\omega}t$ | (Ref. 36) |
| 2 Normal Q.M. with Markov environmental effects on 2 preon composite gauge boson (identical preons) | $<S_x> = 2\hbar\cos\frac{eB}{M_\omega}t \left(\sqrt{P(+)_n^3 P(-)_n} + \sqrt{P(-)_n^3 P(+)_n}\right)$ | (Ref. 36) |

3 Normal Q.M. plus environmental effects on spin 1 gauge boson with no composite structure

$$<S_x> = \frac{\hbar}{\sqrt{2}} \cos \frac{eB}{M_\omega} t$$

$$\times \left[ 2\sqrt{P(+)_n P(0)_n} + 2\sqrt{P(-)_n P(0)_n} \right]$$

$P(+)_n$, $P(0)_n$, $P(-)_n$ = probability of +, 0 -, states calculated from Markov chain with initial probability of ¼ ½, ¼ respectively (Ref. 36)

4 Discrete time difference Q.M. with no Markov environmental effects (2 preon composite structure of gauge boson)

$$<S_x> = \frac{\hbar}{2} \cos(a_1 - a_3)t$$

$$+ \frac{\hbar}{2} \cos(a_3 - a_2)t$$

($a_1$, $a_2$, $a_3$ = parameters depending on internal state of two preon composite with $S_z$ = 1, 0, -1) respectively)

Ref. 36

5 Discrete time difference Q.M. with Markov environmental effects (2 preon composite structure of gauge boson with identical preons)

$$<S_x> = 2\hbar \left[ \sqrt{P(+)_n^3 P(-)_n} \cos(a_1 - a_3)t + \sqrt{P(-)^3 P(+)_n} \cos(a_3 - a_2)t \right]$$

Ref. 36

6. Normal Q.M. with Markov environmental effects on 2 preon composite, ("different preons")

$$\langle S_x \rangle = \hbar \begin{bmatrix} \sqrt{P_1(+)_n^2 P_2(+)_n P_2(-)_n} \\ +\sqrt{P_1(+)_n P_1(-)_n P_2(+)_n^2} \\ +\sqrt{P_1(-)_n P_1(+)_n P_2(-)_n^2} \\ +\sqrt{P_1(-)_n^2 P_2(+)_n P_2(-)_n} \end{bmatrix} \times \cos\frac{eB}{M_\omega}t$$

Here ($P_1(+)_n$, $P_1(-)_n$, $P_2(+)_u$, $P_2(-)_n$ are different for two different preons

Present Study

In Table I, row 2 would be a probe to both discrete time difference effects and the composite structure of leptons if $\tau = n\tau_0$. Row 3 in Table 1 would be a probe to Markov environmental effects on normal quantum mechanics. Row 4 would test for both discrete time difference effects and Markov environmental influences which may or may not include the relationship $\tau_{D.T.} = \tau_{Markov}$ (or the interval in discrete time difference effects may or may not be equal to the interval for Markov jumps). Row 5 in Table I would test for a pure discrete time (not discrete time difference theory) theory and predicts chaotic fluctuations in $\langle S_x \rangle$ as evidenced by the term $(-1)^n (\epsilon_1 + \epsilon_2)$.

Table II for row 2 and 3 would provide a test for the compositenss of a spin 1 gauge boson since the theory predicts distinctly different variations of $\langle S_x \rangle$ with n. Row 4 would provide a test for both discrete time difference effects and the composite structure of gauge bosons since $a_1$, $a_2$, $a_3$ are sensitive to the internal preon parameters. Row 6 would to provide a probe to test for Markov influences and the compositeness of gauge bosons with 2 different types of preons

comprising the substructure.

## 4. New Frontiers for Discrete Time Q.M.

As the discussion above has suggested, discrete time notions emerge from either pre-geometric theories of how the continuum evolved from a discrete set[37] or from a fundamental quantum uncertainty principle applied to space and time themselves.[38] Probing the discrete property of time might involve very high external fields or very rapid physical processes where deviations from the continuum may be seen. In addition to spin polarization precession, elementary particle decays[39] that have an "energy dependent width-energy relation" generated by discrete time effects may also be a probe to discreteness. In an unpublished note[40] I have emphasized that spin correlations of particles emitted in E.P.R. type (two particle correlation experiments) may also provide a sensitive probe to discrete time effects. Whenever short time intervals appear in physics whether in particle decays, resonance phenomena, tunnelling times etc. unaccountable corrections may be ascribed to Markov jump processes and discrete time phenomena in general. It is not in fashion at the present moment to suggest experiments that would probe the discrete nature of time simply because there are so many other uncertainties in Q.M. and particle theory in general. The existence of higher rank gauge groups, of supersymmetry and coupling constant variations all would generate corrections to particle life-times and decay asymmetries that experimental deviations from the Standard model would be more apt to be identified with. This is because of the present "disposition" enjoyed by contemporary physics. However, the history of physics is filled with examples where a new and stunning discovery came at a time when popular belief seemed to discourage it. Such examples include the discovery of special relativity, the breakdown of parity conservation and the explanation of the Planck radiation law in terms of new and radical quantum ideas. In Einstein's famous book

he stresses[41] "that the continuum has legitimacy in that it "serves to represent the complex of our experience", he also points out that any absolute attachment to the notion of continuum physics has no justification since it is based on notions outside of our experience. It is known that special relativity is violated by discrete physics,[42] but gauge invariance is not. Gauge theories might be the accidental result of physics observed in the range (10 TeV > E) emerging from the local invariance under a gauge group of a multiplet of fermions. D. Park has reminded me of the fact that Feynman diagrams and even "gauge invariance" are in a certain sense only valid in perturbation theory.[43] What about the case when photons and electrons are inseparable, or quarks and gluons are inseparable, doesn't something deeper have to replace Q.E.D., Q.C.D. and U(1) and $SU(3)_C$ invariance. Perhaps in this "as yet" unexplored domain new concepts of space and time will emerge.

I'd also like to point out that within the theory of the "Thermodynamics of Irreversible Processes"[44] a discrete correlation time is discussed that in some sense represents the "time scale" for the principle of microscopic reversibility to hold. This correlation time must be bigger than the characteristic molecular interaction time and less than the characteristic time for the decay of fluctuations. Using this analogy, perhaps the discrete time interval in quantum theory is a measure of the time scale for interaction between the particle and the background, being greater than the preon-preon interaction time and less than the decay time for fluctuations from the Minkowski background. Quantum random walks,[45, 46,] Quantum Theory on graphs,[47] the quantization of discrete classical systems[48] and the search for a discrete graphical picture of pregeometry[49, 50] all represent pioneering attempts to model the world from a discrete set of primitive objects. Although there has been a sentiment against modelling Q.M. by Markov processes[51] I feel the systems chosen are to naive to draw any final conclusions regarding the underlying probability laws governing

Quantum theory. To this day, It think it is fair to say that quantum theory is still a theory of "subjective probability", the idea of a pregeometric world with quantum correlations more fundamental than space and time offers[52] us both a more fundamental picture of space and time along with an explanation of how fluctuations from the "present" continuum can be interpreted in terms of discrete time effects. Let us with a spirit of faith look for instances where unexplained corrections to standard physics may be explained by discrete physics, thus revealing a new mathematical and physical picture of the world.

## Acknowledgement

I'd like to thank the Physics Departments at Williams College and Harvard University for the use of their facilities. I'd also like to thank Dr. Santilli for his warm hospitality in extending me the opportunity to speak at this conference.

## References

1. I. J. R. Aitchison and A. J. G. Hey, Gauge Theories in Particle Physics (Adam Higler Ltd., Bristol, 1982).

2. D. C. Cheng and G. K. O'Neil, Elementary Particle Physics (Addison Wesley, Reading, Mass. 1979).

3. H. Georgi and S. Glashow, Phys. Rev. Lett. 32, 438 (1974).

4. S. Weinberg, Phys. Rev. D 13, 974 (1976).

5. E. W. Kolb and M. S. Turner, The Early Universe (Addison-Wesley Pub. Comp. N.Y. 1990), p. 28.

6. P. Candelas, E. T. Horowitz, M. Strominger and E. Witten, Nucl. Phys. B 258, 46 (1985).

7. L. Lyons, Prog. in Particle and Nucl. Phys. (Vol. 10) (Pergamon Press, NY, 1983), p. 254.

8. C. Wolf, Phys. Lett. A, 123, 208 (1987).

9. C. Wolf, Il Nuovo Cimento Note Brevi B 100, 431 (1987).

10. D. B. Lichtenberg, Unitary Symmetry and Elementary Particles (Accademic Press, NY, 1978) p. 157.

11. L. Lyons, Prog. in Particle and Nucl. Phys. (Vol. 10) (Pergamon Press, NY, 1983) p. 229.

12. A. A. Ansel'n J.E.T.P. 53, 23 (1981).

13. H. Harari and N. Seiberg, Phys. Lett. 98B, 269 (1981).

14. R. Barberi, R. N. Mohapatra and A. Mussiero, Phys. Lett. 105B, 369 (1981).

15. I. Montvay, Phys. Lett. 95B, 227 (1980).

16. R. Casalbuoni and R. Gatto, Phys. Lett. 100B, 135 (1981).

17. I. Bars, Phys. Lett. B 106, 105 (1981).

18. I. Bars, Proc. of XXIII Int. Conf. on High Energy Phys., 16-23 July, 1986, Berkley Calif. (World Scientific, Singapore, 1987).

19. H. Harari, Phys. Lett. B 86, 83 (1979).

20. H. Fritzsch and G. Mandelbaum, Phys. Lett. 102B, 319 (1981).

21. C. Wolf, Hadronic J. 13, 22 (1990).

22. C. Wolf, Hadronic J. 11, 227 (1988).

23. C. Wolf, Annales de la Foundation Louis de Broglie, 18 (No. 4), 403 (1993).

24. C. Wolf, Annales de la Foundation Louis de Broglie, 15 (No. 4), 487 (1990).

25. C. Wolf, Hadronic J. 14, 321 (1991).

26. A. Einstein, B. Padolsky and N. Rosen, Phys. Rev. 47, 777 (1935).

27. L. E. Ballentine, Rev. Mod. Phys. 42, 358 (1970).

28. H. P. Stapp, Am. J. of Phys. 40, 1098 (1972).

29. H. Everett, J. A. Wheeler, B. S. DiWitt, L. N. Cooper, D. van Vechten and N. Graham, Many Worlds Interpretation of Q.M., ed., B. S. De Witt and N. Graham (Princeton Univ. Press, Princeton, N.J., 1973).

30. C. Philippidis, C. Dewdney and B. J. Hiely, Il Nuovo Cimento 52, 15 (1979).

31. J. Wheeler, Chap in Quantum Theory and Gravitation, Proc. of a symposium held at Loyola Univ., New Orleans, May 23 - 26, 1979 (Academic, NY, 1980).

32. D. Finkelstein, Int. J. of Theoretical Physics 27 (No. 4), (1985), 473.

33. T. D. Lee, Phys. Lett. 122B, 217 (1983).

34. P. G. Hoel, S. C. Post and C. J. Stone, Intro. to Stochastic Processes (Houghton Mifflin Comp., Boston, 1972), p. 3.

35. C. Wolf, Fizika B3(1), 9 (1994).

36. C. Wolf, submitted to Fizika B. (May 1995).

37. L. Bombelli, J. Lee, D. Meyer and R. Sorkin, Preprint IA-SSNS-HEP-87/23, Inst. of Advanced Study, Princeton, NJ (1987).

38. E. Recami, personal communication at Fourth Workshop on Hadronic Mechanics and Non-Potential Interactions, 22-26 August 1988, Skopje,

Yugoslovia.

39. C. Wolf, Proc. of Fourth Workshop on Hadronic Mechanics and Non Potential Interactions, 22-26 Aug. 1988, Skopje, Yugoslavia (Nova Science Pub. NY 1990), p. 283.

40. C. Wolf, unpublished work (1995).

41. A. Einstein, The Meaning of Realtivity (Princeton University Press, Princeton, NJ, 1955), p. 2

42. N. H. Christ, R. Friedberg and T. D. Lee, Nucl. Phys. B 210, 310 (1982).

43. D. Park, personal communcation (1995).

44. S. R. De Groot, Thermodynamics of Irreversible Processes (North Holland Pub. Comp., Amsterdam, 1951).

45. S. Majid, Int. J. of Mod. Phys. A. 8, 4521 (1993).

46. O. Bang, J. J. Rasmussen and P. L. Christiansen, Physica D 68, 169 (1993).

47. J. Gratus, C. J. Lambert, S. J. Robinson and R. W. Tucker, J. Phys. A 27 (No. 20), 6881, 1994.

48. M. Razavy, Hadronic J. 12 (No. 5), 515 (1994).

49. F. Antonsen, Int. J. of Theoretical Phys. 33 (No. 6), 1189 (1994).

50. A. V. Evabo, Int. J. of Theoretical Phys. 33 (No. 7), 1553 (1994).

51. D. J. Gillespie, Phys. Rev. A 49 (No. 3), 1607, 1994.

52. W. Wootters, Int. J. of Theoretical Phys. 23, 701 (1984).

**HADRONIC JOURNAL 47**, 353 - 380 (2024)
DOI 10.29083/HJ.47.03.2024/SC353 

# THE ART GALLERY OF THE QUANTUM INVERSE PROBLEM

**V. M. Chabanov[1], B. N. Zakhariev[1]**
(All pictures of this report were prepared in collaboration with S. Brandt*, H. D. Dahmen* and T. Stroh*)
* Fachbereich Physik, Universitat Siegen, 57068 Siegen, Germany
[1] Laboratory of Theoretical Physics
Joint Institute for Nuclear Research
Dubna, 141980, Russia

## Abstract

The inverse problem is "the second half" of quantum mechanics which is not widely known yet. The pictures illustrating the fundamental interrelations of spectral and scattering parameters with the details of potential perturbations are presented here. We unify the technique of the exactly solvable models, program INTERQUANTA that proved itself very useful in the picture demonstrations of the direct problem, and the original qualitative theory explaining quantum systems by splitting the observables and potential perturbations in elementary and universal constituents ("atoms, bricks").

Reprinted from: Gill, Tepper L., Editor, "*New Frontiers in Physics, Vol. II*" Hadronic Press, ISBN 1-57485-014-8, p. 171-198 (1996)

## INTRODUCTION

The approach of the inverse problem theory and supersymmetrical quantum mechanics provides potential perturbations that cause changes of any chosen spectral parameters (SP) (without altering other ones). The new language [1-4] that allows universally and concisely explains these potential perturbations opens the way to new success in theory and applications.

The new pictures of the shifts of arbitrary energy levels on the energy scale and corresponding transformations of potentials and wave functions are given here. It is done for different initial potential wells (of finite and infinite depth, of different shapes): rectangular, oscillator, and multi-step-type. Particularly, we shall present the amazing phenomenon of effective annihilation of states by degeneration of neighboring energy levels [5].

The reader will get a clear notion about the significance of the fundamental spectral parameters (weight or norming factors) which together with energy levels form the complete set for one-dimensional systems with the purely discrete spectrum. The physical sense of these parameters is that each of them relating to a proper bound state serves as a lever controlling the region of the main spatial localization of the corresponding state.

In addition to the already published [1-4] pictures illustrating the construction of quantum systems with the desired properties it has sense to show here more perfect and instructive figures that were derived by the INTERQUANTA technique which was elaborated by the creation of picture books of quantum mechanics [6]. We shall give also explanations of every partial flexure (sages and arches) of the corresponding potential perturbations and mention some open problems.

## SHIFTS OF LEVELS IN SQUARE WELLS (infinite and finite),

There are simple rules of spectral management. The potential perturbation which shifts only the chosen energy level up (or down) must have repulsive hills (attractive wells) in the vicinity of local maxima modulo of the corresponding wave function (where the eigenstate is the most sensitive to perturbations). And there must be compensating potential wells (hills) near the knots of the wave function which keep all other energy levels at the previous positions. The main corresponding formulae are given in Appendix I.

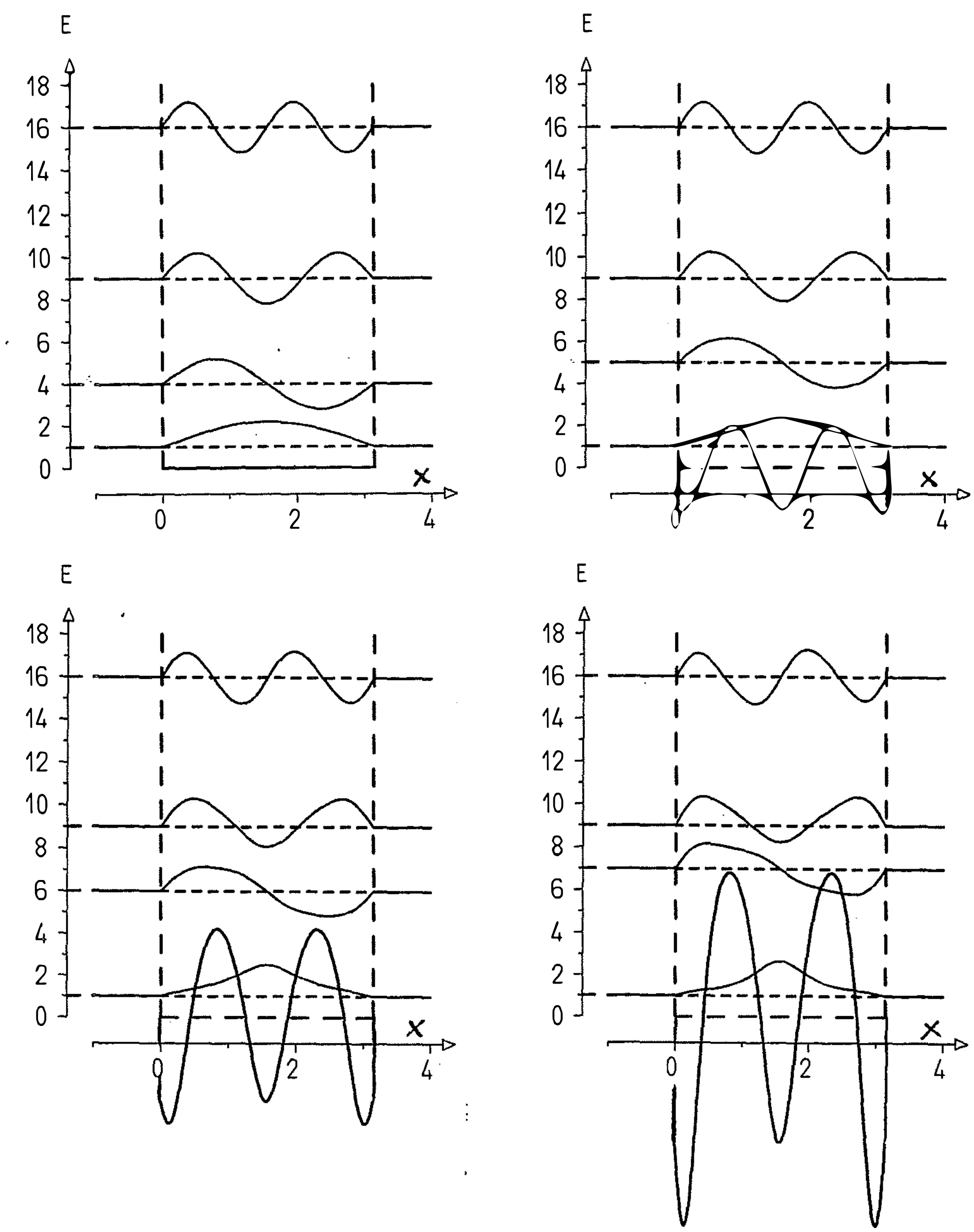


Fig.1a. Gradual shifts up of only the second energy level: $\Delta E_2 \equiv t = 0,\ 1,\ 2,\ 3$ in the infinite rectangular well. Transformations of the four lower bound states and of the flat bottom of the initial potential are shown.

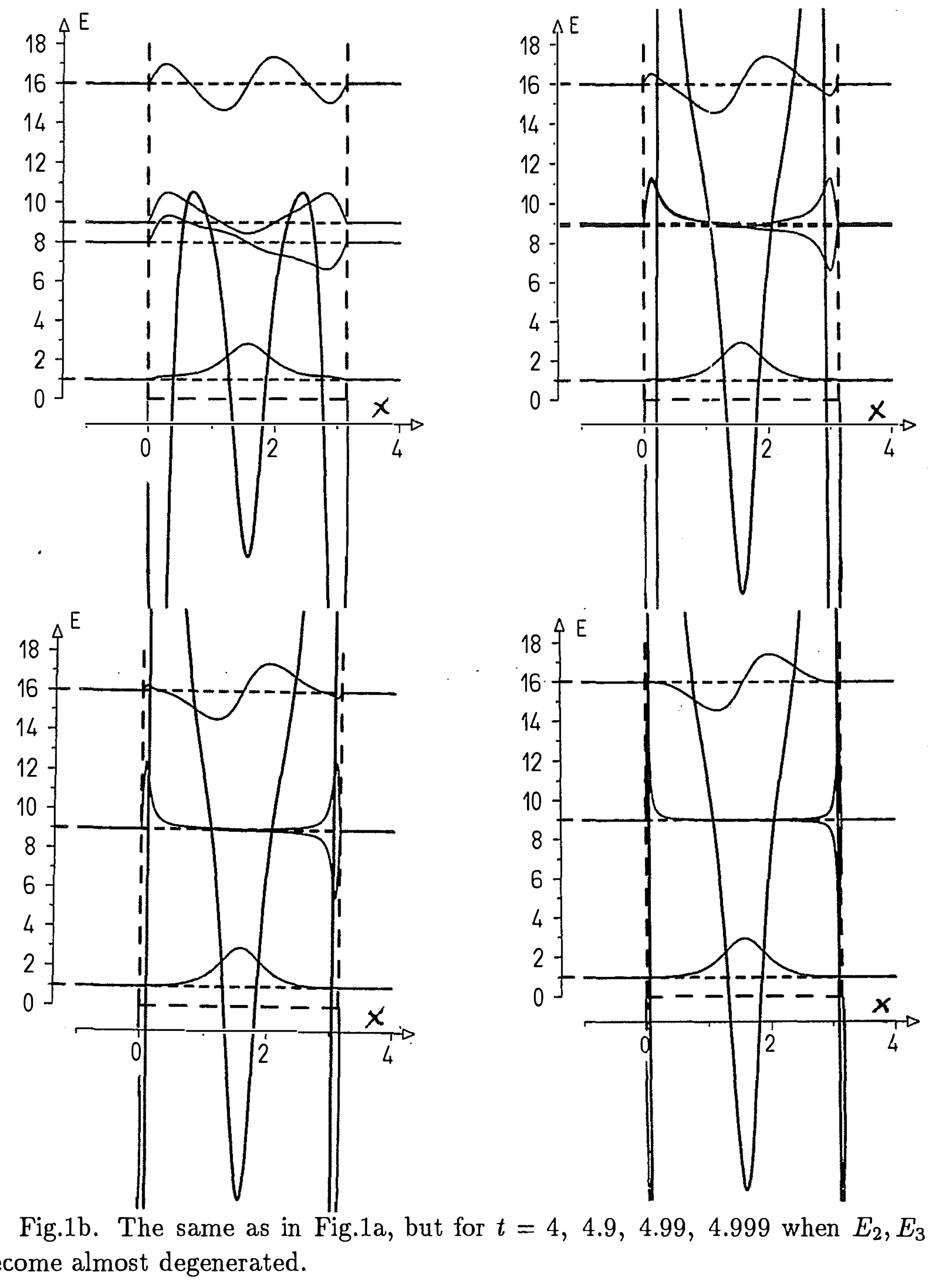


Fig.1b. The same as in Fig.1a, but for $t$ = 4, 4.9, 4.99, 4.999 when $E_2, E_3$ become almost degenerated.

In Fig.1 the gradual deformations of the infinite rectangular potential well of the width $\pi$ and corresponding eigenfunctions are shown in the process of approaching of the second energy level $E_2$ to the third one. The parameter of the energy shift $\Delta E_2 \equiv t$ is gradually changed from $t = 0$ (unperturbed system) to $t = 4.999$ (the case of almost fulfilled degeneration of the energy levels $E_1 \longrightarrow E_2$).

The shape of the potential perturbation has two repulsive hills. At the beginning these hills push the chosen second state near the maxima modulo of $\psi_2(x)$ where this state is the most sensitive to potential perturbations. The three wells of the potential perturbation near the knots of $\psi_2(x)$ are necessary for the compensation of the influence of the potential hills on the other energy levels that must remain at the previous positions. It is possible to shift only one chosen energy level (keeping an infinite number of all other at the same places !) because all eigenstates are orthogonal to one another. The states above the degenerating pair "lose" gradually the half-oscillations from both sides as can be seen for the fourth state in Fig.1b with t=4.9; 4.99; 4.999. When the neighbor energy levels become very close, the degenerating states must simultaneously be orthogonal and similar to one another as the solutions of the same equation at almost the same energy. These contradictory requirements can be satisfied if both states disappear in the middle part of the system. The wave functions are divided into two parts being gradually pressed into the infinite potential walls of the original well. These two parts look more and more like one another by modulus for both the degenerating states as the solutions of the same equation at approximately the same energy.

If a wave packet is as a sum of the degenerating states (second and third) it will be concentrated at the left wall where $\psi_2(x)$ and $\psi_3(x)$ have the same sign and disappear at the right wall where they cancel one another. Taking into account the time dependent phase factors $\exp(-iE_{2,3}T)$ we can see that there accumulates a phase discrepancy between the two states during some time. Therefore the neighbor states change their relative sign and the wave packet disappears at the left and concentrates at the right wall. And so the packet will "jump" from one wall to the opposite one through the barriers and the middle well (without appearing even in the classically allowed region).

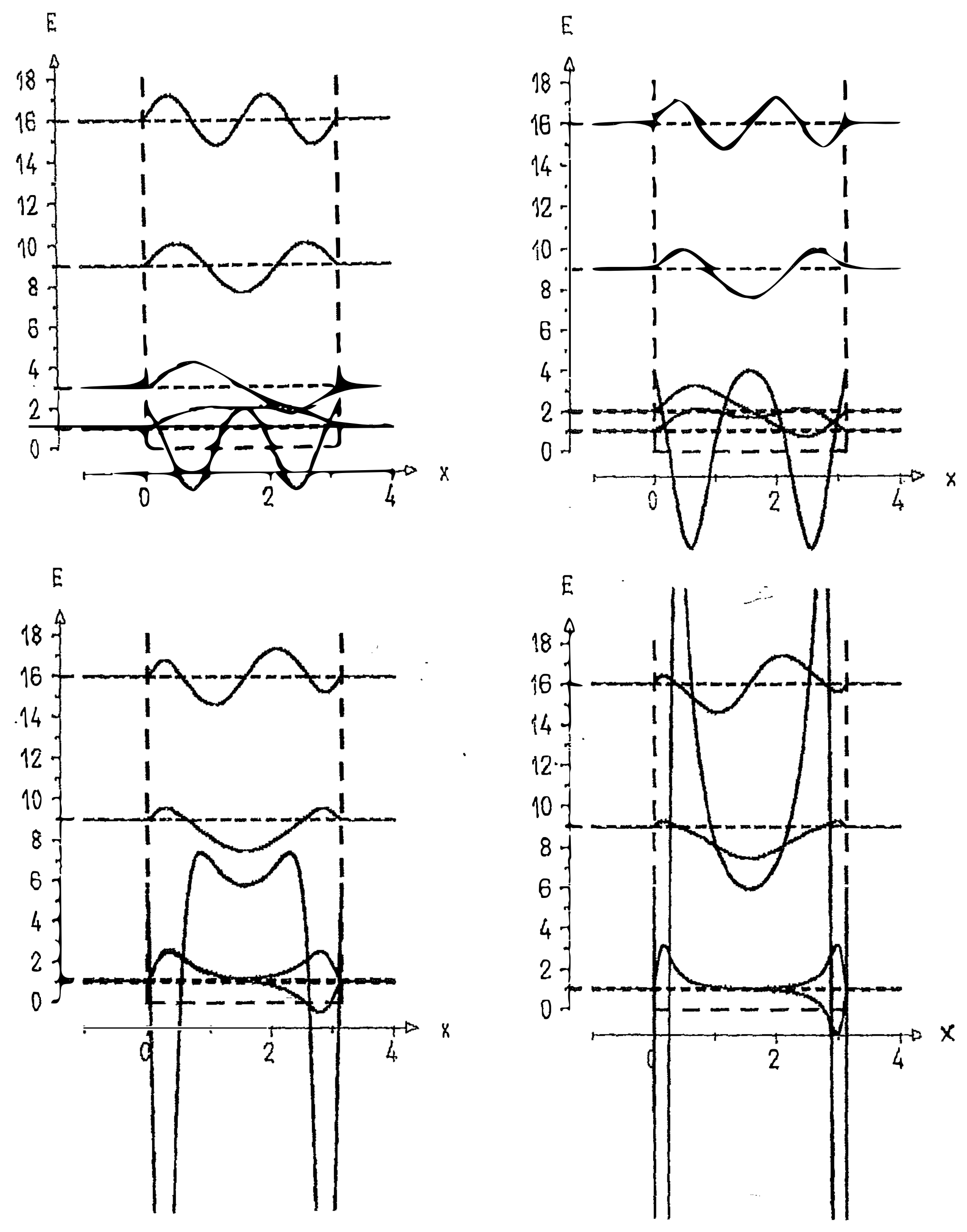


Fig.2. Gradual shifts down of only the second energy level: $\Delta E_2 \equiv t = -1,\ -2,\ -2.9,\ -2.99$ in the infinite rectangular well.

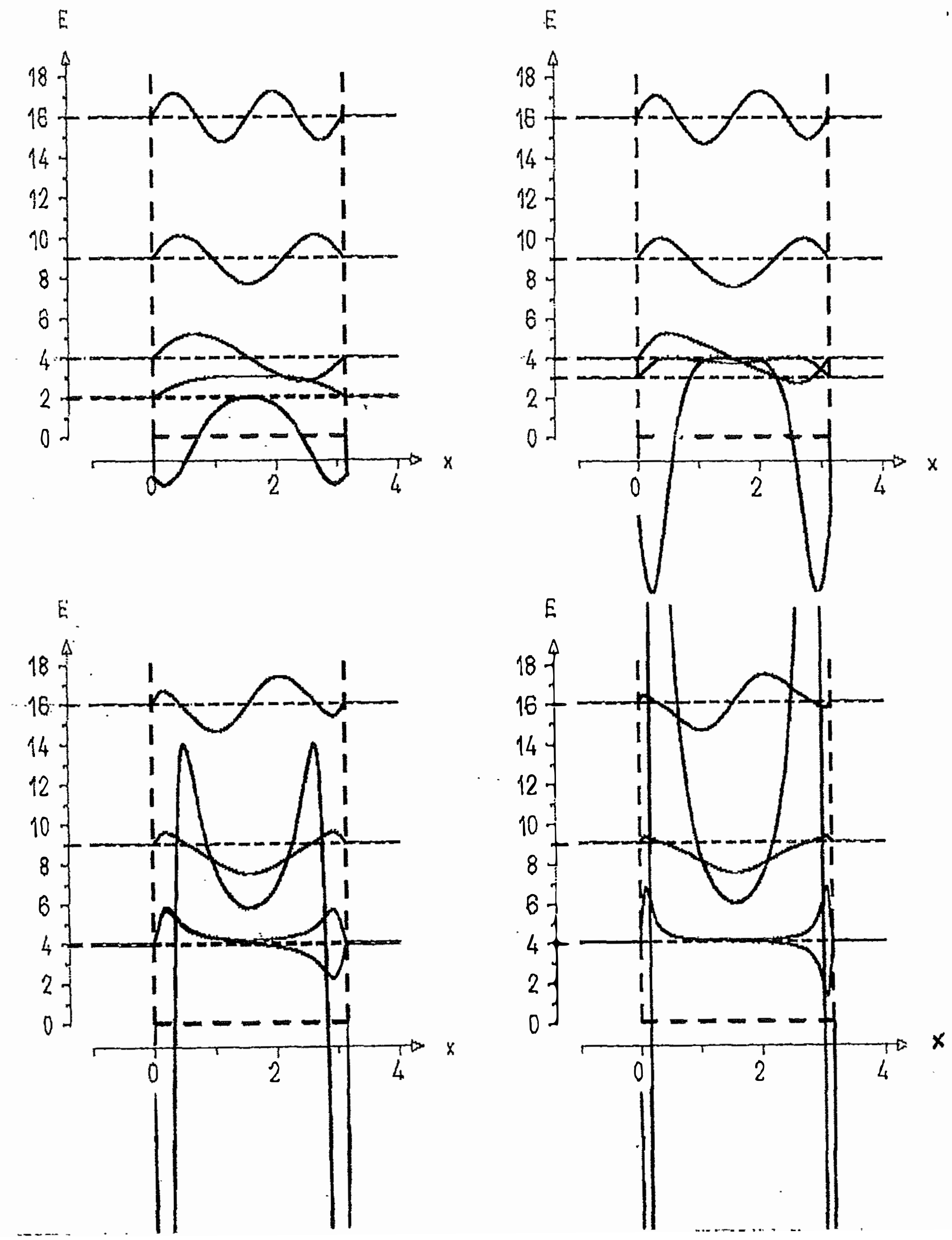


Fig.3. Gradual shifts up of only the ground state energy level: $\Delta E_1 \equiv t = 1,\ 2,\ 2.9,\ 2.99$ in the infinite rectangular well.

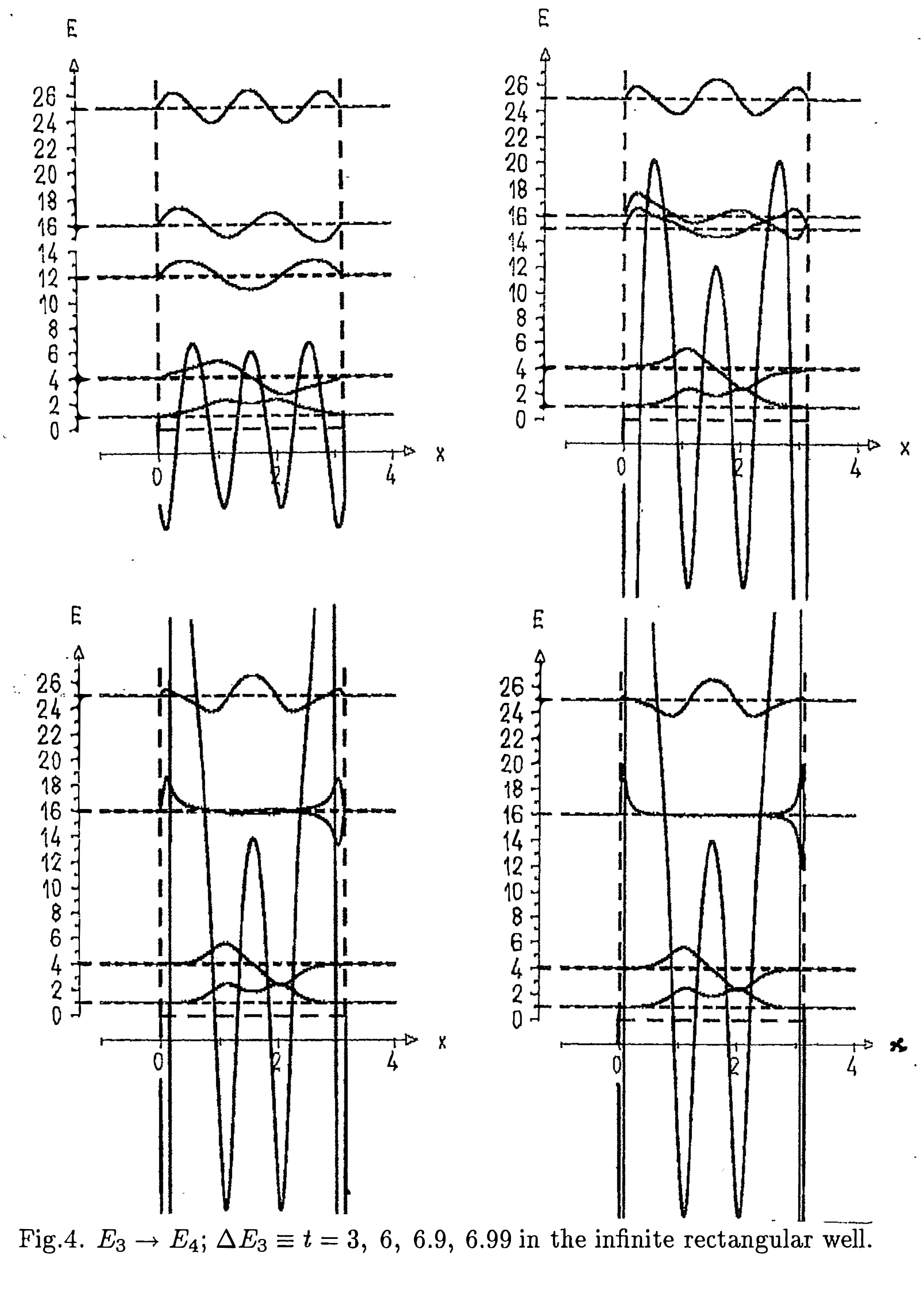


Fig.4. $E_3 \to E_4$; $\Delta E_3 \equiv t = 3,\ 6,\ 6.9,\ 6.99$ in the infinite rectangular well.

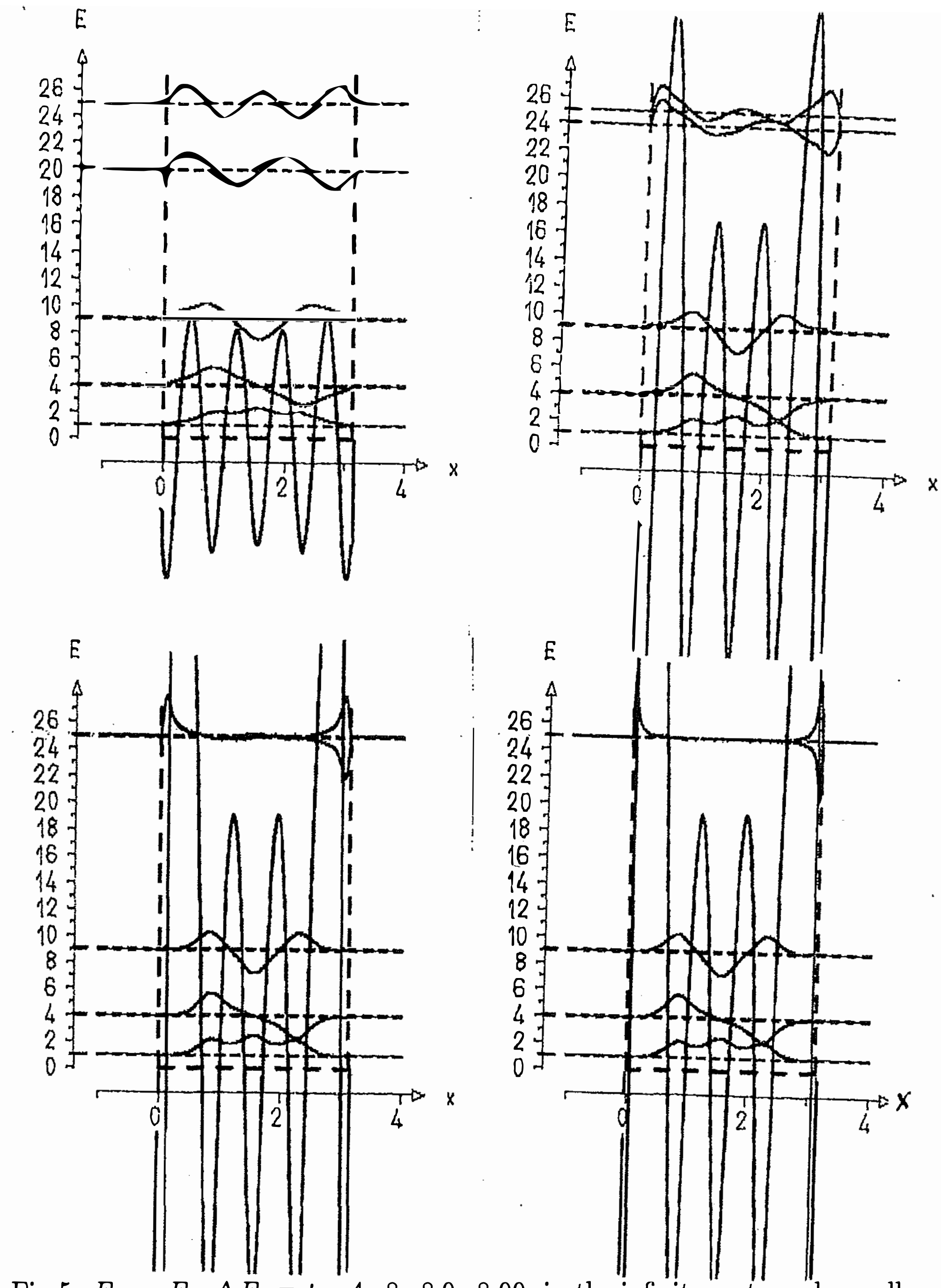


Fig.5. $E_4 \to E_5$; $\Delta E_4 \equiv t = 4,\ 8,\ 8.9,\ 8.99$ in the infinite rectangular well.

Transformations of the infinite rectangular potential well of the width $\pi$ and corresponding eigenfunctions by shifting $E_2 \to E_1$ is shown in Fig.2. There are two wells to pull the second state down where it has maximal probability to find the particle (wave) and auxiliary repulsion in the middle to keep other levels at their previous states. The repulsion in the middle stops increasing when $\psi_2(x)$ and $\psi_3(x)$ become negligible there. So, the middle repulsive hill becomes two-humped.

Fig.3 corresponds to the shift $E_1 \to E_2$ with the repulsive potential perturbation in the middle region and compensating wells near the vertical potential walls where the ground state is small. Again the middle repulsion becomes gradually two-humped.

Pay attention to the fact that the limiting shapes of the perturbation in the middle are the same in both Figs.2,3. After the effective annihilation of $E_2$ and $E_1$ all other states form a new complete set of eigenstates. And the place where degeneration of the disappeared levels occurs (below $E_3$) is of no importance for other states – we get the same middle well. Compare its form with the middle well in Fig.1b. The bottom of the well for the remaining upper states must be higher. The states above the degenerating pair "lose" gradually half-oscillations from both sides as can be seen for the third and fourth states in the Figs. with t=2.9; 2.99.

In Fig.4 the transformations of the infinite rectangular potential well of the width $\pi$ and corresponding eigenfunctions while shifting $E_3 \to E_4$ are shown. Gradually with decreasing $\psi_3(x)$ and $\psi_4(x)$ in the middle region the central potential spike cease to rise (becomes relatively lower: there is no need to push the state stronger where it becomes not sensitive). The same qualitative rule requires three repulsive potential hills to push up only the third energy level (and four auxiliary wells to keep all other levels at their previous places). The second potential peak stops to grow when the 3rd and the 4th states become small in the middle. The shapes of the limiting potentials for the cases $E_3 \to E_4$ and $E_4 \to E_3$ must be the same except the singular behavior at boundary points $x = 0$ and $x = \pi$. There are confined degenerate states in infinite narrow wells behind the infinite high barriers.

In Fig.5 the transformations of the infinite rectangular potential well of the width $\pi$ and corresponding eigenfunctions in the process of shifting $E_4 \to E_5$ are shown. Explanation is qualitatively analogous to that of Figs above.

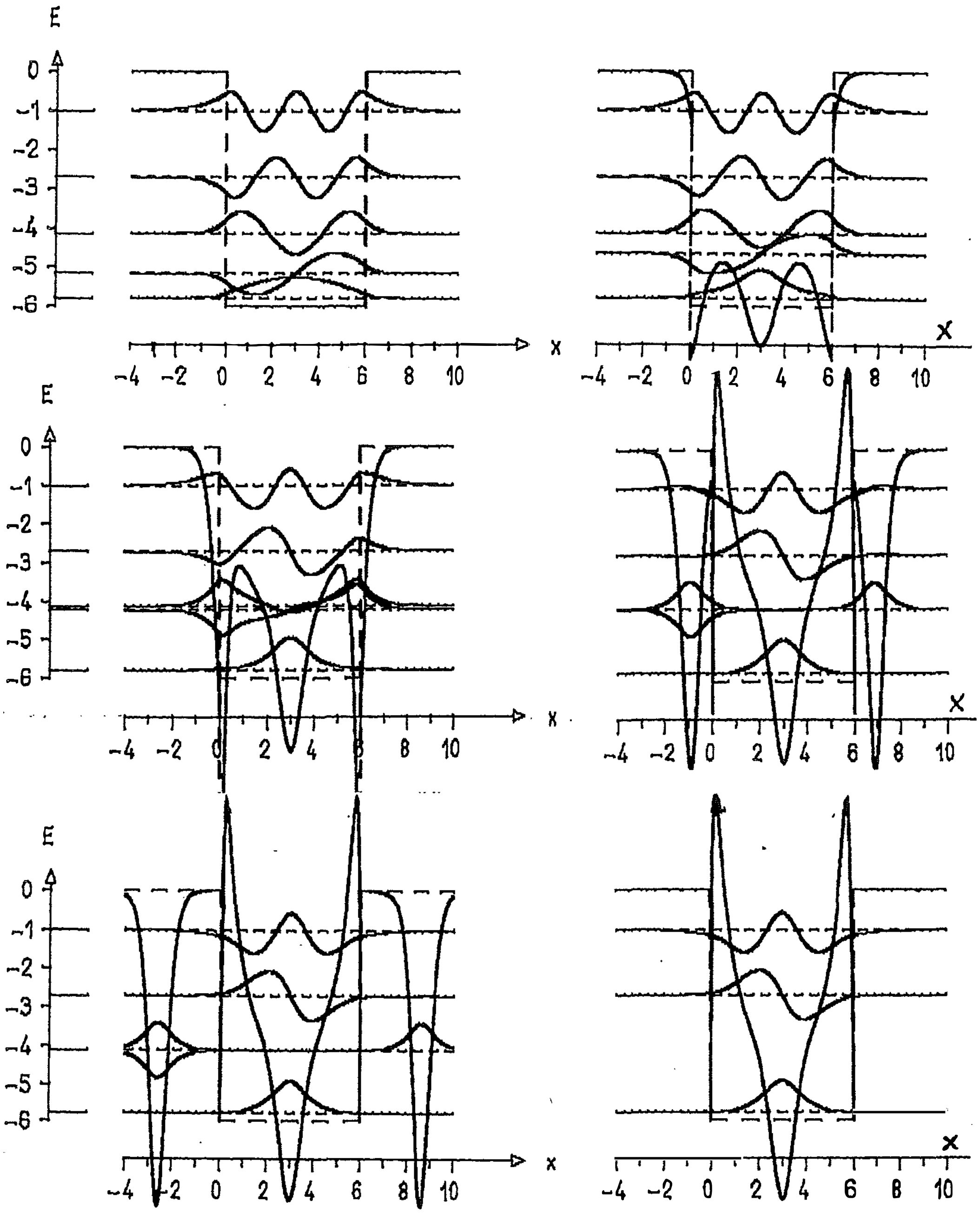


Fig.6. $E_2 \to E_3$; $t \equiv \Delta E_2/(E_3 - E_2); t = 0; 0.5; 0.9; 0.999; 0.999999; 1$ in the finite well.

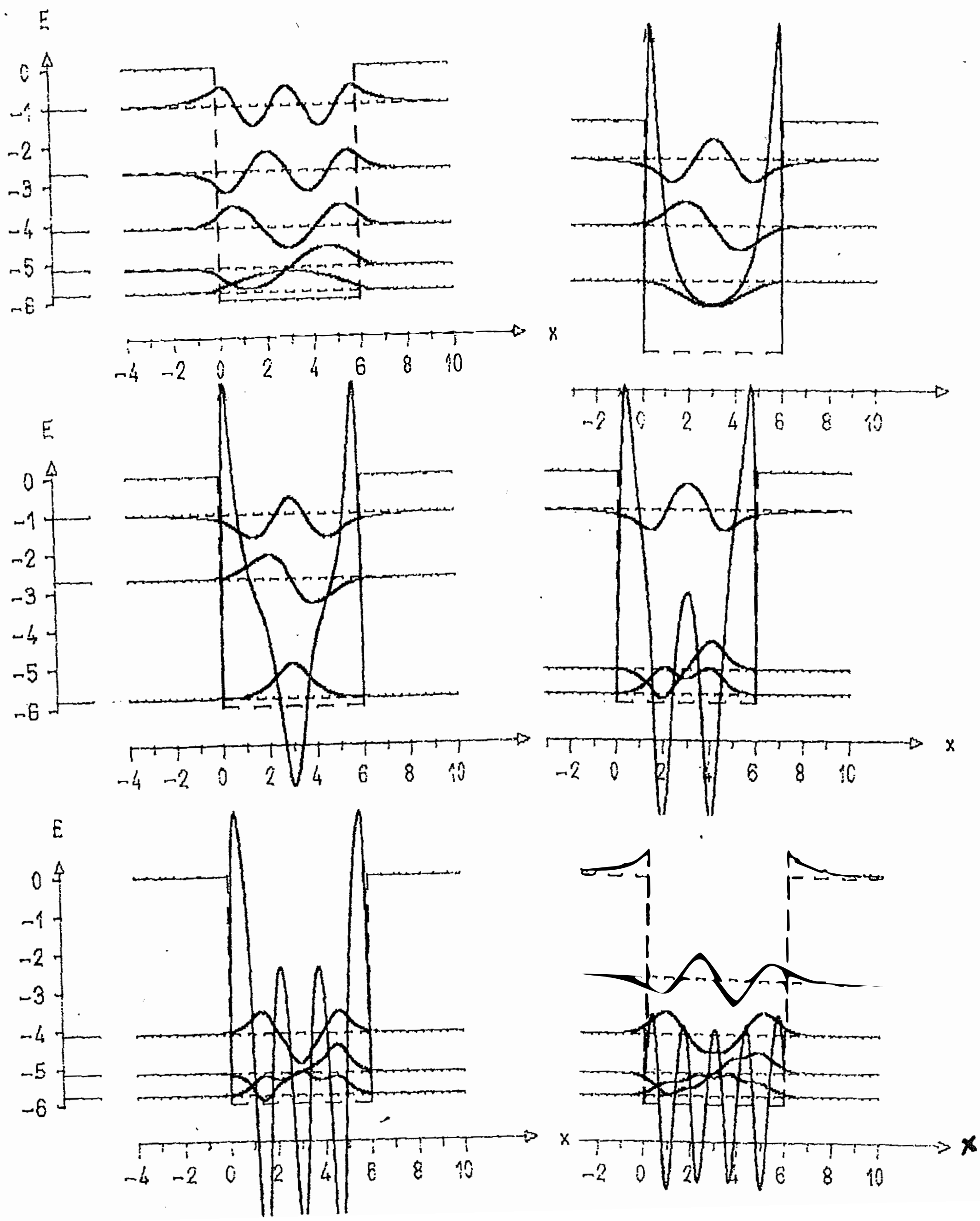


Fig.7. $E_n \rightarrow E_{n+1}$; $\Delta E_n/(E_{n+1} - E_n) \equiv t$: $n = 1, t = 0$; $n = 1, t = 1$; $n = 2, t = 1$; $n = 3, t = 1$; $n = 4, t = 1$; $n = 5, t = 1$ in the finite well.

In Fig.5 there are four potential perturbation hills which push the fourth energy level up and five compensating auxiliary wells. The two potential peaks in the middle stop to grow when the 4th and the 5th states become small in the middle. As has been mentioned above, the shapes of the limiting potentials for the cases $E_4 \rightarrow E_5$ and $E_5 \rightarrow E_4$ must also be the same except the slightly different singular behavior at boundary points (to provide the finite shift of the degenerated energy levels).

The qualitative difference of the shapes of the limiting potentials in Figs 1-5 can be explained according to the universal algorithms of symmetrical shifting of states in the new complete spectra after annihilation of the degenerated states.

For finite potential wells the wave motion in the bound states is not restricted to the finite interval. Fig.6 shows: the deformation of the finite rectangular potential well of the width 6 and depth $V_0 = -6$ and corresponding bound state eigenfunctions in the process of approaching of the second energy level $E_2$ to the third one without changing the reflection coefficients of the scattering states. The degenerating states have here the possibility to separate exactly from one another by going to $\pm\infty$ in the opposite directions. They are carried away by the auxiliary reflectionless soliton-like wells (in order to prevent changing the reflection features of all the states of the continuum spectrum when they are moving away). Also the peaks appearing at the edges of the initial rectangular well preserve the scattering (reflective) features of the initial potential steps which have been smoothed by the degeneration. In Figs 7 and 8 the deformation of the finite rectangular potential well of the width 6 and depth $V_0 = -6$ and corresponding bound state eigenfunctions are shown for $E_1 \rightarrow E_2$; $E_2 \rightarrow E_3$ ; $E_3 \rightarrow E_4$; $E_4 \rightarrow E_5$; $E_5 \rightarrow 0$ ; $E_1$ going down without changing the reflection coefficients. The value $t = 1$ for $n = 5$ corresponds to the upper bound state lifted to the continuous spectrum. The value $t = -1; n = 1$ corresponds to the ground state at the bottom of the initial well.

Pay attention to the different shapes of these peaks in Figs 6,7 and Fig.8. Compare the transformations of potentials inside the interval [0,1] for the infinite and finite initial wells.

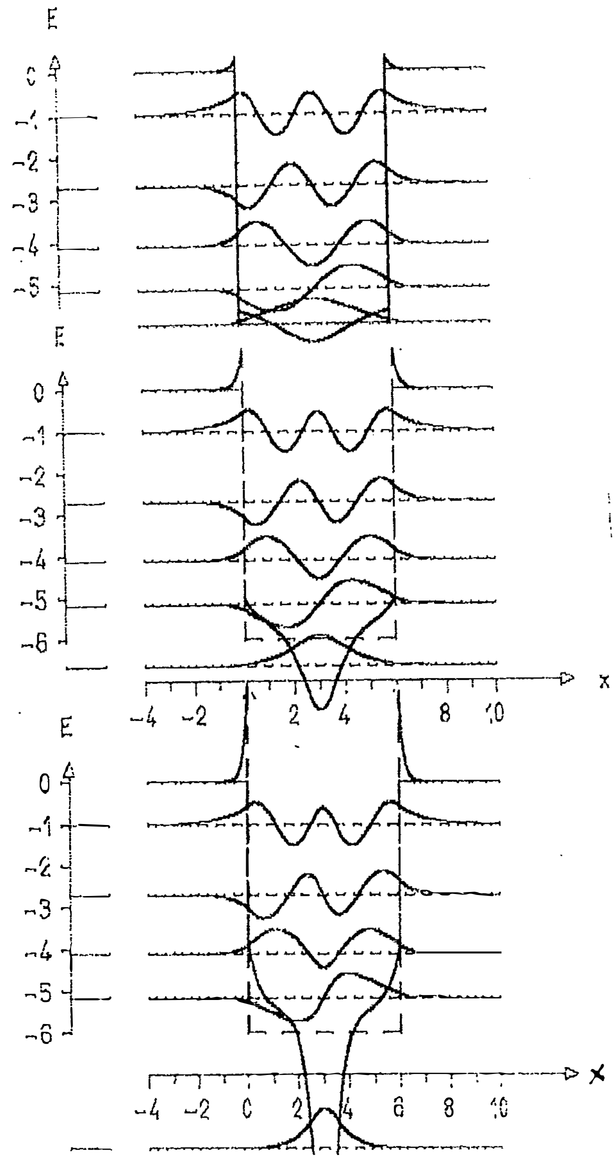


Fig.8. Symmetrical transformations of square potential having finite depth and of corresponding wave functions of all five bound states. when only the ground state energy level is shifted down and all other states remain with the same spectral and scattering parameters. a) $E_1 \to 0$; b) $E_1 \to -4E_1$; c) $E_1 \to -14E_1$. Pay attention to the difference in shapes of the peaks at the ends of the initial well here and in Figs 6 and 7.

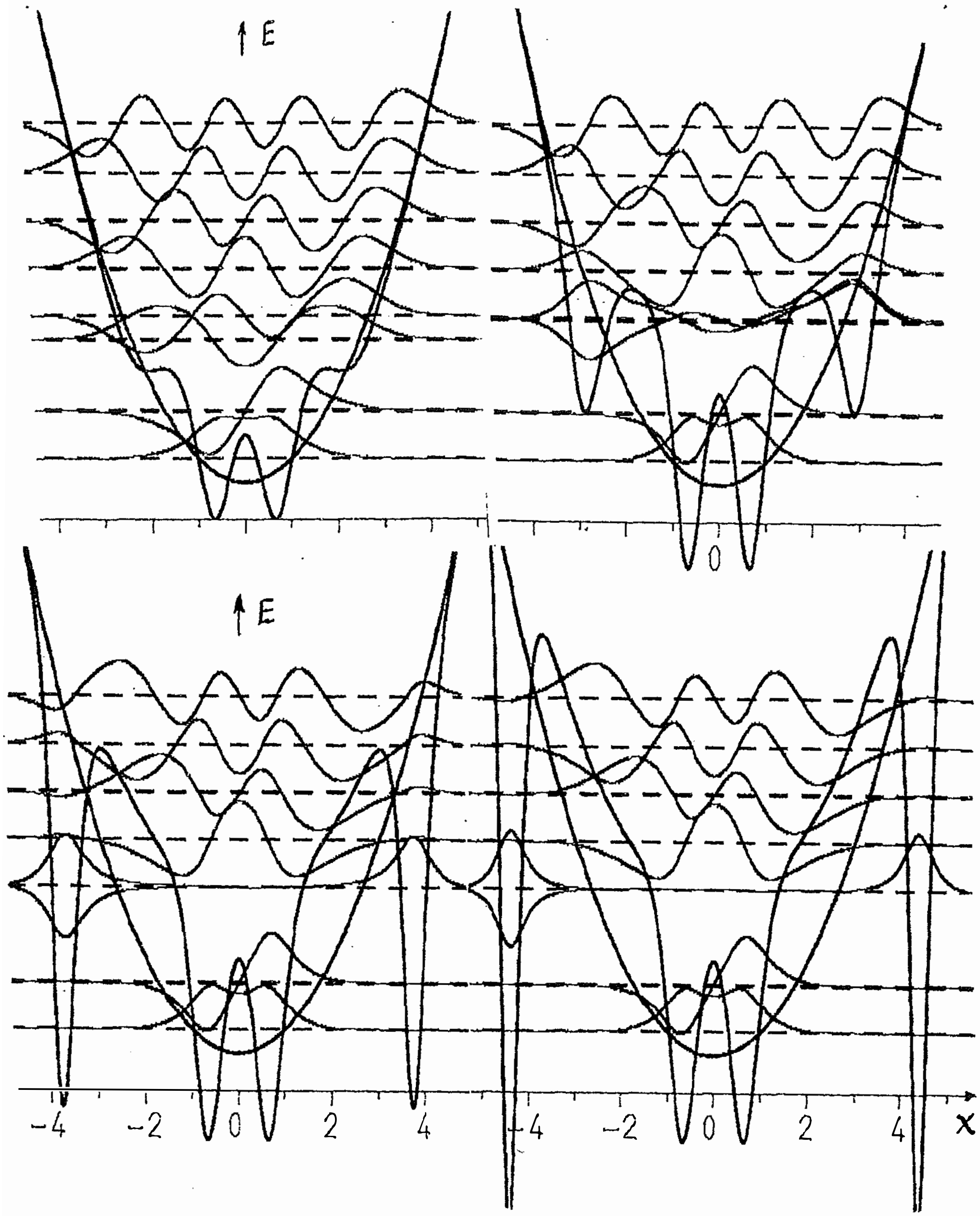


Fig.9. $E_3 \to E_4$; $\Delta E_3 \equiv t = 1,\ 1.9,\ 1.999,\ 1.99999$ in the oscillator well.

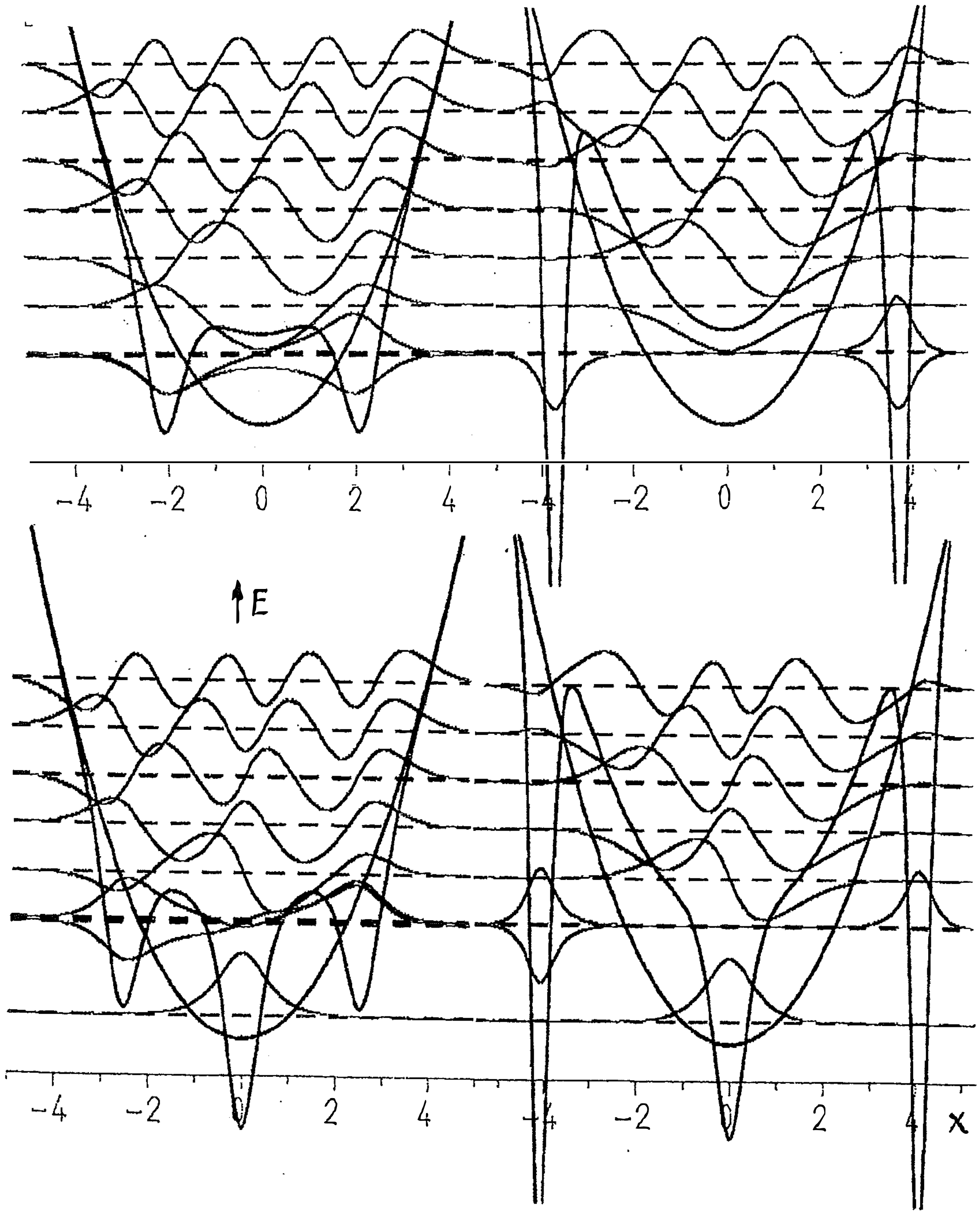


Fig.10. $E_1 \to E_2$; $\Delta E_1 \equiv t = 1.9,\ 1.99999$ and $E_2 \to E_3$; $\Delta E_2 \equiv t = 1.9,\ 1.99999$ in the oscillator well.

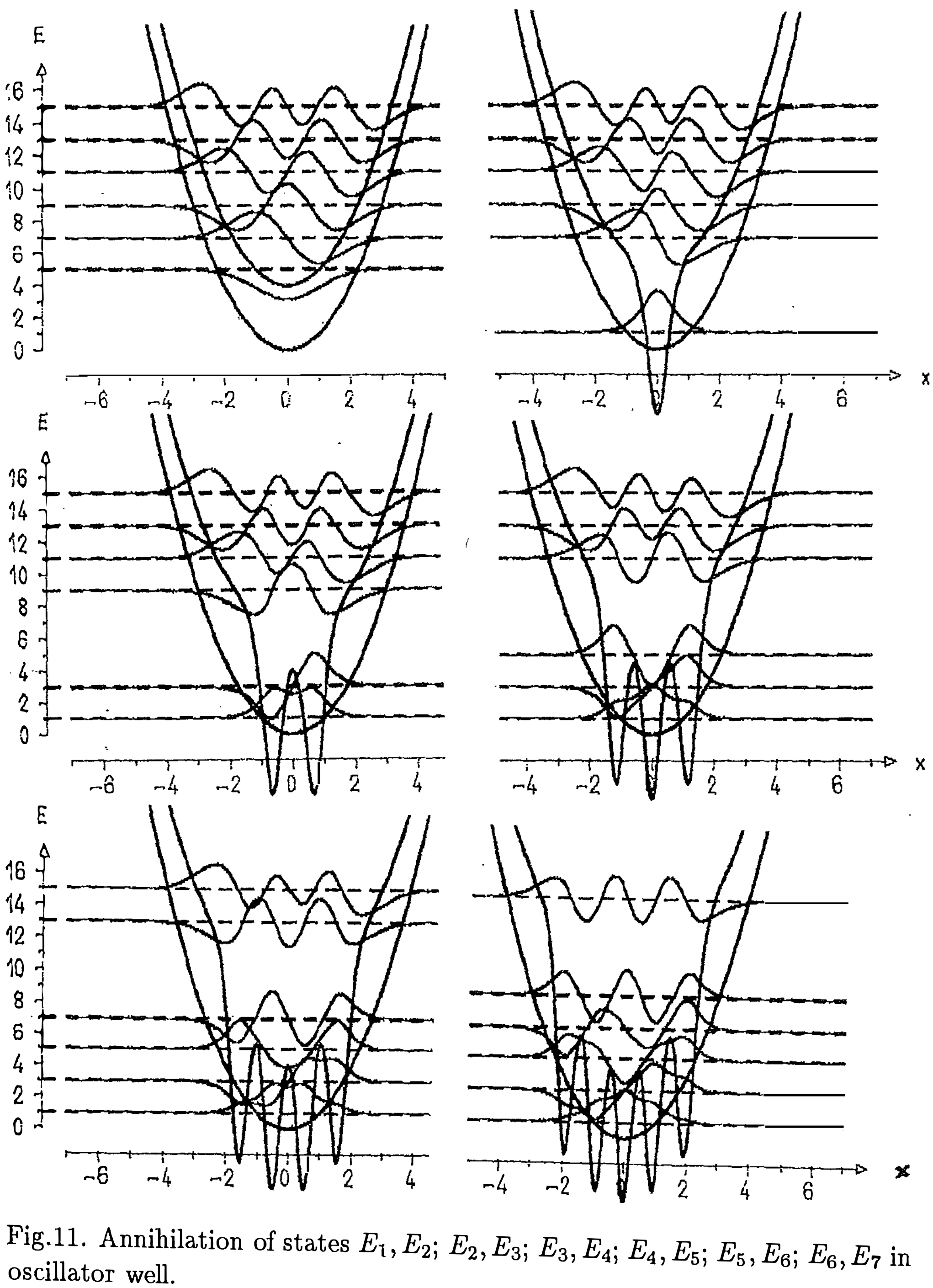


Fig.11. Annihilation of states $E_1, E_2$; $E_2, E_3$; $E_3, E_4$; $E_4, E_5$; $E_5, E_6$; $E_6, E_7$ in the oscillator well.

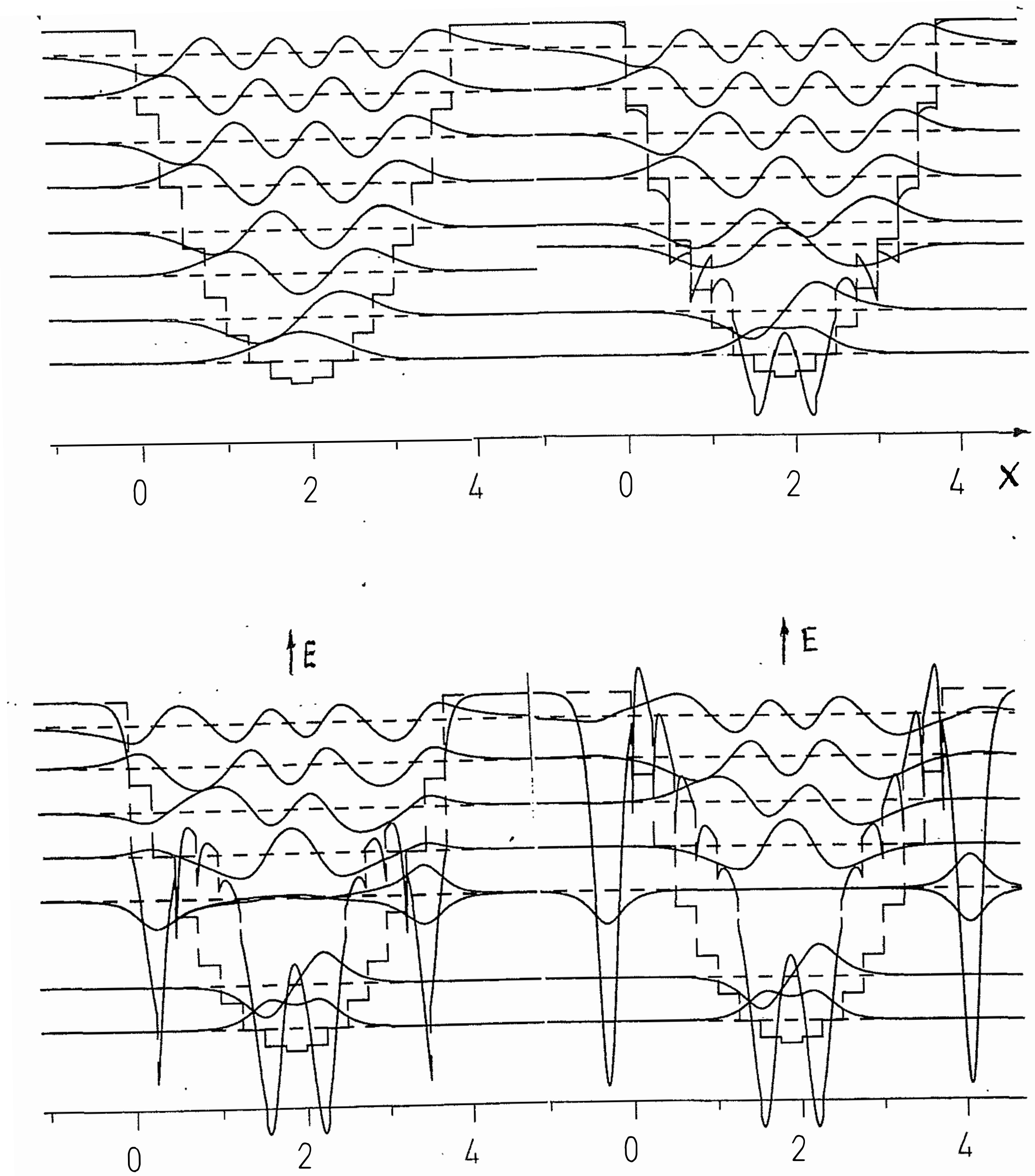


Fig.12. $E_3 \rightarrow E_4$; $\Delta E_3/(E_2 - E_1)$ in the multi-step well with equidistant bound states.

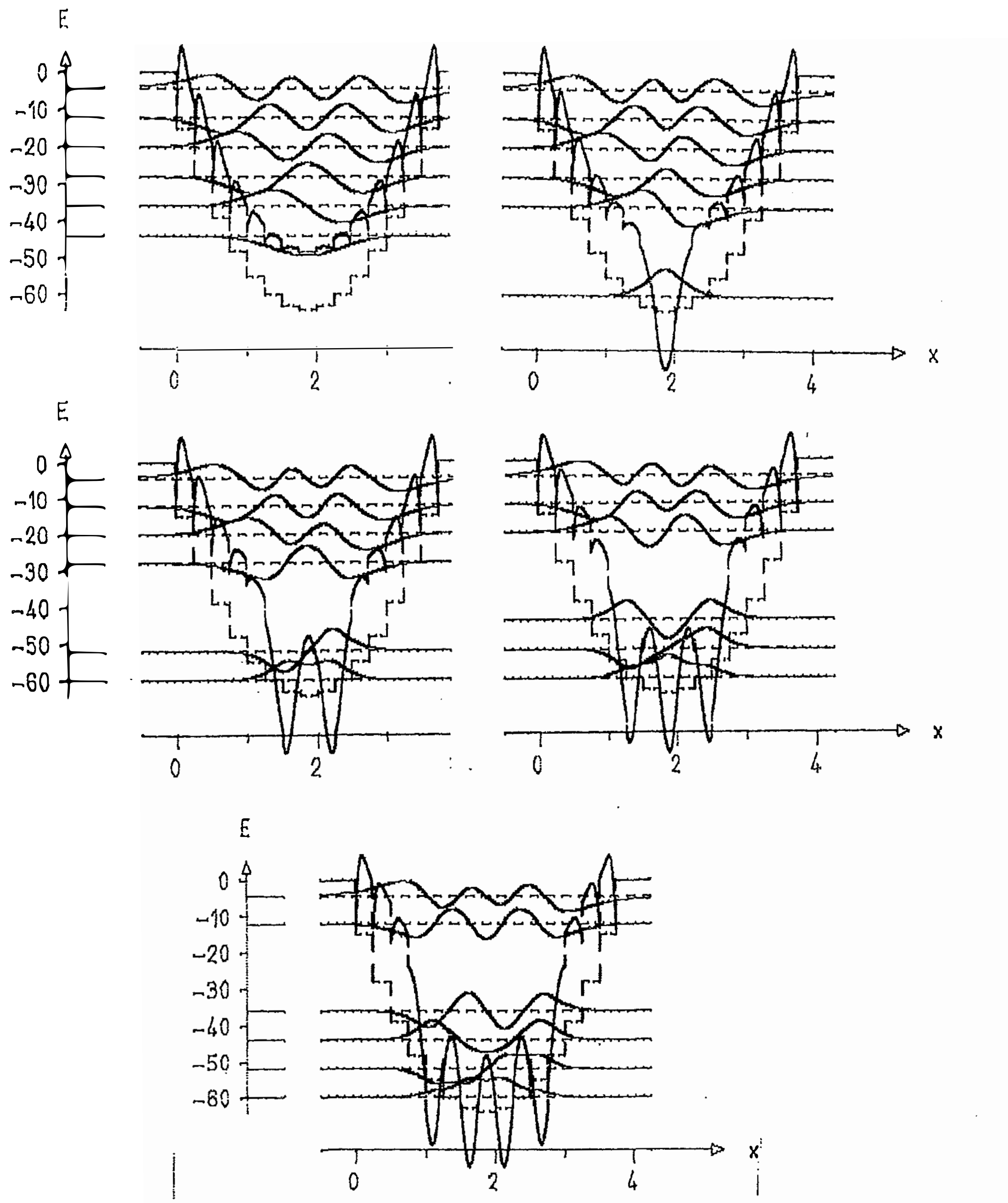


Fig.13. Annihilation of states $E_1, E_2$; $E_2, E_3$; $E_3, E_4$; $E_5, E_6$; $E_6, E_7$ in the multi-step wells.

Fig.9 shows the transformations of the infinite oscillator well and corresponding bound state eigenfunctions in the process $E_3 \to E_4$. All other states remain at their previous places. Pay attention to the auxiliary carrier wells which move in the opposite directions. In the limit they have infinite depth and zero width as the delta-wells. And the corresponding degenerating states disappear from the main middle well. Fig.10 shows the transformations of the infinite oscillator well and corresponding bound state eigenfunctions in the process $E_1 \to E_2$; and $E_2 \to E_3$. The limiting cases of effective annihilation of pairs of degenerated states $E_1, E_2$; $E_2, E_3$; $E_3, E_4$; $E_4, E_5$; $E_5, E_6$; $E_6, E_7$ in the oscillator well are shown in Fig.11. The explanation of forms of the resulting potentials is analogous to the case of the effective deleting of energy levels by making the corresponding spectral weight factors infinite or zero, as it will be shown below.

Fig.12 shows the symmetrical deformations of the finite multi-step potential well and corresponding bound state eigenfunctions in process of approach of the third energy level $E_3$ to the fourth one. The unperturbed initial system is chosen with the equidistant discrete spectrum. It is interesting that the equidistancy requires the initial multi-step well to be approximately of oscillator shape in the range of the lowest part of the spectrum where their energy levels coincide. Compare the shapes of the potential perturbations (find the common and different features) in Fig.12 and Fig.9. Pay attention to the potential peaks corresponding to every step of the initial well (for conservation of the reflection in scattering states by potential deformation).

Let us mention two kinds of the universal form of the auxiliary wells which carry the degenerating bound states out of the main well (for transformations of infinite and finite wells). Every carrier well takes away only half oscillation of the initial wave function. The oscillations which remain in the main well disappear in the limit of degeneration.

In Fig.13 are shown the deformation of the finite multi-step potential well and corresponding bound state eigenfunctions in the limiting cases: $E_1 \to E_2$; $E_2 \to E_3$; $E_2 \to E_3$; $E_3 \to E_4$; $E_4 \to E_5$; $E_5 \to E_6$; $E_6 \to E_7$. Compare the shapes of the perturbed potentials in Figs 13 and 11.

**SHIFTING BOUND STATES IN SPACE (Changing spectral weight factors)**

The spatial shifts of any chosen states are performed by auxiliary wells

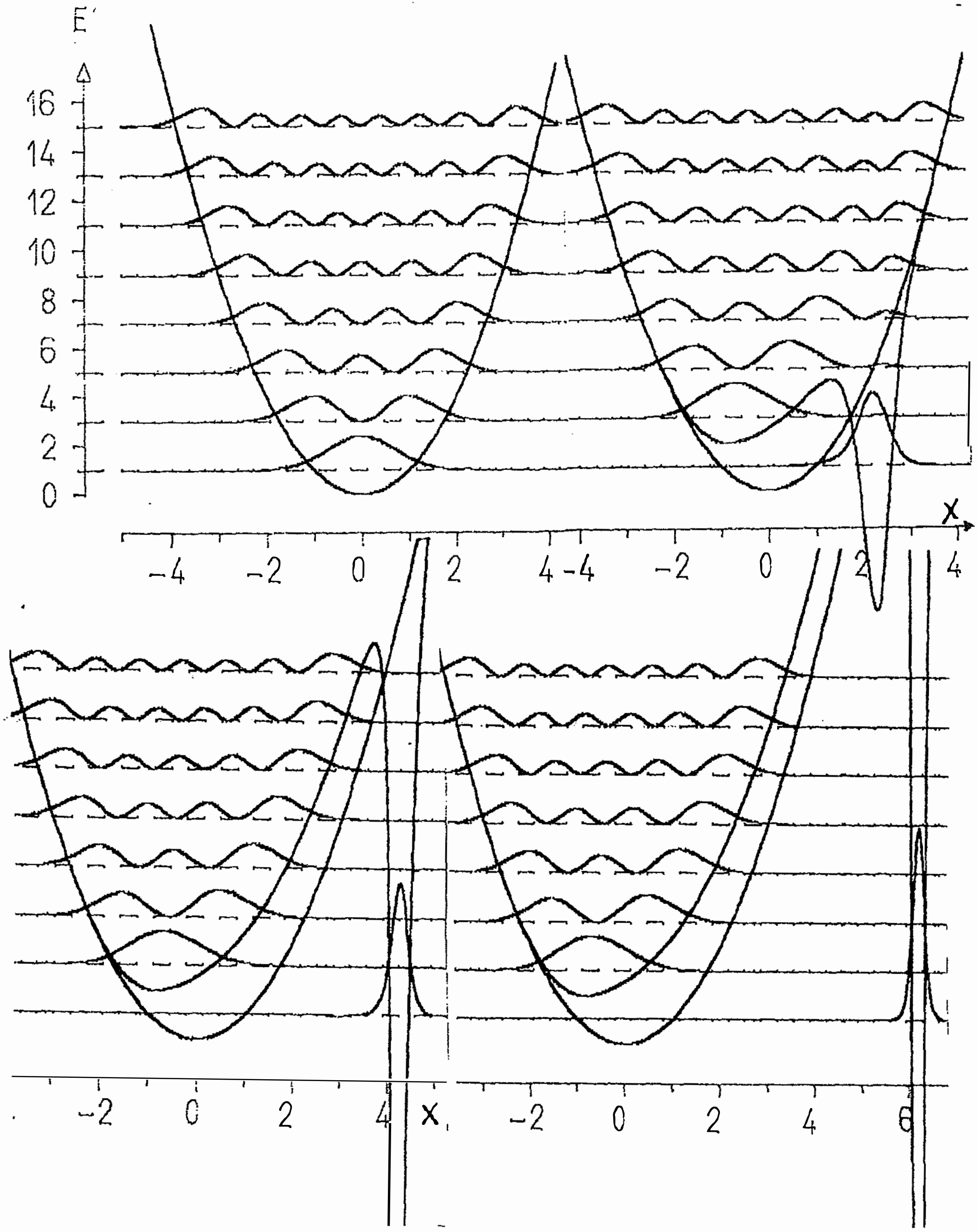


Fig.14. Shifting of the ground state from the oscillator well.

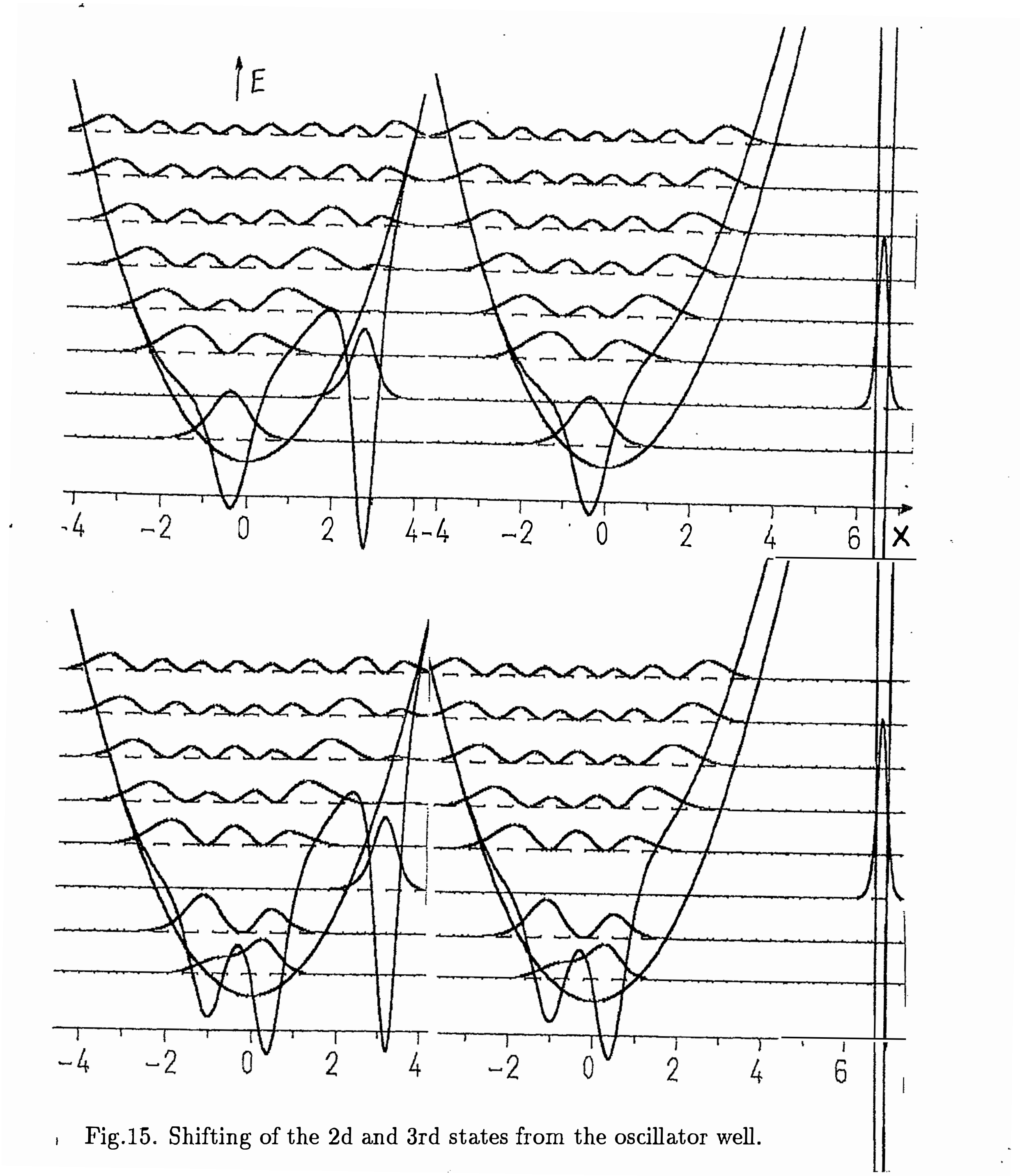


Fig.15. Shifting of the 2d and 3rd states from the oscillator well.

of the perturbation potentials carrying the states to be moved and analogous to that considered above (for shifts of energy levels). This confirms the economy of the algorithmical tools of the qualitative theory of quantum spectral control. There exist favorable conditions for retaining the standing wave in the carrier wells (for a half oscillation only) for the chosen energy. The corresponding formulae are given in Appendix 2.

Fig.14 shows the transformations of the infinite oscillator potential well and the corresponding bound state eigenfunctions in the process of increasing the spectral weight parameter (pre-exponential factor in the asymptotic behavior) $M_1$ of the ground state. Ground state is moved away from the main well by a special auxiliary carrier well. There exist favorable conditions of retaining the standing wave in the carrier wells (for a half oscillation only) for the chosen energy. All other states have their last half-oscillations inside the carrier well but with the disappearing amplitudes.

Fig.15 shows the gradual removing of the second and third states. Only one half-oscillation of the standing wave is carried away. The other oscillations remain in the main well but they have negligible amplitudes (unfavorable conditions for the standing wave there), so that the whole normalization of the removed state is concentrated in the carrier well. All other states remain in the deformed initial well and have their last half-oscillations inside the carrier well but with the disappearing amplitudes (destructive interference). The main well in the limit becomes narrower in comparison with the initial one above the removed state because every upper state lost a half-oscillation and must be shorter. The additional deepenings at the bottom of the main well are needed to keep at the same position the energy levels of the states below the removed one (to pool them down at the previous places when the narrowing of the main well pushes them up according to the rule considered above).

**DELETING OF THE CHOSEN ENERGY LEVELS**

In the limiting case $M_n \to \infty$ we have the effective disappearance of the nth energy level from the bound state spectrum.

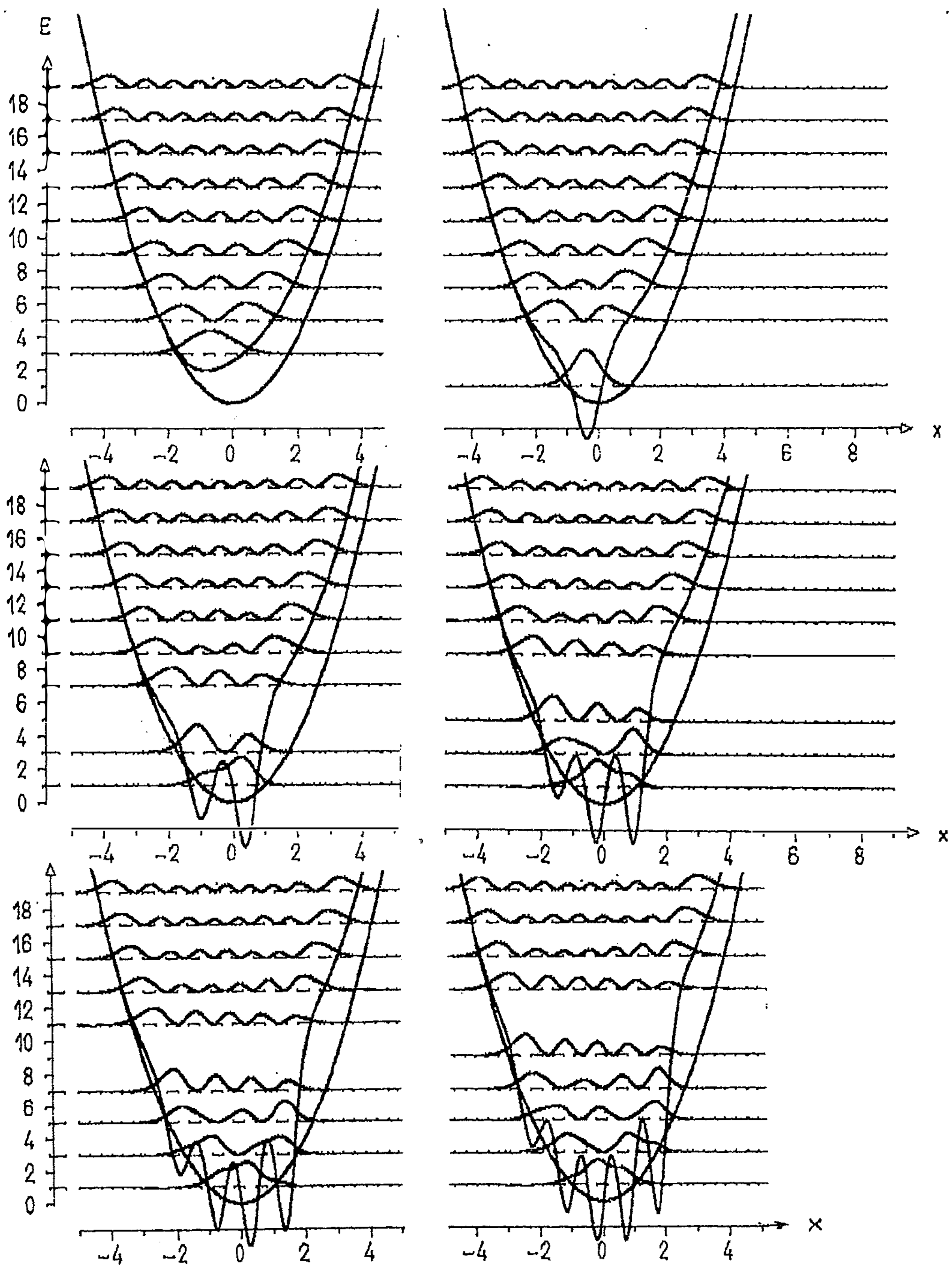


Fig.16. Deleting of states $E_1$; $E_2$; $E_3$; $E_4$; $E_5$; $E_6$ in oscillator well.

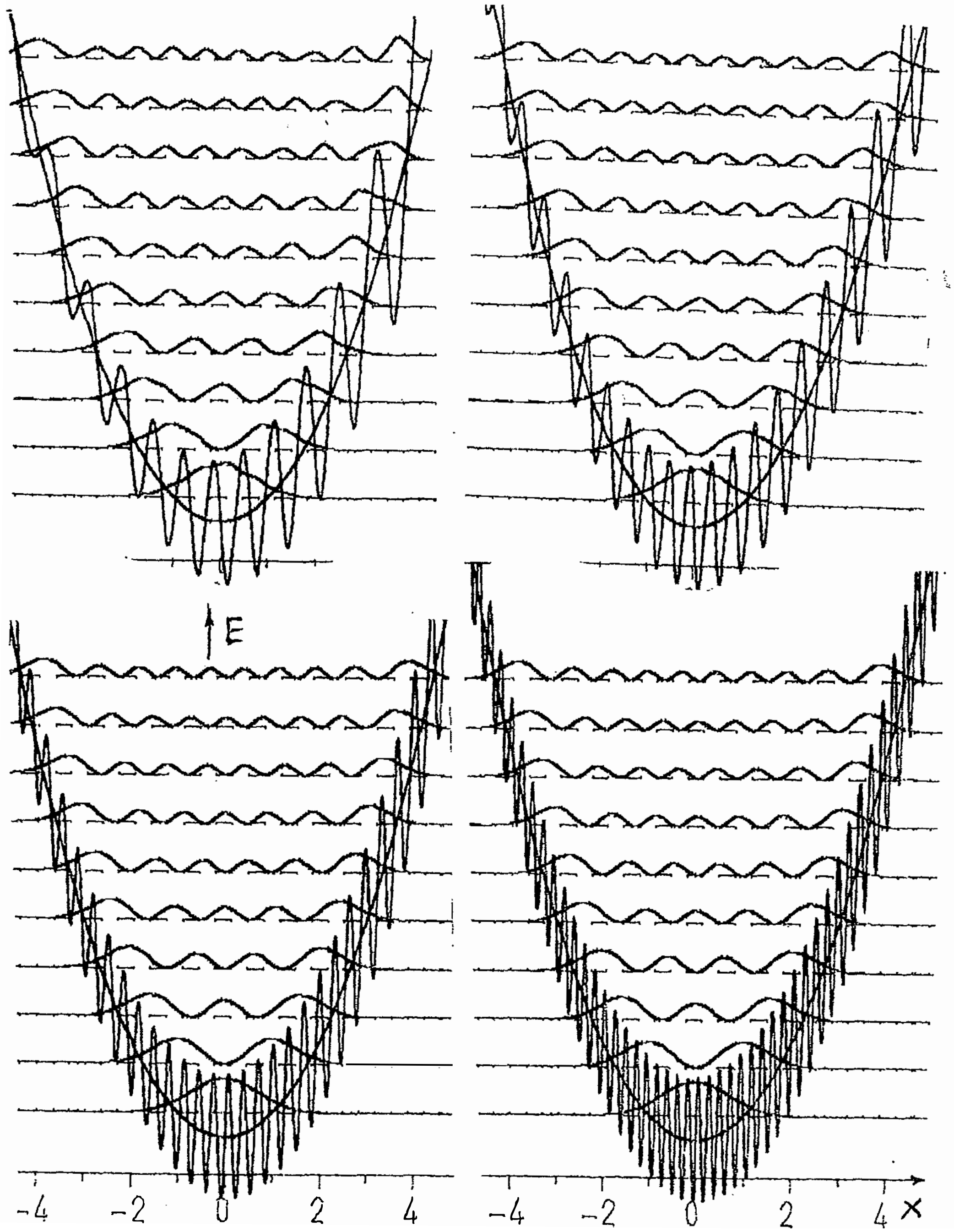


Fig.17. Deleting of states $E_{12}$; $E_{24}$; $E_{49}$; $E_{99}$ in oscillator well.

Fig.16 shows the limiting cases: deletion of states $E_1$; $E_2$; $E_3$; $E_4$; $E_5$; $E_6$. As in Fig.15, all the states above the removed one lost one half-oscillation and became shorter. To keep at the same positions the energy levels below the removed one, we need to pool them down with the proper number of partial wells at the bottom. The most sensitive is the nearest neighbor of the removed state. For more deeper states the narrowing of the upper part of the main well is not so important. So the shape of the bottom is mainly determined by the forces applied to this state.

Fig.17 shows the limiting cases: deletion of states $E_{12}$; $E_{24}$; $E_{49}$; $E_{99}$. Pay attention that the frequent potential oscillations do not alter significantly the wave functions of the lower states (approximately zero average influence).

**Acknowledgments**

The authors (V.M.Ch. and B.N.Z.) are grateful Geisenberg-Landau and RFFR Foundations for the support.

## APPENDIX I

Symmetrical deformations of initial potential wells and bound states by shifting only the chosen $n$th energy level are given below [7].

$$v(x) = \mathring{v}(x) - 2\{\ln \omega(x)\}'', \tag{1}$$

where

$$\omega(x) = [w(x), \mathring{\psi}(x, E_n)]. \tag{2}$$

In this expression symbol [ . , . ] denotes Wronskian:

$$[w(x), \mathring{\psi}(x, E_n)] = w(x)\, \mathring{\psi}'(x, E_n) - w'(x)\, \mathring{\psi}(x, E_n), \tag{3}$$

where $\mathring{\psi}(x, E_n)$ is the n-th (normalized) bound state wave function of the reference system. As w(x) one should take the solutions for initial symmetrical potential such that their parity must be opposite to one of the state to be shifted. For example, in the case of oscillator $v(x) = x^2$ hypergeometrical analogues of sine and cosine should be used:

$$w(x) = exp(-x^2/2)\ {}_1F_1(1/4 - (E_n + t)/4, 1/2, x^2), \text{ n is odd,}$$

or

$$w(x) = exp(-x^2/2)\ {}_1F_1(3/4 - (E_n + t)/4, 3/2, x^2)\ x, \text{ n is even.}$$

And for the rectangular well as $w(x)$ should be taken either sine or cosine (in the case of the well of finite depth these solutions, of course, must be smoothly sewed together with exponentially decreasing solutions outside the well). The expression for eigenfunction at the shifted energy $E_n + t$ is given by

$$\psi(x, E_n + t) = \overset{\circ}{\psi}(x, E_n)/\omega(x). \tag{4}$$

In the case of the whole line eigenfunctions for other (unshifted) energy levels $E_m$ are written as following $(n \neq m)$ :

$$\psi(x, E_m) = \overset{\circ}{\psi}(x, E_m) - -t(1/\omega(x))w(x) \int_{-\infty}^{x} \overset{\circ}{\psi}(y, E_n)\, \overset{\circ}{\psi}(y, E_m) dy. \tag{5}$$

**APPENDIX II**

Spectral parameters which determine the boundary (asymptotic) behavior of bound state wave functions are the levers of control of the main space localization of the chosen states. Let $\overset{\circ}{\psi}(x)$ be an eigenfunction of the reference Hamiltonian $\overset{\circ}{v}(x) = x^2$ related to $\mu$th energy eigenvalue, $M$ and $\overset{\circ}{M}$ be the factors by the decreasing exponential asymptotical tails $\sim x^{\mu}\exp(-x^2/2)$ of $\psi(x)$ and $\overset{\circ}{\psi}(x)$ respectively. If the problem is to alter only the weight factor $\overset{\circ}{M}$ of chosen state provided that all other spectral parameters remain unchanged, then the transformed potential is

$$V(x) = \overset{\circ}{v}(x) - \frac{d}{dx}K(x, x). \tag{6}$$

Here expression for $K$ has the form

$$K(x, y) = \frac{(1 - M^2/\overset{\circ}{M}{}^2)\, \overset{\circ}{\psi}(x)\, \overset{\circ}{\psi}(y)}{1 - (1 - M^2/\overset{\circ}{M}{}^2) \int_x^{\infty} \overset{\circ}{\psi}{}^2(y) dy}. \tag{7}$$

Formula for the eigenfunctions of new Hamiltonian at unaltered energies $E_\nu$ reads

$$\psi_\nu(x) = \overset{\circ}{\psi}_\nu (x) + \int_x^\infty K(x,y) \overset{\circ}{\psi}_\nu (y) dy. \tag{8}$$

It should be noted here that similar formula for $K$ is valid also for varying $c$ in G-L-approach (as well as in the case of finite interval). We must only replace $c$ by $M$ and the integration limits in the denominator (from 0 till $x$).

**REFERENCES**

[1] Zakhariev, B.N., *Lessons on Quantum Intuition* (to be published Dubna, JINR, 1996);

[2] Zakhariev, B.N., N.A.Kostov, E.B.Plekhanov, 1990, Fiz.Elem. Chastits At.Yadra **21** 914 [Sov.J. Part.& Nucl.**21** 384 (1990)];

[3] Zakhariev, B.N., 1992, Fiz.Elem.Chastits At.Yadra **23** 1387 [Sov.J.Part.& Nucl. **23**, 603 (1992)];

[4] Zakhariev, B.N., V.M.Chabanov, 1994, Fiz.Elem.Chastits At. Yadra **25** 1561 [Sov.J.Part.& Nucl. **25**, 662 (1994)]; 1993, Phys.Lett. **B 319**, 13.; 1994, Phys.Rev. **A49**, 3159; **A50** 3948.

[5] Chabanov, V. M., B. N. Zakhariev, S.Brandt, H.D.Dahmen, T.Stroh, 1995 (to be published).

[6] Brandt, S., and H.D.Dahmen, 1985, *The Picture Book of Quantum Mechanics*, (J.Wiley and Sons, New York); 1990, *Quantum Mechanics on the Personal Computer*, (Springer, Heidelberg).

[7] Pöschel, J., and E. Trubovitz, 1987, *Inverse Spectral Theory* (Academic, New York).